FINITE ELEMENT SIMULATION OF MHD MIXED CONVECTION IN A RECTANGULAR CAVITY CONTAINING HEATED BLOCK AND TWO SEMI-CIRCULAR WALL HEATER

by

Sayeda Fahmida Ferdousi
Student No. 0412093007 P
Registration No. 0412093007, Session: April-2012

MASTER OF PHILOSOPHY
IN
MATHEMATICS

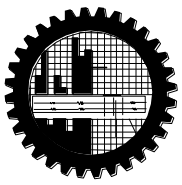

Department of Mathematics
Bangladesh University of Engineering and Technology (BUET),
Dhaka-1000
March - 2017

The thesis titled

FINITE ELEMENT SIMULATION OF MHD MIXED CONVECTION IN A RECTANGULAR CAVITY CONTAINING HEATED BLOCK AND TWO SEMI-CIRCULAR WALL HEATER

Submitted by

Sayeda Fahmida Ferdousi
Student No. 0412093007 P, Registration No. 0412093007, Session: April-2012, a part time student of M. Phil. (Mathematics) has been accepted as satisfactory in partial fulfillment for the degree of Master of Philosophy in Mathematics On 21 March, 2017

BOARD OF EXAMINERS

1. A. Alim

Dr. Md. Abdul Alim — Chairman
Professor — (Supervisor)
Dept. of Mathematics, BUET, Dhaka-1000

2. A. Alim

Head — Member
Dept. of Mathematics — (Ex-Officio)
BUET, Dhaka-1000

3. Mahkhan

Dr. Md. Abdul Hakim Khan — Member
Professor
Dept. of Mathematics, BUET, Dhaka-1000

4. Md. Elias.

Dr. Md. Elias — Member
Professor
Dept. of Mathematics, BUET, Dhaka-1000

5. Laek Sazzad Andallah

Dr. Laek Sazzad Andallah — Member
Professor — (External)
Department of Mathematics
Jahangirnagar University, Savar, Dhaka

ii

AUTHOR'S DECLARATION

I hereby announce that the work which is being presented in this thesis entitled

"FINITE ELEMENT SIMULATION OF MHD MIXED CONVECTION IN A RECTANGULAR CAVITY CONTAINING HEATED BLOCK AND TWO SEMI-CIRCULAR WALL HEATER"

submitted in partial fulfillment of the requirements of the degree of Master of Philosophy, department of Mathematics, BUET, Dhaka, is an authentic record of my own work.

The work is also original except where indicated by and attached with special reference in the context and no part of it has been submitted for any attempt to get other degrees or diplomas.

All views expressed in the dissertation are those of the author and in no way or by no means represent those of Bangladesh University of Engineering and Technology, Dhaka. This dissertation has not been submitted to any other University for examination either in home or abroad.

(Sayeda Fahmida Ferdousi)
Date: 21 March, 2017

iii

ACKNOWLEDGEMENT

I would like to affirm the notable recognizance of Almighty's continual mercy, because no work would have been possible to accomplish the goal line without help of Him. With great pleasure the author takes this opportunity to place on record her deepest respect and sincerest gratitude to her Supervisor Dr. Md. Abdul Alim, Professor, Department of Mathematics, Bangladesh University of Engineering and Technology, Dhaka for his expert guidance and valuable suggestions throughout this work. It would not have been possible to carry out this study successfully without continuous inspiration, guidance, constant support, intuitive suggestions and relentless encouragement from supervisor.

I am also intensely grateful to Professor Dr. Md. Abdul Hakim Khan and Prof. Dr. Md. Elias, Department of Mathematics, BUET for their wise and liberal co-operation in providing me all necessary help from the department during my course of M.Phil degree. I am also grateful to all my honorable teachers without help of them my achievement would not be possible. I wish to thank to the all staff of the Department of Mathematics, Bangladesh University of Engineering and Technology, for their cooperation in this work.

Finally, I express my heartiest respect to my father S.M.A. Ferdous, mother Farida Ferdous, husband Md. Mahmudul Hasan, beloved son Md. Nihad Farwan and all of my family members for creating a delightful atmosphere as well as excusing me from family duties in order to complete the courses, research studies and final production of the thesis work.

Author

ABSTRACT

Mixed convective flow in lid driven cavities occurs as a result of two competing mechanisms. The first one is due to shear flow caused by the movement of one of the walls of the enclosure, while the following one is due to the buoyancy flow produced by thermal non-homogeneity of the enclosure boundaries. Analysis of mixed convective flow in a lid-driven enclosure finds application in material processing, flow and heat transfer in solar ponds, dynamics of lakes, reservoirs and cooling ponds, crystal growing, float glass production, metal casting, food processing, galvanizing and metal coating.

In this thesis all mechanisms of convection such as natural, mixed and forced convection have been studied. The relative direction between the buoyancy force and the externally imposed flow is important. In the case where the buoyancy force and external force both are present termed as mixed convection flow. This study depends on various non-dimensional parameters and geometrical conditions which are abstracted below.

A numerical simulation of two dimensional laminar steady flow for MHD mixed convection within rectangular cavity with two semi-circular wall heater and heated block in the middle has been performed. Two different shapes of heated block i.e. trapezoidal and rectangular has been considered. Present study consists a concentrated heated block in the middle and two concentrated semi-circular wall heater, adiabatic upper and bottom wall except two semi-circular wall heater, left and right cold and low concentrated wall and moving upper wall. The fluid is concerned with various values of Hartmann number; *Ha=0,Ha=50,Ha=100* and *Ha=150*, Richardson number ; *Ri=0.1,Ri=1,Ri=5* and *Ri=10*, buoyancy ratio; *Br=2, Br=5, Br=10* and *Br=20* with different shapes of heated and concentrated obstacle areas as *A=0.042* and *A=0.028*. Also the value of Prandtl number; *Pr=7* and Lewis number; *Le=2* have been kept fixed in the present study.

The properties of the fluid are presumed to be constant. The physical problems are represented mathematically by different sets of governing equations along with the corresponding boundary conditions. The non-dimensional governing equations are discretized by using Galerkin weighted residual method of finite element formulation.

Numerical simulation results are presented in terms of streamlines, isotherms, average Nusselt number along with the left and right semi-circular wall. We also plotted average Nusselt number Vs Richardson number for different shaped obstacle along the two semi-circular wall heater with MHD and without MHD, average Nusselt number Vs Richardson number for different values of Ha along the two semi-circular wall heater with trapezoidal and rectangular obstacle and average Nusselt number Vs Richardson number along the two semi-circular wall for different values of Br with MHD for trapezoidal and rectangular obstacle. The range of Richardson number is selected on the basis of calculation covering forced, mixed and free convection dominated regions. The computational results indicate that the average Nusselt number at the two semi-circular wall depends on the dimensionless parameters and the shapes of obstacle. Comparison with previously published work are presented and the results are found to be in excellent agreement.

CONTENTS

NOMENCLATURE

B_0	magnetic induction
C_p	Specific heat at constant pressure (J/kg K)
g	gravitational acceleration (m/s^2)
h	convective heat transfer coefficient (W/m^2 K)
Ha	Hartmann number
k	thermal conductivity of fluid(W/m K)
L	Length of the enclosure(m)
H	Height of the enclosure (m)
N	Total number of nodes
Nu_{av}	Average Nusselt number
P	non-dimensional pressure
p	pressure
Pr	Prandtl number
Ri	Richardson number
Re	Reynold's number
Le	Lewis number
Br	Buoyancy ratio
T	Temperature
T_H	High Temperature at hot wall
T_L	Low Temperature at cold wall
C	Concentration of species
C_H	High Concentration

C_L Low Concentration

D Mass Diffusivity (m^2/s)

U x component of dimensionless velocity

u x component of velocity (m/s)

V y component of dimensionless velocity

v y component of velocity (m/s)

u_0 Lid velocity

x, y Cartesian coordinates

X, Y dimensionless Cartesian coordinates

Greek symbols

α Thermal diffusivity

β_T Coefficient of thermal expansion

β_C Compositional expansion coefficient

ν Kinematic Viscosity

ρ Density of the fluid

θ Non-dimensional Fluid temperature

μ Dynamic viscosity of the fluid

ΔT Temperature difference

Ψ Streamfunction

ν Kinematic viscosity of the fluid

σ Fluid electrical conductivity

Subscripts

T Temperature

C Concentration

H High

L Low

LIST OF TABLES

LIST OF FIGURES

CHAPTER 1

INTRODUCTION

1.1 Introduction

Heat transfer is that science which seeks to predict the energy transfer which may take place between material bodies as a result of a temperature difference. Thermodynamics teaches that this energy transfer is defined as heat. The science of heat transfer seeks not merely to explain how heat energy may be transferred, but also to predict the rate at which the exchange will take place under certain specified conditions.

The phenomenon of heat transfer was known to human being even in the primitive age when they used to use solar energy as a source of heat. Heat transfer in its initial stage was conceived with the invention of fire in the early age of human civilization. Since then its knowledge and use has been progressively increasing each day as it is directly related to the growth of human civilization. With the invention of stream engine by James watt in 1765 A. D., the phenomenon of heat transfer got its first industrial recognition and after that its use extended to a great extent and spread out in different spheres of engineering fields. In the past three decades, digital computers, numerical techniques and development of numerical models of heat transfer have made it possible to calculate heat transfer of considerable complexity and thereby create a new approach to the design of heat transfer equipment.

The study of temperature and heat transfer is of great importance to the engineers because of its almost universal occurrence in many branches of science and engineering. Although heat transfer analysis is most important for the proper sizing of fuel elements in the nuclear reactors cores to prevent burnout, the performance of aircraft also depends upon the case with which the structure and engines can be cooled. The design of chemical plants is usually done on the basis of heat transfer analysis and the analogous mass transfer processes. The transfer and conversion of energy from one form to another is the basis to all heat transfer process and hence, they are governed by the first as well as the second law of thermodynamics. Heat transfer is commonly associated with fluid dynamics. The knowledge of temperature

distribution is essential in heat transfer studies because of the fact that the heat flow takes place only wherever there is a temperature gradient in a system. The heat flux which is defined as the amount of heat transfer per unit area in per unit time can be calculated from the physical laws relating to the temperature gradient and the heat flux.

The study of the universe has led to the realization that all physical phenomena are subject to natural laws. The term natural might well be used to describe the framework or system of fundamental and universal importance within this system is the mechanisms for the transfer of heat. Heat transfer is a branch of applied thermodynamics. It estimates the rate at which heat is transferred across the system boundaries subjected to specific temperature differences and the temperature distribution of the system during the process. Whereas classical thermodynamics deals with the amount of heat transferred during the process. Heat transfer processes have always been an integral part of our environment.

1.2 Heat Transfer Mechanism

Heat is the form of energy that can be transferred from one system to another as a result of temperature difference. A thermodynamic analysis is concerned with the amount of heat transfer as a system undergoes a process from one equilibrium state to another. The science that deals with the determination of the rates of such energy transfers is the heat transfer. The transfer of energy as heat is always from the higher temperature medium to the lower temperature one, and heat transfer stops when the two mediums reach the same temperature.

Heat can be transferred in three mechanisms or modes: conduction, convection and radiation. All modes of heat transfer require the existence of a temperature difference, and all modes are from the high temperature medium to a lower temperature one. In reality, the combined effect of these three modes of heat transfer control temperature distribution in a medium.

1.2.1 Convective heat transfer

Convection is a type of heat transfer which occurs generally in fluids. The transfer of heat from surface and a moving liquid or generally fluid at various temperature is termed as convection. This is due to the movement of atoms or molecules present in the liquids or gases. The heat transfer from solid to fluid or fluid to solid consists of two transfer process. One is conduction and other one is advection. A convective transfer involves the combined process of conduction and advection. Advection means the heat transfer due to the bulk fluid

flow. The conduction or diffusion is taking place the boundary layer of the solids. So the combined effect of transfer is termed as convection.

Convection is one of the major modes of heat transfer and mass transfer. Convective heat and mass transfer take place through both diffusion which means random Brownian motion of individual particles in the fluid and by advection, in which matter or heat is transported by the larger-scale motion of currents in the fluid. In the context of heat and mass transfer, the term "convection" is used to refer to the sum of advective and diffusive transfer. The term "convection" may have slightly different but related usages in different contexts. The broader sense is in fluid mechanics, where "convection" refers to the motion of fluid (regardless of cause). However in thermodynamics "convection" often refers specifically to heat transfer by convection. Additionally, convection includes fluid movement both by bulk motion (advection) and by the motion of individual particles (diffusion). However in some cases, convection is taken to mean only advective phenomena. For instance, in the transport equation, which describes a number of different transport phenomena, terms are separated into "convective" and "diffusive" effects. A similar differentiation is made in the Navier–Stokes equations. In such cases the precise meaning of the term may be clear only from context. Convection occurs on a large scale in atmospheres, oceans, and planetary mantles. Fluid movement during convection may be invisibly slow, or it may be obvious and rapid, as in a hurricane. On astronomical scales, convection of gas and dust is thought to occur in the accretion disks of black holes, at speeds which may closely approach that of light.

1.2.2 Mixed Convection

Mixed convection occurs when natural convection and forced convection mechanisms act together to transfer heat. This is also defined as situations where both pressure forces and buoyant forces interact. How much each form of convection contributes to the heat transfer is largely determined by the flow, temperature, geometry, and orientation. Combined forced and natural convection is necessary where the forced convection is not enough to dissipate all of the heat required. At this point, combining natural convection with forced convection will often deliver the desired results. Examples of these processes are nuclear reactor technology and some aspects of electronic cooling.

1.2.3 Internal and External Flows

A fluid flow is classified as being internal or external, depending on whether the fluid is forced to flow in a confined channel or over a surface. An internal flow is bounded on all sides by solid surfaces except, possibly, for an inlet and exit. Flows through a pipe or in an air-conditioning duct are the examples of internal flow. Internal flows are dominated by the influence of viscosity throughout the flow field. The internal flow configuration represents a convenient geometry for the heating and cooling of fluids used in the chemical processing, environmental control, and energy conversion areas. The flow of an unbounded fluid over a surface is external flow. The flows over curved surfaces such as sphere, cylinder, airfoil, or turbine blade are the example of external flow. In external flows the viscous effects are limited to boundary layers near solid surfaces.

1.2.4 Boundary Layer

Since fluid motion is the distinguishing feature of heat convection, it is necessary to understand some of the principles of fluid dynamics in order to describe adequately the processes of convection. When a fluid flows over a body, the velocity and temperature distribution at the immediate vicinity of the surface strongly influenced by the convective heat transfer. In order to simplify the analysis of convective heat transfer the boundary layer concept frequently is introduced to model the velocity and temperature fields near the solid surface in order to simplify the analysis of convective heat transfer. So we are concerned with two different kinds of boundary layers, the velocity boundary layer and the thermal boundary layer.

The velocity boundary layer is defined as the narrow region, near the solid surface, over which velocity gradients and shear stresses are large, but in the region outside the boundary layer, called the potential-flow region, the velocity gradients and shear stresses are negligible. The exact limit of the boundary layer cannot be precisely defined because of the asymptotic nature of the velocity variation. The limit of the boundary layer is usually taken to be at the distance from the surface, at which the fluid velocity is equal to a predetermined percentage of the free stream value, $\boldsymbol{U}_{\infty}$. This percentage depends on the accuracy desired, 99 or 95% being customary. Although, outside the boundary layer region the flow is assumed to be inviscid, but inside the boundary layer the viscous flow may be either laminar or turbulent. In the case of laminar boundary layer, fluid motion is highly ordered and it is possible to

identify streamlines along which particles move. Fluid motion along a streamline is characterized by velocity components in both the *x* and *y* directions. Since the velocity component v is in the direction normal to the surface, it can contribute significantly to the transfer of momentum, energy or species through the boundary layer. Fluid motion normal to the surface is necessitated by boundary layer growth in the x direction. In contrast, fluid motion in the turbulent boundary layer is highly irregular and is characterized by velocity fluctuations. These fluctuations enhance the transfer of momentum, energy and species and hence increase surface friction, as well as convection transfer rates. Due to fluid mixing resulting from the fluctuations, turbulent boundary layer thicknesses are larger and boundary layer profiles are flatter than in laminar flow. The thermal boundary layer may be defined (in the same sense that the velocity boundary layer was defined above) as the narrow region between the surface and the point at which the fluid temperature has reached a certain percentage of ambient temperature. Outside the thermal boundary layer the fluid is assumed to be a heat sink at a uniform temperature of $\boldsymbol{T}_\infty$. The thermal boundary layer is generally not coincident with the velocity boundary layer, although it is certainly dependent on it. If the fluid has high thermal conductivity, it will be thicker than the velocity boundary layer, and if conductivity is low, it will be thinner than the velocity boundary layer.

1.2.5 Streamfunction

The fluid motion is displayed using the streamfunction ($\boldsymbol{\psi}$) obtained from velocity components $\boldsymbol{U}$ and $\boldsymbol{V}$. The relationships between streamfunction ($\boldsymbol{\psi}$) and velocity components for two-dimensional flows are

$$U = \frac{\partial \psi}{\partial Y} \qquad \text{and} \qquad V = -\frac{\partial \psi}{\partial X}$$

which yield a single equation

$$\frac{\partial^2 \psi}{\partial X^2} + \frac{\partial^2 \psi}{\partial Y^2} = \frac{\partial U}{\partial Y} - \frac{\partial V}{\partial X}$$

Using the above definition of the streamfunction, the positive sign of w denotes anti-clockwise circulation and the clockwise circulation is represented by the negative sign of ψ.

1.2.6 Thermal Conductivity

Thermal conductivity of a material can be defined as the rate of heat transfer through a unit thickness of the material per unit area per unit temperature difference. Therefore the thermal conductivity of a material is a measure of the ability of the material to conduct heat. A high value for thermal conductivity indicates that the material is a good heat conductor, and a low value for thermal conductivity indicates that the material is a poor heat conductor or insulator. For example the materials such as copper and silver that are good electric conductors are also good heat conductors, and have high values of thermal conductivity. Materials such as rubber, wood are poor conductors of heat and have low conductivity values. The rate of heat conduction through a medium depends on the geometry of the medium, its thickness, and the material of the medium, as well as the temperature difference across the medium. The proportionality constant k is called thermal conductivity of the material.

1.2.7 Thermal Diffusivity

The time dependent heat conduction equation for constant $\boldsymbol{k}$ contains a quantity $\boldsymbol{\alpha}$, called the thermal diffusivity. Thermal diffusivity represents how fast heat diffuses through a material and is defined as

$$\alpha = \frac{\kappa}{\rho C_P}$$

Here the thermal conductivity κ represents how well a material conducts heat, and the heat capacity $\boldsymbol{\rho C_p}$ represents how much energy a material stores per unit volume. Therefore, the thermal diffusivity of a material can be viewed as the ratio of the heat conducted through the material to the heat stored per unit volume. A material that has a high thermal conductivity or a low heat capacity will obviously have a large thermal diffusivity. The larger thermal diffusivity means that the propagation of heat into the medium is faster. A small value of thermal diffusivity means the material mostly absorbs the heat and a small amount of heat is conducted further.

1.2.8 Tilted Enclosure

The tilted enclosure geometry has received considerable attention in the heat transfer literature because of mostly growing interest of solar collector technology. The angle of tilt has a dramatic impact on the flow housed by the enclosure. Consider an enclosure heated

from below is rotated about a reference axis. When the tilted angle becomes 90º, the flow and thermal fields inside the enclosure experience the heating from side condition. Thereby convective currents may pronounce over the diffusive currents. When the enclosure rotates to 180º, the heat transfer mechanism switches to the diffusion because the top wall is heated.

1.2.9 Boussinesq Approximation

The governing equations for convection flow are coupled elliptic partial differential equations and are, therefore, of considerable complexity. The major problems in obtaining a solution to these equations lie in the inevitable variation of density with temperature, or concentration, and in their partial, elliptic nature. Several approximations are generally made to considerably simplify these equations. Among them Boussinesq approximation is considered here. In flows accompanied by heat transfer, the fluid properties are normally functions of temperature. The variations may be small and yet be the cause of the fluid motion. If the density variation is not large, one may treat the density as constant in the unsteady and convection terms, and treat it as variable only in the gravitational term. This is called the Boussinesq approximation.

1.3 Mass Transfer Mechanism

Mass transfer is the net movement of mass from high concentration to low concentration. Mass transfer occurs in many processes, such as absorption, evaporation, adsorption, drying, precipitation, membrane filtration, and distillation. Mass transfer is used by different scientific disciplines for different processes and mechanisms. The phrase is commonly used in engineering for physical processes that involve diffusive and convective transport of chemical species within physical systems. Convection mass transfer refers to the transfer of mass due to an externally imposed flow and diffusion mass transfer is the transfer of mass due to the random molecular motion.

Some common examples of mass transfer processes are the evaporation of water from a pond to the atmosphere, the purification of blood in the kidneys and liver, and the distillation of alcohol. In industrial processes, mass transfer operations include separation of chemical components in distillation columns, absorbers such as scrubbers, absorbers such as activated carbon beds, and liquid-liquid extraction. Mass transfer is often coupled to additional

transport processes, for instance in industrial cooling towers. These towers couple heat transfer to mass transfer by allowing hot water to flow in contact with hotter air and evaporate as it absorbs heat from the air.

1.4 Diffusion mass transfer

Diffusion is transfer of mass due to the random molecular motion. It is the net movement of particles from an area of high concentration to low concentration due to the random movement of particles. It is a passive process which means no energy is needed.

1.5 Magneto-Hydrodynamics

Magneto-hydrodynamics (MHD) is the academic discipline which studies the dynamics of electrically conducting fluids. Examples of such fluids include plasmas, liquid metals and salt water. The word Magneto-hydrodynamics (MHD) is derived from “magneto-” meaning “magnetic field”, and “hydro” meaning “liquid”, and “dynamics” meaning “movement”. The field of MHD was initiated by Hannes Alfven, for which he received the Noble Prize in Physics in 1970. The idea of MHD is that magnetic fields which induce currents in a moving conducting fluid, and create forces on the fluid, and also change the magnetic field itself. The set of equations which describe MHD are a combination of the Nevier-Stokes equations of fluid dynamics and Maxwell’s equations of electromagnetism. These differential equations have to be solved simultaneously, either analytically or numerically. MHD is a continuum theory and as such it cannot treat kinetic phenomena, i.e. those in which the existence of discrete particles or of a non-thermal velocities distribution are important. The simple form of MHD, Ideal MHD, assumes that fluid has so little resistivity that it can be treated as a perfect conductor. This is the limit of infinite magnetic Reynolds number in ideal MHD, Lenz’s law dictates that the fluid is in a sense tied to the magnetic fields lines. To explain, in ideal MHD a small rope like volume of the fluid surrounding a field line will continue to lie along a magnetic field line, even as it is twisted and distorted by fluid flows in the system The connection between magnetic field lines and fluid in ideal MHD fixes the topology of the magnetic field in the fluid-for example, if a set of magnetic field lines are tied into a knot, then they will remain so as long as the fluid/plasma has negligible resistivity. This difficulty in reconnecting magnetic field lines makes it possible to store energy by moving the fluid or the source of the magnetic field. The energy can then become available if the conditions for

ideal MHD break down allowing magnetic reconnection that release the stored energy from the magnetic field.

The ideal MHD equations consist of the continuity equation, the momentum equation, and Ampere's Law in the limit of no electric field and no electron diffusivity, and a temperature evolution equation. As with any fluid description to a kinetic system, a closure approximation must be applied to highest moment of the particle distribution equation. This is often accomplished with approximations to the heat flux through a condition of adiabaticity or isothermality.

Ideal MHD is only strictly applicable when:

1. The plasma is strongly collisional, so that the time scale of collisions is shorter than the other characteristic times in the system, and the particle distributions are therefore close to Maxwellian.

2. The resistivity due to these collisions is small. In particular, the typical magnetic diffusion times over any scale length present in the system must be longer than any time scale of interest.

3. We are interested in length scales much longer than the ion skin depth and Larmor radius perpendicular to the field, long enough along the field to ignore Landau damping, and time scales much longer than the ion gyration time (system is smooth and slowly evolving).

1.6 Dimensionless Parameter

The dimensionless parameters can be thought of as measures of the relative importance of certain aspects of the flow. Some dimensionless parameters related to our study are discussed below:

1.6.1 Nusselt Number, *Nu*

The Nusselt number represents the enhancement of heat transfer through a fluid layer as a result of convection relative to conduction across the same fluid layer, and is defined as

$$\boldsymbol{Nu = hL / k}$$

where k is the thermal conductivity of the fluid, h is the heat transfer coefficient and L is the characteristics length. The Nusselt number is named after Wilhelm Nusselt, who made significant contributions to convective heat transfer in the first half of the twentieth century,

and it is viewed as the dimensionless convection heat transfer coefficient. The larger Nusselt number indicates a large temperature gradient at the surface and hence, high heat transfer by convection. A Nusselt number of $\boldsymbol{Nu = 1}$, for a fluid layer represents heat transfer across the layer by pure conduction. To understand the physical significance of the Nusselt number, consider the following daily life problems. We remedy to forced convection whenever we want to increase the rate of heat transfer from a hot object. In free convection flow velocities are produced by the buoyancy forces hence there are no externally induced flow velocities.

1.6.2 Reynold's Number, *Re*

Reynold's number is a dimensionless number which is the ratio of of momentum forces to viscous forces defined as

$$\boldsymbol{Re = \frac{inertial\ forces}{viscous\ forces} = \frac{\rho v L}{\mu} = \frac{vL}{\nu}}.$$

Where:

$\boldsymbol{v}$ is the maximum velocity of the object relative to the fluid ($\boldsymbol{m/s}$)

$\boldsymbol{L}$ is a characteristic linear dimension (travelled length of the fluid)($\boldsymbol{m}$)

$\boldsymbol{\mu}$ is the dynamic viscosity of the fluid ($\boldsymbol{Pa.s}$ or $\boldsymbol{Kg\ m^{-1}s^{-1}}$)

$\boldsymbol{\nu}$ is the kinematic viscosity ($\boldsymbol{m^2/s}$)

$\boldsymbol{\rho}$ is the density of the fluid ($\boldsymbol{Kg/m^3}$)

It is a dimensionless number used in fluid mechanics to indicate whether fluid flow past a body or in a duct is steady or turbulent. Also help to predict similar flow patterns in different fluid flow situations. The concept was introduced by George Gabriel Stokes in 1851, but the Reynolds number is named after Osborne Reynolds (1842–1912), who popularized its use in 1883. Reynolds numbers frequently arise when performing scaling of fluid dynamics problems, and as such can be used to determine dynamic similitude between two different cases of fluid flow. They are also used to characterize different flow regimes within a similar fluid, such as laminar or turbulent flow:

Laminar flow occurs at low Reynolds numbers, where viscous forces are dominant, and is characterized by smooth, constant fluid motion;

Turbulent flow occurs at high Reynolds numbers and is dominated by inertial forces, which tend to produce chaotic eddies, vortices and other flow instabilities.

1.6.3 Richardson's Number, *Ri*

The Richardson number, $\boldsymbol{Ri}$ is named after Lewis Fry Richardson. It is a dimensionless number that expresses the ratio of the buoyancy term to the flow gradient term. i.e.

$$\boldsymbol{Ri} = \frac{\textbf{buoyancy term}}{\textbf{flow gradient term}}$$

In the thermal convection problems, $\boldsymbol{Ri}$ represents the importance of natural convection relative to the forced convection. $\boldsymbol{Ri}$ defined as

$$\boldsymbol{Ri} = \frac{\boldsymbol{g\beta}\left(\boldsymbol{T_{hot} - T_{ref}}\right)\boldsymbol{L}}{\boldsymbol{v^2}} = \frac{\boldsymbol{Gr}}{\boldsymbol{Re^2}}$$

Typically, the natural convection is negligible when < 0.1 , forced convection is negligible when $\boldsymbol{Ri} > 10$, and neither is negligible when $\boldsymbol{0.1} < Ri < 10$. Usually the forced convection is large relative to natural convection except in the case of extremely low forced flow velocities.

1.6.4 Prandtl Number, *Pr*

The relative thickness of the velocity and the thermal boundary layers is best described by the dimensionless parameter Prandtl number, defined as

$$\boldsymbol{Pr} = \frac{\boldsymbol{Kinematic\ Viscosity}}{\boldsymbol{Thermal\ Diffusivity}} = \frac{\boldsymbol{\nu}}{\boldsymbol{\alpha}} = \frac{\boldsymbol{\mu C_p}}{\boldsymbol{k}}$$

Where:

$\boldsymbol{\nu}$ is the kinematic viscosity of the fluid ($\boldsymbol{\nu} = \frac{\mu}{\rho}$) ($\boldsymbol{m^2/s}$)

$\boldsymbol{k}$ is the thermal conductivity of the fluid ($\boldsymbol{Wm^{-1}K^{-1}}$)

$\boldsymbol{C_p}$ is the specific heat of the fluid ($\boldsymbol{JKg^{-1}K^{-1}}$)

$\boldsymbol{\alpha}$ is the thermal diffusivity of the fluid $\left(\boldsymbol{\alpha} = \frac{k}{\rho C_p}\right)$ ($\boldsymbol{m^2/s}$)

It is named after Ludwig Prandtl, who introduced the concept of boundary layer in 1904 and made significant contributes to boundary layer theory. The Prandtl numbers of fluids range from less than 0.01 for liquid metals to more than 100,000 for heavy oils. Note that, the Prandtl numbers of gases are about 1, which indicates that both momentum and heat dissipate

through the fluid at about the same rate. Consequently the thermal boundary layer is much thicker for liquid metals and much thinner for oils relative to the velocity boundary layer.

1.6.5 Hartmann Number, *Ha*

Hartmann number is the ratio of electromagnetic force to the viscous force first introduces by Hartmann. It is defined by

$$\boldsymbol{Ha = \frac{Electromagnetic\ Force}{Viscous\ Force} = B_0 L \sqrt{\frac{\sigma}{\mu}}}$$

Where:

$\boldsymbol{B_0}$ is the magnetic field ($\boldsymbol{Nm^{-1}A^{-1}}$)

$\boldsymbol{L}$ is the characteristic length scale

$\boldsymbol{\sigma}$ is the electrical conductivity ($\boldsymbol{\Omega m}$)

$\boldsymbol{\mu}$ is the viscosity

In addition, it is a dimensionless quantity characterizing flow of conducting fluid in a transverse magnetic field, being the product of the magnetic flux density, a representative length and square root of the ratio of electrical conductivity to viscosity.

1.6.6 Lewis Number, *Le*

Lewis number (Le) is a dimensionless number defined as the ratio of thermal diffusivity to mass diffusivity. It is used to characterize fluid flows where there is simultaneous heat and mass transfer by convection and defined as:

$$\boldsymbol{Le = \frac{\alpha}{D}}$$

where $\boldsymbol{\alpha}$ is the thermal diffusivity and $\boldsymbol{D}$ is the mass diffusivity.

The Lewis number can also be expressed in terms of the Prandtl number and the Schmidt number:

$$\boldsymbol{Le = \frac{Pr}{Sc}}$$

It is named after Warren K. Lewis (1882–1975) who was the first head of the Chemical Engineering Department at MIT. Some workers in the field of combustion assume

(incorrectly) that the Lewis number was named for Bernard Lewis (1899–1993), who for many years was a major figure in the field of combustion research.

1.6.7 Sherwood Number, *Sh*

The Sherwood number (also called the mass transfer Nusselt number) is a dimensionless number used in mass-transfer operation. It represents the ratio of the total rate of mass transfer to the rate of diffusive mass transport alone and is named in honor of Thomas Kilgore Sherwood. It is defined as

$$\boldsymbol{Sh = \frac{KL}{D} = \frac{Convective\ mass\ transfer\ coefficient}{Diffusive\ mass\ transfer\ coefficient}}$$

Where

L is a characteristic length ($\boldsymbol{m}$)

D is mass diffusivity ($\boldsymbol{m^2 s^{-1}}$)

K is the mass transfer coefficient ($\boldsymbol{ms^{-1}}$)

1.7 Main Objective of the work

The aim of the proposed study is to present the effect of MHD mixed convection flow around a heated obstacle placed in a lid driven rectangular cavity with two semi-circular wall heater. Results will be presented for non-dimensional governing and physical parameters in terms of streamlines, isotherms and average heat transfer rate along the semi-circular wall heater.

The specific objectives of the present research work are:

- To prepare the mathematical model regarding the effects of MHD mixed convection flow around a heated obstacle placed in a lid driven rectangular cavity with two semi-circular wall heater.
- To solve the model equations using finite element method.
- To investigate the effects of Richardson number *Ri*, Hartmann number *Ha* and Buoyancy ratio *Br*.
- To investigate the effects of the size of the heated obstacle on the flow field and temperature distribution.
- To present the numerical results graphically for different values of the relevant physical parameters along the wall heater used in the model.
- To compare the results with other published works.

1.8 Outline of the thesis

The discussion contains six chapters. The thesis is concerned with the analysis of the effects on heat flow for MHD mixed convection with lid driven rectangular cavity. There are many cavity configurations for the study of combined effect of natural and forced convection flow. In this study we have considered a rectangular cavity containing a centered heated (trapezoidal or rectangular) obstacle.

In chapter 1, a general framework for the description of convective heat transfers has been presented and discussed their properties, also relevant discussion on dimensionless parameters. In this chapter, a brief introduction is presented with aim and objective and also inspiration behind the selection of current work.

In this chapter 2, a brief discussion of literature review of the past studies on fluid flow and heat transfer in cavities or channels is presented. In this state-of-the art review, different aspects of the previous studies have been mentioned categorically

In Chapter 3, the computational techniques of the problem for viscous incompressible flow have been discussed.

in Chapter 4, Mathematical modeling of the problem for uniform heating have been discussed.

In Chapter 5, Numerical analysis and comparison with others work have been discussed.

In Chapter 6, results of the relevant parametric study have been performed.

Finally, in conclusion part, the main achievements have been summarized.

CHAPTER 2

LITERATURE REVIEW

Numerous transport processes survive in nature have industrial applications in which the heat and mass transfer occur concurrently as a result of combines buoyancy effects of thermal and species diffusion. Analysis of mixed convection usually induced in closed cavities or channels containing heating elements in the middle or wall heater are important from both theoretical and practical points of view. The fundamental problem of mixed convection in cavity has received considerable attention from researchers. Most of the cavities commonly used in industries are cylindrical, rectangular, trapezoidal and triangular etc. rectangular cavities have received a considerable attention for its application in various fields. Many numerical investigations on mixed convection in different types of cavities have been investigated in the recent years.

Magnetohydrodynamics (MHD) is the academic discipline which studies the dynamic of electrically conducting fluids. Examples of such fluids include plasmas, liquid metals and salt water. The MHD was originally applied to astrophysical and geophysical problems, where it is still very important. Engineers employ MHD principles in the design of heat exchanger, pumps and flow meters, in space vehicle propulsion, control and re-entry in creating novel power generating systems and developing confinement schemes for controlled fusion.

Mixed convection flow in channels, ducts and cavities may occur in many applications, such as in heat exchangers, ventilation of rooms, double glazing, nuclear reactor insulation, solar energy collection, chemical processing equipment, microelectronic cooling, crystal growth in liquids, to name just a few of these applications studied by Aydin et al (1999). Obstacle or partition is used to enhance heat transfer in cavities. There are many studies on natural convection and mixed convection in an obstructed cavity in the literatures. House et al. (1990) studied natural convection in a vertical square cavity with heat conducting body. Dong and Li (2004) performed the conjugate effect of natural convection and conduction in a complicated enclosure. Öztop et al. (2009) studied fluid flow due to combined convection in

lid-driven enclosure having a circular body. They found that the most effective parameter on the flow field and temperature distribution is the orientation of moving lid. Moallemi et al. (1992) studied Prandtl number effect on laminar mixed convection heat transfer in a lid driven cavity. Hasanuzzaman et al (2012) studied magnetohydrodynamic natural convection in trapezoidal cavities. They discuss the effect of magnetic field on natural convection heat transfer in trapezoidal enclosure with different inclination angles. It is found that heat transfer decreased by 20.70% and 16.15% as φ increases from 0 to 60 at Ra=$\mathbf{10^5}$and $\mathbf{10^6}$ respectively. On the other hand, heat transfer decreased by 20.28% and 13.42% as Ha increases from 0 to 50 for Ra=$\mathbf{10^5}$and $\mathbf{10^6}$respectively. Rahman et al (2012) studied computational analysis of mixed convection in a channel with a cavity heated from different sides. They found that highest heat transfer is obtained when the isothermal heater is located at the right vertical wall. Basak et al (2009) analyzed finite element simulation of natural convection within porous trapezoidal enclosures for various inclination angles: effect of various wall heating. K. Khanafer and S.M. Aithal (2013) studied laminar mixed convection flow and heat transfer characteristics in a lid driven cavity with a circular cylinder. Results obtained in this study indicate that placing the cylinder near the bottom wall increased the maximum average Nusselt number while moving the cylinder near the top wall resulted in the lowest average Nusselt number on the bottom wall. Rahman et al (2011) studied conjugated effect of joule heating and magneto-hydrodynamic on double-diffusive mixed convection in a horizontal channel with an open cavity. The result shows that the aforesaid parameters have noticeable effect on the flow pattern and heat and mass transfer. Y. Varol et al (2006) analyzed natural convection in a triangle enclosure with flush mounted heater on the wall. They observed that the most important parameter on heat transfer and flow field is the position of heater which can be a control parameter in the above system. Billah et al (2011) studied numerical analysis of fluid flow due to mixed convection in a lid-driven cavity having a heated circular hollow cylinder. They found that the flow field and temperature distribution strongly depend on the cylinder diameter and also the solid–fluid thermal conductivity ratio at the three convective regimes. Teamah (2008) analyzed numerical simulation of double diffusive natural convection in rectangular enclosure in the presences of magnetic field and heat source. S. Sivasankaran (2011) studied hydro-magnetic combined convection in a lid-driven cavity with sinusoidal boundary conditions on both sidewalls. They found that the flow behavior and heat transfer rate inside the cavity are strongly affected by the presence of the magnetic field. Al-Salem et al (2011) studied effects of moving lid direction on MHD

mixed convection in a linearly heated cavity. They found that direction of lid is more effective on heat transfer and fluid flow in the case of mixed convection than it is the case in forced convection. Heat transfer is also decreased with increasing of magnetic field for all studied parameters. Nithyadevi (2009) studied double diffusive natural convection in a partially heated enclosure with Soret and Dufour effects. Oztop et al (2011) analyzed MHD mixed convection in a lid-driven cavity with corner heater. A.W. Islam et al (2012) studied mixed convection in a lid driven square cavity with an isothermally heated square blockage inside. From the analysis of the mixed convection process, it is found that for any size of the blockage placed anywhere in the cavity, the average Nusselt number does not change significantly with increasing Richardson number until it approaches the value of the order of 1 beyond which the average Nusselt number increases rapidly with the Richardson number. The most preferable heat transfer is obtained when the blockage is placed around the top left and the bottom right corners of the cavity. Basak et al (2009) analyzed the mixed convection flows within a square cavity with linearly heated side walls. A detailed analysis of flow pattern shows that as the value of $\boldsymbol{Re}$ increases from 1 to $\mathbf{10^2}$, there occurs a transition from natural convection to forced convection depending on the value of $\boldsymbol{Gr}$ irrespective of $\boldsymbol{Pr}$. Nasrin et al (2012) studied combined convection flow in triangular wavy chamber filled with water–CuO nanofluid: Effect of viscosity models. Ching et al (2012) studied finite element simulation of mixed convection heat and mass transfer in a right triangular enclosure. They found that the increase of buoyancy ratio enhances the heat and mass transfer rate for all values of Richardson number and for each direction of the sliding wall motion. Bhuiyan et al (2014) studied combined effect of Hartmann and Rayleigh numbers on free convective flow in a square cavity with different positions of heated elliptic obstacle. They investigated if the Hartman number increases, the local Nusselt number decreases for bottom left configuration, but changes randomly for top right configuration. Rahman et al (2011) studied Magnetohydrodynamic mixed convection in a horizontal channel with an open cavity. The results indicate that the mentioned parameters in this paper strongly affect the flow phenomenon and temperature field inside the cavity whereas in the channel these effects are less significant. Hossain and Alim (2014) investigated MHD free convection within trapezoidal cavity with non-uniformly heated bottom wall. They found that the average and local Nusselt number at the non-uniform heating of bottom wall of the cavity is depending on the dimensionless parameters and also tilts angles. Parvin and Hossain (2012) studied finite element simulation of MHD combined convection through a triangular wavy channel. The

study reveals that the flow as well as thermal field strongly depends on the aforesaid parameters. Al-Amiri et al (2007) studied effect of sinusoidal wavy bottom surface on mixed convection heat transfer in a lid-driven cavity. The results of this investigation illustrate that the average Nusselt number increases with an increase in both the amplitude of the wavy surface and Reynolds number. Rahman et al [27] studied natural convection effects on heat and mass transfer in a curvilinear triangular cavity. They found that average Nusselt and Sherwood numbers increase as Br increases. Also, average Nusselt decreases and Sherwood numbers increases as Le increases. Serrano-Arellano et al (2014) studied numerical investigation of transient heat and mass transfer by natural convection in a ventilated cavity: outlet air gap located close to heat source. Rahman et al (2010) studied numerical study on the conjugate effect of joule heating and magnato-hydrodynamics mixed convection in an obstructed lid-driven square cavity. They also found that the parameters ***Ha*** and ***J*** have notable effect on flow fields, temperature distributions and heat transfer in the cavity. Ray and Chatterjee (2014) investigated MHD mixed convection in a lid-driven cavity including heat conducting circular solid object and corner heaters with Joule heating. The result indicates a major influence of the prevailing convection method and the applied magnetic field on the flow as well as the thermal field, while the effect of Joule heating is found to be of very small significance. Öztop et al (2012) studied MHD natural convection in an enclosure from two semi-circular heaters on the bottom wall. They found that the distance between the semi-circular heaters is the most important parameter affecting the heat and fluid flow fields. Rahman et al (2011) studied MHD mixed convection with joule heating effect in a lid-driven cavity with a heated semi-circular source using finite element technique. Chandra and Chhabra (2011) studied flow over and forced convection heat transfer in Newtonian fluids from a semi-circular cylinder. Khalil Khanafer (2014) studied comparison of flow and heat transfer characteristics in a lid-driven cavity between flexible and modified geometry of a heated bottom wall. This investigation shows the benefits of using flexible walls when augmentation of heat transfer is sought at high Grashof numbers. M. Hasanuzzaman et al (2012) investigated effects of Lewis number on heat and mass transfer in a triangular cavity. They found that heat transfer decreased as Le increases. On the other hand, mass transfer rate increased as Le increases. S. Sivasankaran et al (2010) studied numerical study on mixed convection in a lid-driven cavity with non-uniform heating on both sidewalls. The results show that heat transfer rate is increased on increasing amplitude ratio. A. Koca et al (2007)

studied the effects of Prandtl number on natural convection in triangular enclosures with localized heating from below.

CHAPTER 3

COMPUTATIONAL TECHNIQUE

3.1 Computational Technique

Computational fluid dynamics (CFD) has been rapidly gaining popularity over the past several years for technological as well as scientific interests. For many problems of industrial interest, experimental techniques are extremely expensive or even impossible due to the complex nature of the flow configuration. Analytical methods are often useful in studying the basic physics involved in a certain flow problem, however, in many interesting problems; these methods have limited direct applicability. The dramatic increase in computational power over the past several years has led to a heightened interest in numerical simulations as a cost effective method of providing additional flow information, not readily available from experiments, for industrial applications, as well as a complementary tool in the investigation of the fundamental physics of turbulent flows, where analytical solutions have so far been unattainable. It is not expected (or advocated), however, that numerical simulations replace theory or experiment, but that they be used in conjunction with these other methods to provide a more complete understanding of the physical problem at hand.

Mathematical model of physical phenomena may be ordinary or partial differential equations, which have been the subject of analytical and numerical investigations. The partial differential equations of fluid mechanics and heat transfer are solvable for only a limited number of flows. To obtain an approximate solution numerically, we have to use a discretization method, which approximated the differential equations by a system of algebraic equations, which can then be solved on a computer. The approximations are applied to small domains in space and / or time so the numerical solution provides results at discrete locations in space and time. Much as the accuracy of experimental data depends on the quality of the tools used, the accuracy of numerical solutions depend on the quality of discretizations used .Computational fluid dynamics (CFD) computation involves the formation of a set numbers that constitutes a practical approximation of a real life system. The outcome of computation

process improves the understanding of the performance of a system. Thereby, engineers need CFD codes that can make physically realistic results with good quality accuracy in simulations with finite grids. Contained within the broad field of computational fluid dynamics are activities that cover the range from the automation of well established engineering design methods to the use of detailed solutions of the Navier-Stokes equations as substitutes for experimental research into the nature of complex flows. CFD have been used for solving wide range of fluid dynamics problem. It is more frequently used in fields of engineering where the geometry is complicated or some important feature that cannot be dealt with standard methods.

3.1.1 Merits and Demerits of Numerical Method

As computational power grows, the need for more advanced numerical algorithms also increases. There are many different techniques for constructing numerical solutions of fluid flow problems, e.g. finite difference methods(FD), finite volume methods (FV), and finite element methods(FE), to name a few, and all have their strengths and weaknesses. Since the goal of the present research lies in the development of methods which may ultimately be used for large-scale applications of industrial interest, finite element methods have been chosen, given their accuracy as well as their ability to approximate arbitrarily complex geometric configurations. The finite element method applied to fluid dynamics has reached level of maturity over the past two decades such that it is now being successfully applied to industrial strength problems including turbulent flows.

Finite element method is an ideal numerical approach for solving a system of partial differential equations. The finite element method produces equations for each element independently of all other elements. Only when the equations are collected together and assembled into a global matrix are the interactions between elements taken into account. Despite these ideal characteristics, the finite element method dominates in most of the computational fluid dynamics. The present research is an attempt to bring the FE technique again into light through a novel formulation of two dimensional incompressible thermal flow problems. As the formulation establishes a priority of finite element technique over the FD and FV method, the philosophy and approach of the three methods are recapitulated here in brief. The finite difference method relies on the philosophy that the body is in one single piece but the parameters are evaluated only at some selected points within the body, satisfying the governing differential equations approximately, where as the finite volume

method relies on the philosophy that the body is divided into a finite number of control volumes, On the other hand, in the finite element method, the body is divided into a number of elements. The Finite element method works when all other methods fail and it's managing complex geometrical bodies and boundaries. There are many commercial packages such as ANSYS, MATLAB and COMSOL MULTIPHYSICS for computing practical problems. The demerits of this method, it considers the body is not in one piece, but it is an assemblage of elements connected only at nodes and Finite element solution is highly dependent on the element type.

Accurate and reliable prediction of complex geometry is of great importance to meet the severe demand of greater reliability as well as economic challenge. It is noted that these complex geometries occurs most frequently in CFD. Presented methods have a common feature: they generate equations for the values of the unknown functions at a finite number of points in the computational domain. But there are also several differences. The finite difference and the finite volume methods generate numerical equations at the reference point based on the values at neighboring points. The finite element method takes care of boundary conditions of Neumann type while the other two methods can easily apply to the Dirichlet conditions. The finite difference method could be easily extended to multidimensional spatial domains if the chosen grid is regular (the cells must look cuboids, in a topological sense). The grid indexing is simple but some difficulties appear for the domain with a complex geometry. For the finite element method there are no restrictions on the connection of the elements when the sides (or faces) of the elements are correctly aligned and have the same nodes for the neighboring elements. This flexibility allows us to model a very complex geometry. The finite volume method could also use irregular grids like the grids for the finite element methods, but keeps the simplicity of writing the equations like that for the finite difference method. Of course, the presence of a complex geometry slows down the computational programs. Another benefit of the finite element method is that of the specific mode to deduce the equations for each element that are then assembled. Therefore, the addition of new elements by refinement of the existing ones is not a major problem. For the other methods, the mesh refinement is a major task and could involve the rewriting of the program. But for all the methods used for the discrete analogue of the initial equation, the obtained system of simultaneous equations must be solved. That is why, the present work emphasizes the use of finite element techniques to solve flow and heat transfer problems. The details of this method are explained in the following section.

3.2 Elements of Numerical Solution Methods

Several components of numerical solution methods are available in Ferziger and Perić (1997), here only the main steps will be demonstrate in the following.

3.2.1 Mathematical Model

The starting point of any numerical method is the mathematical model, i.e. the set of partial differential equations and boundary conditions. A solution method is usually designed for a particular set of equations. Trying to produce a general-purpose solution method, i.e. one which is applicable to all flows, is impractical, is not impossible and as with most general purpose tools, they are usually not optimum for any one application.

3.2.2 Discretization Process

After selecting the mathematical model, one has to choose a suitable discretization method, i.e. a method of approximating the differential equations by a system of algebraic equations for the variable at some set of discrete locations in space and time.

3.2.3 Numerical Grid

The numerical grid defines the discrete locations, at which the variables are to be calculated, which is essentially a discrete representation of the geometric domain on which the problem is to be solved. It divided the solution domain into a finite number of sub-domains (elements, control volumes etc). Some of the options available are structural (regular) grid, block structured grid, unstructured grids etc.

3.2.4 Finite Approximations

Following the choice of grid type, one has to select the approximations to be used in the discretization process. In a finite difference method, approximations for the derivatives at the grid points have to be selected. In a finite volume method, one has to select the methods of approximating surface and volume integrals. In a finite element method, one has to choose the functions and weighting functions.

3.2.5 Solution Technique

Discretization yields a large system of non-linear algebraic equations. The method of solution depends on the problem. For unsteady flows, methods based on those used for initial value

problems for ordinary differential equation (marching in time) is used. At each time step an elliptic problem has to be solved. Pseudo-time marching or an equivalent iteration scheme usually solves steady flow problems. Since the equations are non-linear, an iteration scheme is used to solve them. These methods use successive linearization of the equations and the resulting linear systems are almost always solved by iterative techniques. The choice of solver depends on the grid type and the number of nodes involved in each algebraic equation.

3.3 Discretization Approaches

The first step to numerically solve a mathematical model of physical phenomena is its numerical discretization. This means that each component of the differential equations is transformed into a "numerical analogue" which can be represented in the computer and then processed by a computer program, built on some algorithm. There are several discritization methods available for the high performance numerical computation in CFD.

- Finite difference method (FDM)
- Finite volume method (FVM)
- Finite element method (FEM)
- Boundary element method (BEM)
- Boundary volume method (BVM)

In the present numerical computation, Galerkin finite element method (FEM), George R. Buchanan, Finite Element Analysis, Schaum's Outline Series, McGraw-Hill, 1995 has been used.

3.4 Finite Element Method

The finite element method (FEM) is a powerful computational technique for solving problems which are described by partial differential equations or can be formulated as functional minimization. The basic idea of the finite element method is to view a given domain as an assemblage of simple geometric shapes, called finite elements, for which it is possible to systematically generate the approximation functions needed in the solution of partial differential equations by the variation or weighted residual method. The computational domains with irregular geometries by a collection of finite elements makes the method a valuable practical tool for the solution of boundary, initial and Eigen value problems arising in various fields of engineering. The approximation functions, which satisfy the governing equations and boundary conditions, are often constructed using ideas from interpolation

theory. Approximating functions in finite elements are determined in terms of nodal values of a physical field which is sought. A continuous physical problem is transformed into a discretized finite element problem with unknown nodal values. For a linear problem, a system of linear algebraic equations should be solved. Values inside finite elements can be recovered using nodal values. The major steps involved in finite element analysis of a typical problem are:

- Discretization of the domain into a set of finite elements (mesh generation).
- Weighted-integral or weak formulation of the differential equation to be analyzed.
- Development of the finite element model of the problem using its weighted-integral or weak form.
- Assembly of finite elements to obtain the global system of algebraic equations.
- Imposition of boundary conditions.
- Solution of equations.
- Post-computation of solution and quantities of interest.

3.4.1 MESH GENERATION

In finite element method, the mesh generation is the technique to subdivide a domain into a set of subdomains, called finite elements. Figure 3.1 shows a domain, is subdivided into a set of subdomains, with boundary .

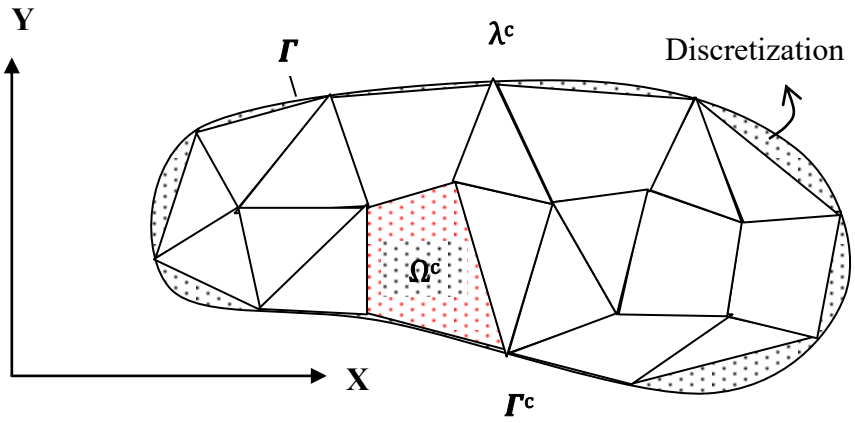

Figure 3.1: Finite element discretization of a domain

The present numerical technique will discretize the computational domain into unstructured triangles by Delaunay Triangular method. The Delaunay triangulation is a geometric structure

that has enjoyed great popularity in mesh generation since the mesh generation was in its infancy. In two dimensions, the Delaunay triangulation of a vertex set maximizes the minimum angle among all possible triangulations of that vertex set. Figure 3.2 shows the mesh mode for the present numerical computation. Mesh generation has been done meticulously

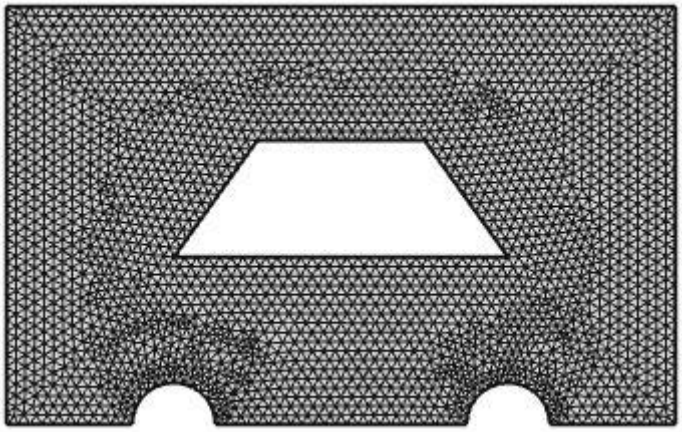

Figure 3.2 (a) Current mesh structure of elements for rectangular enclosure with trapezoidal obstacle area 0.042.

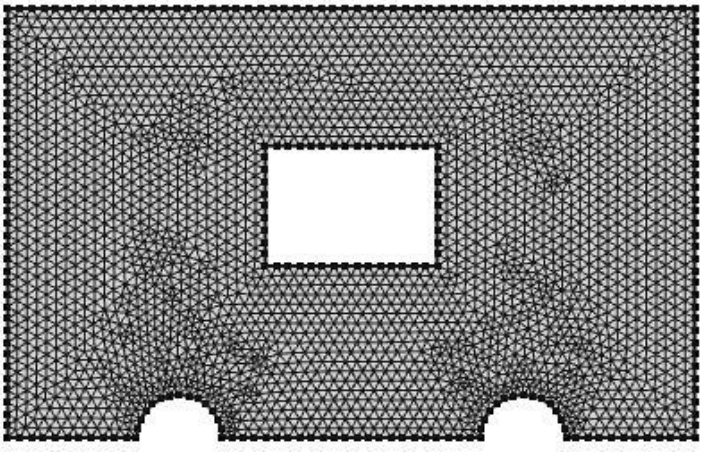

Figure 3.2 (b) Current mesh structure of elements for rectangular enclosure with rectangular obstacle area 0.028.

3.4.2 Finite Element Formulation and Computational Technique

Viscous incompressible thermal flows have been the subject of our investigation. The problem is relatively complex due to the coupling between the energy equation and the Navier-Stokes equations, which govern the fluid motion. These equations comprise a set of coupled nonlinear partial differential equations, which is difficult to solve especially with

complicated geometries and boundary conditions. The finite element formulation and computational procedure for Navier-Stokes equations along with energy equation and mass equation will be discuss in chapter 4 and chapter 5.

3.5 Algorithm

The algorithm was originally put forward by the iterative Newton-Raphson algorithm; the discrete forms of the continuity, momentum and energy equations are solved to find out the value of the velocity and the temperature. It is essential to guess the initial values of the variables. Then the numerical solutions of the variables are obtained while the convergent criterion is fulfilled. The simple algorithm is shown by the flow chart below.

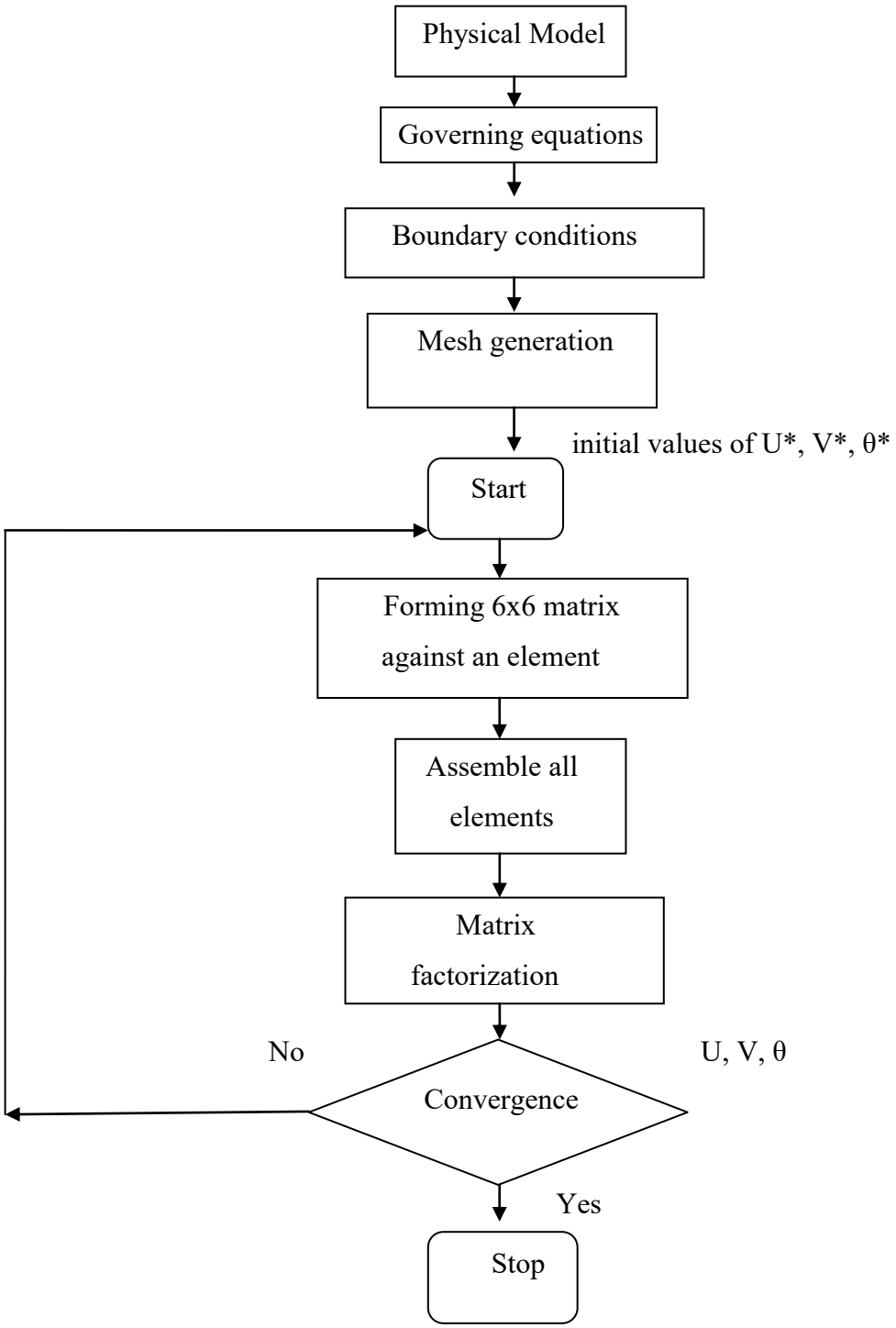

Figure 3.3: Flow chart of the computational procedure

3.5.1 Solution of System of Equations

A system of linear algebraic equations has been solved by the UMFPACK with MATLAB interface. UMFPACK is a set of routines for solving asymmetric sparse linear systems Ax = b, using the Asymmetric Multi Frontal method and direct sparse LU factorization. Five primary UMFPACK routines are required to factorize A or Ax = b:

- Pre-orders the columns of A to reduce fill-in and performs a symbolic analysis.
- Numerically scales and then factorizes a sparse matrix.
- Solves a sparse linear system using the numeric factorization.
- Frees the Symbolic object.
- Frees the Numeric object.

Additional routines are:

- Passing a different column ordering
- Changing default parameters
- Manipulating sparse matrices
- Getting LU factors
- Solving the LU factors
- Computing determinant

UMFPACK factorizes PAQ, PRAQ, or PR−1AQ into the product LU, where L and U are lower and upper triangular, respectively, P and Q are permutation matrices, and R is a diagonal matrix of row scaling factors (or R = I if row-scaling is not used). Both P and Q are chosen to reduce fill-in (new nonzeros in L and U that are not present in A). The permutation P has the dual role of reducing fill-in and maintaining numerical accuracy (via relaxed partial pivoting and row interchanges). The sparse matrix A can be square or rectangular, singular or non-singular, and real or complex (or any combination). Only square matrices A can be used to solve Ax = b or related systems. Rectangular matrices can only be factorized. UMFPACK first finds a column pre-ordering that reduces fill-in, without regard to numerical values. It scales and analyzes the matrix, and then automatically selects one of three strategies for pre-

ordering the rows and columns: asymmetric, 2-by-2 and symmetric. These strategies are described below.

One notable attribute of the UMFPACK is that whenever a matrix is factored, the factorization is stored as a part of the original matrix so that further operations on the matrix can reuse this factorization. Whenever a factorization or decomposition is calculated, it is preserved as a list (element) in the factor slot of the original object. In this way a sequence of operations, such as determining the condition number of a matrix and then solving a linear system based on the matrix, do not require multiple factorizations of the intermediate results.

Conceptually, the simplest representation of a sparse matrix is as a triplet of an integer vector i giving the row numbers, an integer vector j giving the column numbers, and a numeric vector x giving the non-zero values in the matrix. The triplet representation is row-oriented if elements in the same row were adjacent and column-oriented if elements in the same column were adjacent. The compressed sparse row (csr) or compressed sparse column (csc) representation is similar to row-oriented triplet or column-oriented triplet respectively. These compressed representations remove the redundant row or column in indices and provide faster access to a given location in the matrix.

3.6 Chapter Summary

This chapter has presented a tutorial introduction to computational method with advantages of numerical investigation, because numerical method has played a central role in this thesis. Various components of numerical method have been also explained. Finally, the major steps involved in finite element analysis of a typical problem have been discussed.

CHAPTER 4

MATHEMATICAL MODELING OF THE PROBLEM

4.1 Mathematical Modeling

The starting point of any numerical method is the mathematical model, i.e. the set of partial differential equations and boundary conditions. A solution method is usually designed for a particular set of equations. Trying to produce a general-purpose solution method, i.e. one which is applicable to all flows, is impractical, is not impossible and as with most general purpose tools, they are usually not optimum for any one application.

The generalized governing equations are based on the conservation laws of mass, momentum and energy. As the heat transfer depends upon a number of factors, a dimensional analysis is presented to show the important non-dimensional parameters which will influence the dimensionless heat transfer parameter, i.e. Nusselt number.

4.2 Physical model

The physical model is shown in Fig. 4.1,along with the important geometric parameters. A rectangular cavity of height *H* and wide *L* containing different shapes of obstacle (trapezoidal or rectangular) whose areas are *A=0.042* and *A=0.028* considered. Two semi-circular wall heaters are constructed at the bottom wall. The obstacle and the two semi-circular wall are maintained at higher temperature and higher concentrated than the two vertical walls. The upper wall and the bottom wall except two semi-circular walls are kept adiabatic. The upper horizontal wall is moving with a uniform velocity by unity and the other walls are at no slip condition. The left and right vertical walls are subjected to low temperature $\boldsymbol{T_L}$ and low concentration $\boldsymbol{C_L}$, two semi-circular wall and the obstacle area are subjected to high temperature $\boldsymbol{T_H}$ and high concentration $\boldsymbol{C_H}$. The heat transfer and fluid temperature will be illustrated for commonly used fluids with $\boldsymbol{Pr = 7}$. Hartmann number are considered $\boldsymbol{Ha = 0}$ to $\boldsymbol{Ha = 150}$ to analyze the effect of magnetic field. The fluid is considered incompressible, Newtonian and the flow is assumed to be laminar. The boundary conditions for velocity are considered as no slip on solid boundaries except the upper wall.

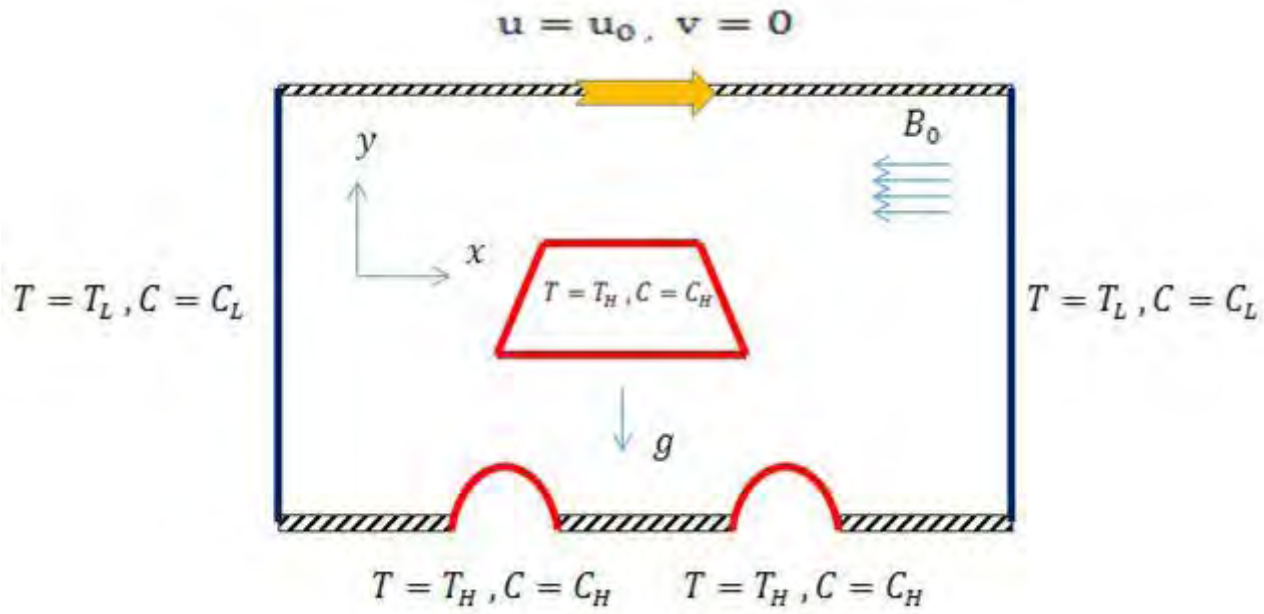

Figure 4.1 (a): Schematic diagram of the cavity with trapezoidal obstacle Area = 0.042

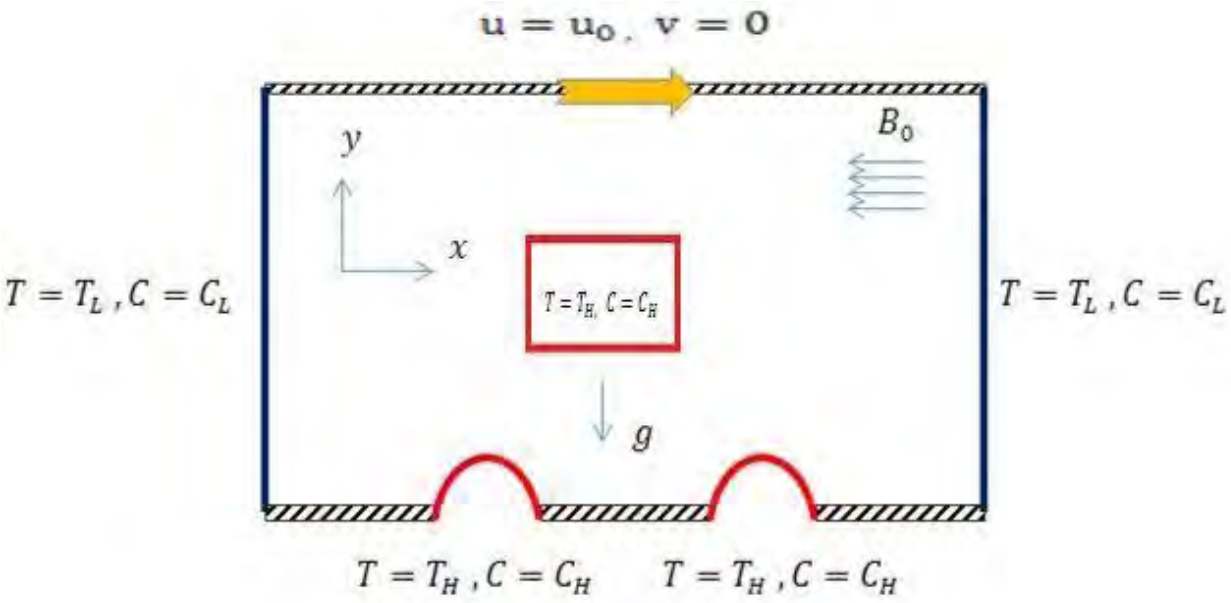

Figure 4.1 (b): Schematic diagram of the cavity with rectangular obstacle Area = 0.028

4.3 Mathematical Formulation

The several steps of the mathematical formulation for the above physical configurations are shown as follows.

4.3.1 Governing Equations

The fundamental laws which are used to solve the fluid flow and heat transfer problems, are the conservation of mass (continuity equation), conservation of momentum (momentum equations), conservation of energy (energy equation) and conservation of mass (mass equation) and constitute a set of coupled, nonlinear, partial differential equations. The viscous dissipation term in the energy equation is neglected. For the treatment of the buoyancy term in the momentum equation, Boussinesq approximation is employed to account for the variations of density as a function of temperature, and to couple in this way the temperature field to the flow field. Also for laminar incompressible thermal flow, the buoyancy force is included here as a body force in the v-momentum equation. The governing equations for steady mixed convection flow can be written as:

Continuity Equation

$$\frac{\partial u}{\partial x} + \frac{\partial v}{\partial y} = 0 \tag{4.1}$$

Momentum Equations

$$\rho \left(u \frac{\partial u}{\partial x} + v \frac{\partial u}{\partial y} \right) = -\frac{\partial p}{\partial x} + \mu \left(\frac{\partial^2 u}{\partial x^2} + \frac{\partial^2 u}{\partial y^2} \right) \tag{4.2}$$

$$\rho \left(u \frac{\partial v}{\partial x} + v \frac{\partial v}{\partial y} \right) = -\frac{\partial p}{\partial y} + \mu \left(\frac{\partial^2 v}{\partial x^2} + \frac{\partial^2 v}{\partial y^2} \right) + \rho g \beta_T (T - T_L) + \rho g \beta_C (C - C_L) - \sigma {B_0}^2 v \tag{4.3}$$

Energy Equation

$$\left(u \frac{\partial T}{\partial x} + v \frac{\partial T}{\partial y} \right) = \alpha \left(\frac{\partial^2 T}{\partial x^2} + \frac{\partial^2 T}{\partial y^2} \right) \tag{4.4}$$

Mass Equation

$$\left(u \frac{\partial C}{\partial x} + v \frac{\partial C}{\partial y} \right) = D \left(\frac{\partial^2 C}{\partial x^2} + \frac{\partial^2 C}{\partial y^2} \right) \tag{4.5}$$

where x and y are the distances measured along the horizontal and vertical directions respectively; u and v are the velocity components in the x and y directions respectively; T

denote the fluid temperature, $\boldsymbol{C}$ denotes the concentration, $\boldsymbol{T_L}$ and $\boldsymbol{C_L}$ denotes the low temperature and concentration respectively, $\boldsymbol{p}$ is the pressure and $\boldsymbol{\rho}$ is the fluid density, $\boldsymbol{g}$ is the gravitational constant, $\boldsymbol{\beta}$ is the volumetric coefficient of thermal expansion, $\boldsymbol{\alpha}$ denotes the thermal conductivity and $\boldsymbol{D}$ denotes the mass diffusivity.

4.3.2 Boundary Conditions

The boundary conditions for the present problem are specified as follows:

At the left and right wall:

$$\boldsymbol{u(0,y) = v(0,y) = 0,\ T = T_L,\ C = C_L} \qquad \forall \quad \boldsymbol{0 \le y \le H} \tag{4.6}$$

At the upper wall:

$$\boldsymbol{u(x,0) = u_0,\ \ v(x,0) = 0,\ \ \frac{\partial}{\partial y}\left(\frac{T-T_L}{T_H-T_L}\right) = 0} \qquad \forall \quad \boldsymbol{y = H} \tag{4.7}$$

On the middle obstacle and semi-circular wall obstacle,

$$\boldsymbol{u(x,y) = 0,\ \ v(x,y) = 0,\ \ T = T_H, C = C_H} \qquad \forall \quad \boldsymbol{0 \le x \le L, 0 \le y \le H} \tag{4.8}$$

At the bottom wall without semi-circular wall heater,

$$\boldsymbol{u(x,0) = 0,\ \ v(x,0) = 0,\ \ \frac{\partial}{\partial y}\left(\frac{T-T_L}{T_H-T_L}\right) = 0} \qquad \forall \quad \boldsymbol{y = 0} \tag{4.9}$$

where $\boldsymbol{x}$ and $\boldsymbol{y}$ are the distances measured along the horizontal and vertical directions, respectively; u and v are the velocity components in the $\boldsymbol{x}$ and $\boldsymbol{y}$-direction, respectively; $\boldsymbol{H = 0.5}$ is the height and $\boldsymbol{L = 0.8}$ is the width of the rectangular cavity with middle obstacle with area $\boldsymbol{A = 0.042}$ and $\boldsymbol{0.028}$; $\boldsymbol{T}$ denotes the temperature; $\boldsymbol{T_H}$ and $\boldsymbol{T_L}$ are heated and cold temperature respectively; $\boldsymbol{C}$ denotes the concentration; $\boldsymbol{C_H}$ and $\boldsymbol{C_L}$ are high and low concentration respectively.

The local Nusselt number at the heated surface of the cavity which is defined by the following expression:

$$\boldsymbol{Nu = \frac{h(x)\,L}{K}}$$

Such local values have been further averaged over the entire heated surface to obtain the surface averaged or overall mean Nusselt number at the bottom, left and right walls are

$$\boldsymbol{Nu = \int_0^L Nu\ dx}$$

Where L and h(x) are the length and the local convection heat transfer coefficient of the heated wall respectively. The average Nusselt number can be used in process engineering design calculations to estimate the rate transfer from the heated surface.

4.3.3 Non-Dimensional Variables

Non-dimensional variables or numbers used for making the governing equations (4.1−4.5) into dimensionless form are stated as follows:

$$X = \frac{x}{L}, Y = \frac{y}{L}, U = \frac{u}{u_0}, V = \frac{v}{u_0}, P = \frac{(p + \rho g y)}{\rho\, {u_0}^2}, \theta = \frac{T - T_L}{T_H - T_L}, C = \frac{C - C_L}{C_H - C_L}, Pr = \frac{\nu}{\alpha},$$

$$Le = \frac{\alpha}{D}, Ri = \frac{g\beta_T (T_H - T_L) L}{{u_0}^2} = \frac{Gr}{Re^2}, Br = \frac{\beta_C (C_H - C_L)}{\beta_T (T_H - T_L)}, Ha^2 = \frac{\sigma\, {B_0}^2 L^2}{\mu}, Re = \frac{L u_0}{\nu},$$

$$\alpha = \frac{k}{\rho C_p}, \nu = \frac{\mu}{\rho}, Gr = \frac{g\beta \Delta T L^3}{\nu^2}$$

Where X and Y are the coordinates varying along horizontal and vertical directions, respectively, U and V are the velocity components in the X and Y directions, respectively, θ is the dimensionless temperature and P is the dimensionless pressure and $\Delta T = T_H - T_L$ is the temperature difference,α thermal diffusivity of the fluid, C and D are the concentration of species and the mass diffusivity respectively.

The dimensionless parameters are the Nusselt number Nu, Prandtl number Pr, Hartmann number Ha, Richardson number Ri, Reynold's number Re, Sherwood number Sh and Lewis number Le.

4.3.4 Non-Dimensional Governing Equations

The non-dimensional governing equations for steady two-dimensional mixed convection flow in the square cavity after substitution the non-dimensional variables or numbers into the equations (4.1-4.5), we get,

Continuity Equation

$$\frac{\partial U}{\partial X} + \frac{\partial V}{\partial Y} = 0 \tag{4.10}$$

Momentum Equations

$$U \frac{\partial U}{\partial X} + V \frac{\partial U}{\partial Y} = -\frac{\partial P}{\partial X} + \frac{1}{Re}\left(\frac{\partial^2 U}{\partial X^2} + \frac{\partial^2 U}{\partial Y^2}\right) \tag{4.11}$$

$$\boldsymbol{U}\ \frac{\partial \boldsymbol{V}}{\partial \boldsymbol{X}} + \boldsymbol{V}\ \frac{\partial \boldsymbol{V}}{\partial \boldsymbol{Y}} = -\frac{\partial \boldsymbol{P}}{\partial \boldsymbol{Y}} + \frac{\mathbf{1}}{\boldsymbol{Re}}\left(\frac{\partial^2 \boldsymbol{V}}{\partial \boldsymbol{X}^2} + \frac{\partial^2 \boldsymbol{V}}{\partial \boldsymbol{Y}^2}\right) + \boldsymbol{Ri}(\boldsymbol{\theta} + \boldsymbol{Br}\ \boldsymbol{C}) - \boldsymbol{Ha}^2\frac{\mathbf{1}}{\boldsymbol{Re}}\ \boldsymbol{V} \quad (4.12)$$

Thermal Energy Equation

$$\boldsymbol{U}\ \frac{\partial \boldsymbol{\theta}}{\partial \boldsymbol{X}} + \boldsymbol{V}\ \frac{\partial \boldsymbol{\theta}}{\partial \boldsymbol{Y}} = \frac{\mathbf{1}}{\boldsymbol{PrRe}}\left(\frac{\partial^2 \boldsymbol{\theta}}{\partial \boldsymbol{X}^2} + \frac{\partial^2 \boldsymbol{\theta}}{\partial \boldsymbol{Y}^2}\right) \quad \textbf{(4.13)}$$

Mass Energy Equation

$$\boldsymbol{U}\ \frac{\partial \boldsymbol{C}}{\partial \boldsymbol{X}} + \boldsymbol{V}\ \frac{\partial \boldsymbol{C}}{\partial \boldsymbol{Y}} = \frac{\mathbf{1}}{\boldsymbol{LePrRe}}\left(\frac{\partial^2 \boldsymbol{C}}{\partial \boldsymbol{X}^2} + \frac{\partial^2 \boldsymbol{C}}{\partial \boldsymbol{Y}^2}\right) \quad (4.14)$$

4.3.5 Non-Dimensional Boundary Conditions

The non- dimensional boundary conditions under consideration can be written as

At the left and right wall

$$U = 0, V = 0, \theta = 0, C = 0 \quad \forall \quad 0 < Y < 1 \quad (4.15)$$

At the upper wall

$$U = 1, V = 0, \ \frac{\partial \theta}{\partial Y} = 0 \quad \forall \quad Y = 1 \quad (4.16)$$

On the middle obstacle and semi-circular wall obstacle

$$U = 0, V = 0, \theta = 1, C = 1 \quad \forall \quad 0 \le X \le 1, \ 0 \le Y \le 1 \quad (4.17)$$

At the bottom wall without semi-circular wall heater

$$U = 0, V = 0, \ \frac{\partial \theta}{\partial Y} = 0 \quad \forall \quad Y = 0 \quad (4.18)$$

The local Nusselt number at the heated surface of the cavity is defined by the following expression:

$$Nu = -\frac{\partial \theta}{\partial n}$$

where n denotes the normal direction on a plane.

The average heat transfer rate evaluated along the heated surface and semi-circular wall heater based on the dimensionless quantities may be expressed respectively as

$\frac{1}{L_s}\int_0^{L_s} Nu\ \ ds$ and $\frac{1}{L}\int_0^{L}\ Nu\ ds$

where L_s and L denotes the arc length of the semi-circular wall heater and length of the heated wall respectively.

4.4 Numerical Solution

The governing equations along with the boundary conditions are solved numerically, employing Galerkin weighted residual finite element techniques discussed below.

4.4.1 Finite Element Formulation

The numerical procedure used to solve the governing equations for the present work is based on the Galerkin weighted residual method of finite-element formulation. The non-linear parametric solution method is chosen to solve the governing equations. This approach will result in substantially fast convergence assurance. A non-uniform triangular mesh arrangement is implemented in the present investigation especially near the walls to capture the rapid changes in the dependent variables.

The velocity and thermal energy equations (4.10)-(4.14) result in a set of non-linear coupled equations for which an iterative scheme is adopted. To ensure convergence of the numerical algorithm the following criteria is applied to all dependent variables over the solution domain

$$\sum \left| {\psi_{ij}}^{n} - {\psi_{ij}}^{n-1} \right| \leq 10^{-5}$$

where ψ represents a dependent variable U, V, P, T and C; the indexes i, j indicate a grid point; and the index n is the current iteration at the grid level. The six node triangular element is used in this work for the development of the finite element equations. All six nodes are associated with velocities as well as temperature; only the corner nodes are associated with pressure. This means that a lower order polynomial is chosen for pressure and which is satisfied through continuity equation. The velocity component and the temperature distributions and linear interpolation for the pressure distribution according to their highest derivative orders in the differential equations (4.10)-(4.14) as

$$U(X,Y) = N_\alpha U_\alpha \tag{4.19}$$

$$V(X,Y) = N_\alpha V_\alpha \tag{4.20}$$

$$\theta(X,Y) = N_\alpha \theta_\alpha \tag{4.21}$$

$$C(X,Y) = N_\alpha C_\alpha \tag{4.22}$$

$$P(X,Y) = H_\lambda \, P_\lambda \tag{4.23}$$

where $\alpha = 1, 2, \ldots \ldots, 6$; $\lambda = 1, 2, 3$; N_α are the element interpolation functions for the velocity components and the temperature, and H_λ are the element interpolation functions for the pressure.

To derive the finite element equations, the method of Weighed Residuals Zienkiewicz (1991), George R. Buchanan, Finite Element Analysis, Schaum's Outline Series, McGraw-Hill, 1995 is applied to the equations (4.10) - (4.14) as

$$\int_A N_\alpha \left(\frac{\partial U}{\partial X} + \frac{\partial V}{\partial Y}\right) dA = 0 \tag{4.24}$$

$$\int_A N_\alpha \left(U \frac{\partial U}{\partial X} + V \frac{\partial U}{\partial Y}\right) = -\int_A H_\lambda \left(\frac{\partial P}{\partial X}\right) dA + \frac{1}{Re} \int_A N_\alpha \left(\frac{\partial^2 U}{\partial X^2} + \frac{\partial^2 U}{\partial Y^2}\right) dA \tag{4.25}$$

$$\int_A N_\alpha \left(U \frac{\partial V}{\partial X} + V \frac{\partial V}{\partial Y}\right) dA = -\int_A H_\lambda \left(\frac{\partial P}{\partial Y}\right) + \frac{1}{Re} \int_A N_\alpha \left(\frac{\partial^2 V}{\partial X^2} + \frac{\partial^2 V}{\partial Y^2}\right) + Ri \int_A N_\alpha \, \theta \, dA + Ri \, Br \, AN\alpha C \, dA - Ha21Re \, AN\alpha V \, dA \tag{4.26}$$

$$\int_A N_\alpha \left(U \frac{\partial \theta}{\partial X} + V \frac{\partial \theta}{\partial Y}\right) dA = \frac{1}{PrRe} \int_A N_\alpha \left(\frac{\partial^2 \theta}{\partial X^2} + \frac{\partial^2 \theta}{\partial Y^2}\right) dA \tag{4.27}$$

$$\int_A N_\alpha \left(U \frac{\partial C}{\partial X} + V \frac{\partial C}{\partial Y}\right) dA = \frac{1}{LePrRe} \int_A N_\alpha \left(\frac{\partial^2 C}{\partial X^2} + \frac{\partial^2 C}{\partial Y^2}\right) dA \tag{4.28}$$

where A is the element area.

Gauss's theorem is then applied to equations (4.25) - (4.28) to generate the boundary integral terms associated with the surface tractions, heat flux and diffusion flux. Then equations (4.25) - (4.28) becomes,

$$\int_A N_\alpha \left(U \frac{\partial U}{\partial X} + V \frac{\partial U}{\partial Y}\right) + \int_A H_\lambda \left(\frac{\partial P}{\partial X}\right) dA - \frac{1}{Re} \int_A \left(\frac{\partial N_\alpha}{\partial x} \frac{\partial U}{\partial x} + \frac{\partial N_\alpha}{\partial Y} \frac{\partial U}{\partial Y}\right) dA = \int_{S_0} N_\alpha \, S_x \, dS_0 \tag{4.29}$$

$$\int_A N_\alpha \left(U \frac{\partial V}{\partial X} + V \frac{\partial V}{\partial Y}\right) dA + \int_A H_\lambda \left(\frac{\partial P}{\partial Y}\right) - \frac{1}{Re} \int_A \left(\frac{\partial N_\alpha}{\partial x} \frac{\partial V}{\partial x} + \frac{\partial N_\alpha}{\partial Y} \frac{\partial V}{\partial Y}\right) - Ri \int_A N_\alpha \, \theta \, dA - Ri \, Br \, AN\alpha C \, dA + Ha21Re \, AN\alpha V \, dA = S0 N\alpha \, Sy \, dS0 \tag{4.30}$$

$$\int_A N_\alpha \left(U \frac{\partial \theta}{\partial X} + V \frac{\partial \theta}{\partial Y}\right) dA - \frac{1}{PrRe} \int_A \left(\frac{\partial N_\alpha}{\partial x} \frac{\partial \theta}{\partial x} + \frac{\partial N_\alpha}{\partial Y} \frac{\partial \theta}{\partial Y}\right) dA = \int_{S_w} N_\alpha \, q_w \, dS_w \tag{4.31}$$

$$\int_A N_\alpha \left(U \frac{\partial C}{\partial X} + V \frac{\partial C}{\partial Y}\right) dA - \frac{1}{LePrRe} \int_A \left(\frac{\partial N_\alpha}{\partial x} \frac{\partial C}{\partial x} + \frac{\partial N_\alpha}{\partial Y} \frac{\partial C}{\partial Y}\right) dA = \int_{S_w} N_\alpha \, J_w \, dS_w \tag{4.32}$$

Here (4.25) - (4.26) specifying surface tractions (S_x, S_y) along the outflow boundary S_0 and (4.27) - (4.28) specifying velocity components and fluid temperature or heat flux (q_w) and diffusion flux (J_w) that flows into or out from domain along wall boundary S_w.

CHAPTER 5

NUMERICAL SIMULATION AND COMPARISON

The heat and mass transfer and fluid flow in a two dimensional rectangular cavity with height H and width L with a centered heated obstacle and two semi-circular wall heater is considered as shown in a schematic diagram of figure 4.1 of chapter 4. In this physical system, dimensional governing equations (4.1-4.5) and non-dimensional governing equations (4.10-4.14) are solved in section 4.4.1 in previous chapter 4. for boundary conditions, left and right walls (i.e. side walls) are subjected to cold temperature (T_L) and low concentration (C_L) , the centered obstacle and two semi-circular walls are subjected to high temperature (T_H) and high concentration (C_H), also upper wall and lower wall except two semi-circular wall heater are thermally insulated and upper wall has a moving velocity as shown in section 4.2. Numerical technique of finite element formulation has also been discussed in section 4.4.1. In this chapter grid independence test, code validation, comparison and results have been discussed.

5.1 Grid Independence Test

Test for the accuracy of grid fineness has been carried out to find out the optimum grid number.

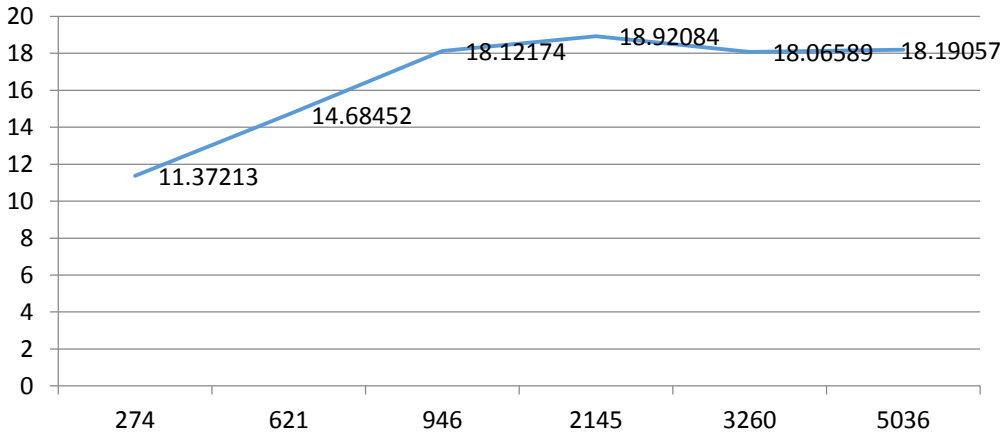

Figure 5.1: Convergence of average Nusselt number with grid refinement for $Pr = 7, Ha = 0, A = 0.042$ and $Re = 100$

Nodes	169	357	532	1163	1740	2654
(Element)	274	621	946	2145	3260	5036
Nu	11.37213	14.68452	18.12174	18.92084	18.06589	18.19057
Time(s)	14	14	16	25	36	47

Table 5.1: Grid sensitivity check at $Pr = 7, Ha = 0, A = 0.042$ and $Re = 100$

In order to obtain grid independent solution, a grid refinement study is performed for a rectangular cavity with $Pr = 7, A = 0.042$ and $Re = 100$. Figure 5.1 showsthe convergence of the average Nusselt number Nu at the heated surface with grid refinement. It is observed that grid independence is achieved with 2145 elements where there is insignificant change in *Nu* with further increase of mesh elements. Six different non-uniform grids with the following number of nodes and elements were considered for the

grid refinement test: 169 nodes, 274 elements; 357 nodes, 621 elements; 532 nodes, 946 elements; 1163 nodes, 2145 elements; 1740 nodes, 3260 elements; 2654 nodes, 5036 elements. From these values 1163 nodes, 2145 elements can be chosen throughout the simulation to optimize the relation between the accuracy required and the computing time.

5.2 Code Validation

5.2.1 Code validation through data

Ri	Present	Y.C. Ching [21]
0.01	30.258	32.386
0.1	27.687	28.653
1	12.323	12.231
10	11.029	11.5689

Table 5.2: Code validation for heated wall with Pr=0.71, Re=100,Ha=0

For the validation of the code, a triangular cavity without MHD is considered with fluid by finite element weighted residual method whose vertical wall was moving upward with a velocity and maintained at cooled condition. The inclined wall is hot, whereas the bottom wall is under adiabatic conditions. Average Nusselt number is calculated for different values of Richardson number *Ri=0.01* to *Ri=10.* Also Prandtl number is kept fixed at *Pr=0.71* and *Re=100.*

The results are compared with the literature Y.C.Ching [21] to validate the present numerical code. The average Nusselt number presented in Table 5.2 for different values of Richardson number along the heated inclined wall with fixed Prandtl number.

5.2.2 Code validation through streamlines and isotherms

To validate the present numerical code, the results for mixed convection flow in an triangular enclosure with moving cooled vertical wall, heated inclined wall and adiabatic bottom wall have been compared with the present model. Figure 5.2 demonstrate the comparison of streamline and isotherm at Ching et al. [21] with the regenerated model for

Pr=1, Br=20 , Le=2 and *Ri=5*.Also figure 5.3 shows the comparison of streamline and isotherm at present model with the result presented in figure 5.2 for *Pr=1, Br=20 , Le=2* and *Ri=5*.

As seen from both figures presented in 5.2 and 5.3 the obtained results shows very good agreement.

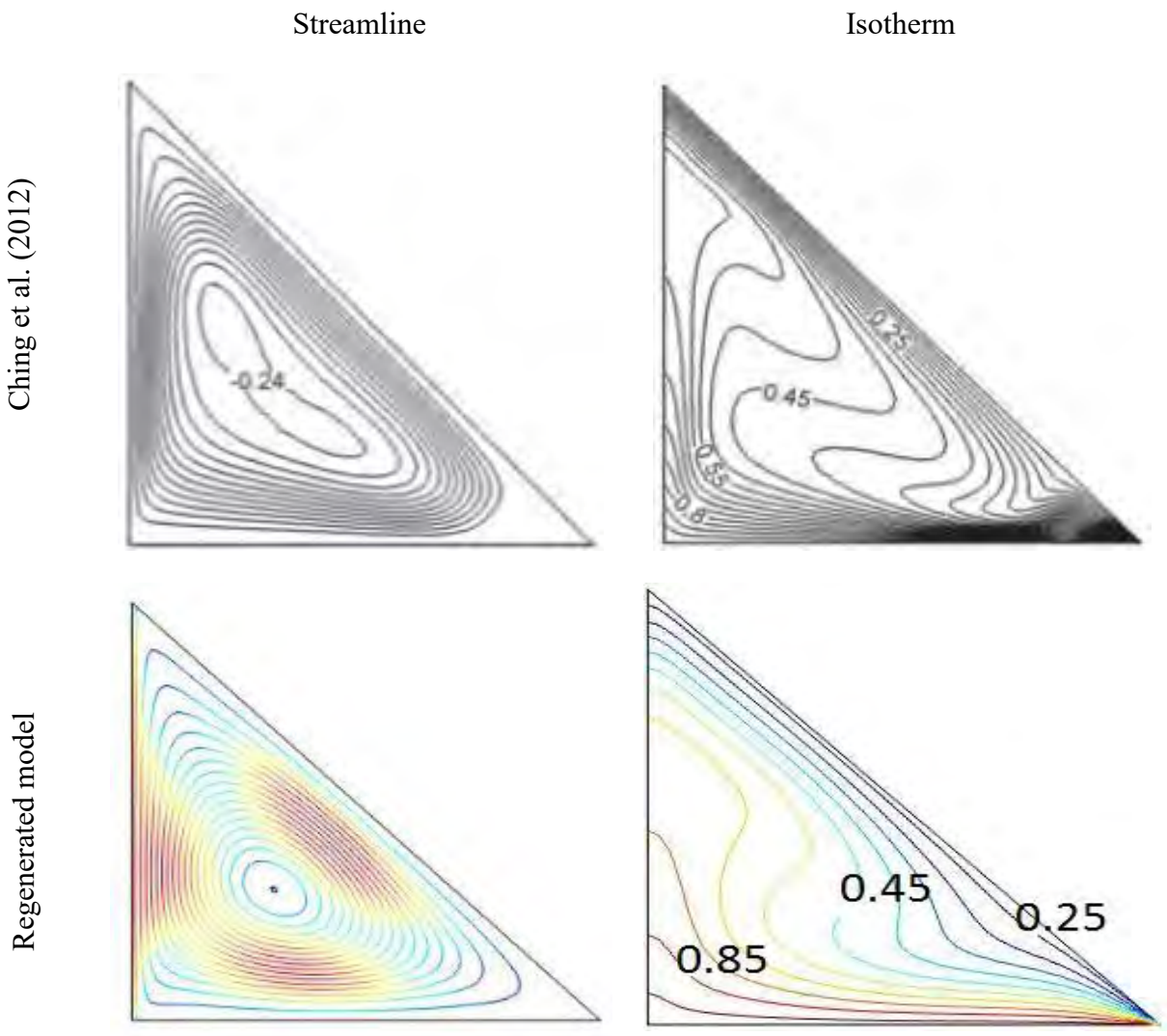

Figure 5.2: Comparison of streamlines and isotherms with Pr=1, Br=20 , Le=2 and Ri=5.

Present Model

Streamline

Isotherm

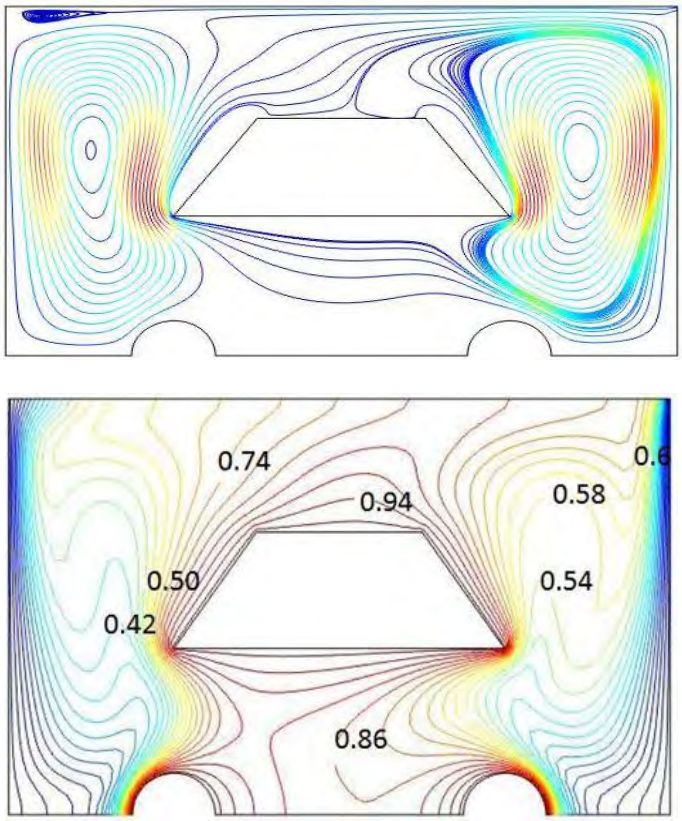

Figure 5.3: Comparison of streamline and isotherm with Pr=1, Br=20 , Le=2 and Ri=5 according Present model

5.3 Comparison between without and with MHD

After validation of the code, a rectangular cavity with fluid in presence of MHD is considered whose vertical walls (i.e. side walls) are subjected to cold temperature, middle obstacle and two semi-circular wall are subjected to hot temperature while the upper and bottom wall except two semi-circular wall are kept thermally insulated. Average Nusselt number is calculated for four different Richardson number and two different obstacle areas $A = 0.042$ and $A = 0.028$ while the Prandtl number is kept fixed at $Pr = 7$ along the left and right semi-circular wall heater respectively.

Ri	Average Nusselt number			
	Present work without MHD		Present work with MHD	
	A = 0.042	A = 0.028	A = 0.042	A = 0.028
0.1	10.0383	12.0834	4.7519	5.4818
1	21.4403	25.2814	11.4664	12.6083
5	33.2847	38.9765	27.8648	29.0452
10	40.0748	45.8042	37.0442	37.6899

Table 5.3: Comparison of average Nusselt number along the left semi-circular wall heater with Pr=7 and Re=100 (without and with MHD)

Ri	Average Nusselt number			
	Present work without MHD		Present work with MHD	
	A = 0.042	A = 0.028	A = 0.042	A = 0.028
0.1	18.8839	19.4481	5.6127	6.7954
1	24.5412	27.3028	12.4158	13.8999
5	32.8020	39.3562	28.8039	30.2725
10	39.8014	47.1523	38.1933	39.1586

Table 5.4: Comparison of average Nusselt number along the right semi-circular wall heater with Pr=7 and Re=100 (without and with MHD)

The results are compared between the presence and absence of MHD effect. For comparison average Nusselt number along two semi-circular wall heater and temperature of the fluid are presented for different Richardson numbers and two different obstacle areas with fixed Prrandtl number and Reynolds number *Re=100* in Table 5.3 and 5.4.

5.3.1 Average Nusselt number in presence and absence of magnetic field:

When there is trapezoidal obstacle of area $A = 0.042$, from table 5.3 as Richardson number increases from 0.1 to 1 i.e. when heat transfer is happening from forced convection to mixed convection region, the average Nusselt number increases. But further increase of Richardson number from 1 to 10 i.e. when heat transfer is happening from mixed convection to free convection region, the average Nusselt number also increases more rapidly. The same phenomena happens when there is a rectangular obstacle of area $A = 0.028$. But obstacle size also has significant effect on heat transfer. In both cases as Richardson number increases from 0.1 to 10 heat transfer increases but table 5.3 shows that when there is rectangular obstacle heat transfer increases more rapidly than using trapezoidal obstacle. The entire phenomena happens when there is no magnetic field.

In the presence of magnetic field, from table 5.3 as Richardson number increases from 0.1 to 10 average heat transfer increases. But when we compare the two results with MHD and without MHD we observed from table 5.3, as Richardson number increases from 0.1 to 1 i.e. when heat transfer happening from forced convection to mixed convection region, the average Nusselt number decreases. But further increase of Richardson number from 1 to 10 i.e. when heat transfer happening from mixed convection to free convection region, the average Nusselt number increases slowly. The obstacle size also has significant effect on heat transfer in the presence of magnetic field. In that case as Richardson number increases from 0.1 to 1 heat transfer rate decreases rapidly. For further increase of Richardson number i.e. when varies from 1 to 10 heat transfer rate increase slowly when there is trapezoidal obstacle but when there is rectangular obstacle average Nusselt number decreases as above.

CHAPTER 6

RESULT AND DISCUSSION

6.1 Results and Discussion

A numerical study has been performed through finite element method to analyze the laminar mixed convection heat transfer and fluid flow in a lid driven rectangular cavity containing heated block and two semi-circular wall heater. Effect of parameters such as Richardson number Ri, Reynolds number Re, Hartmann number Ha, Buoyancy ratio Br and the area of the heated block A (trapezoidal & rectangular) on heat transfer and fluid flow of the cavity have been analyzed. The results are presented in two parts. The first part has focused on fluid flow and temperature fields which explain through the streamlines and isotherms for different cases. The second part has focused on heat transfer rate through the explanation of average Nusselt number along the left and right semi-circular wall heater for different cases. The range of Richardson number Ri for this investigation is chosen from 0.1 to 10 to obtain the characteristics on forced convection, mixed convection and natural convection region based on $Ri = \frac{Gr}{Re^2}$. The range of Prandtl number is chosen 7 for water at 20 C and it kept fixed for all cases. Reynolds number is also kept fixed $Re = 100$. Results are obtained for two different shapes of heated block namely trapezoidal and rectangular heated block which contained area 0.042 and 0.028 respectively. Hartmann number is vary from 0 to 150 , buoyancy ratio vary from 0 to 20 and Lewis number is kept fixed $Le = 20$.

6.1.1 Effect of fluid flow and temperature with trapezoidal obstacle in absence of magnetic field

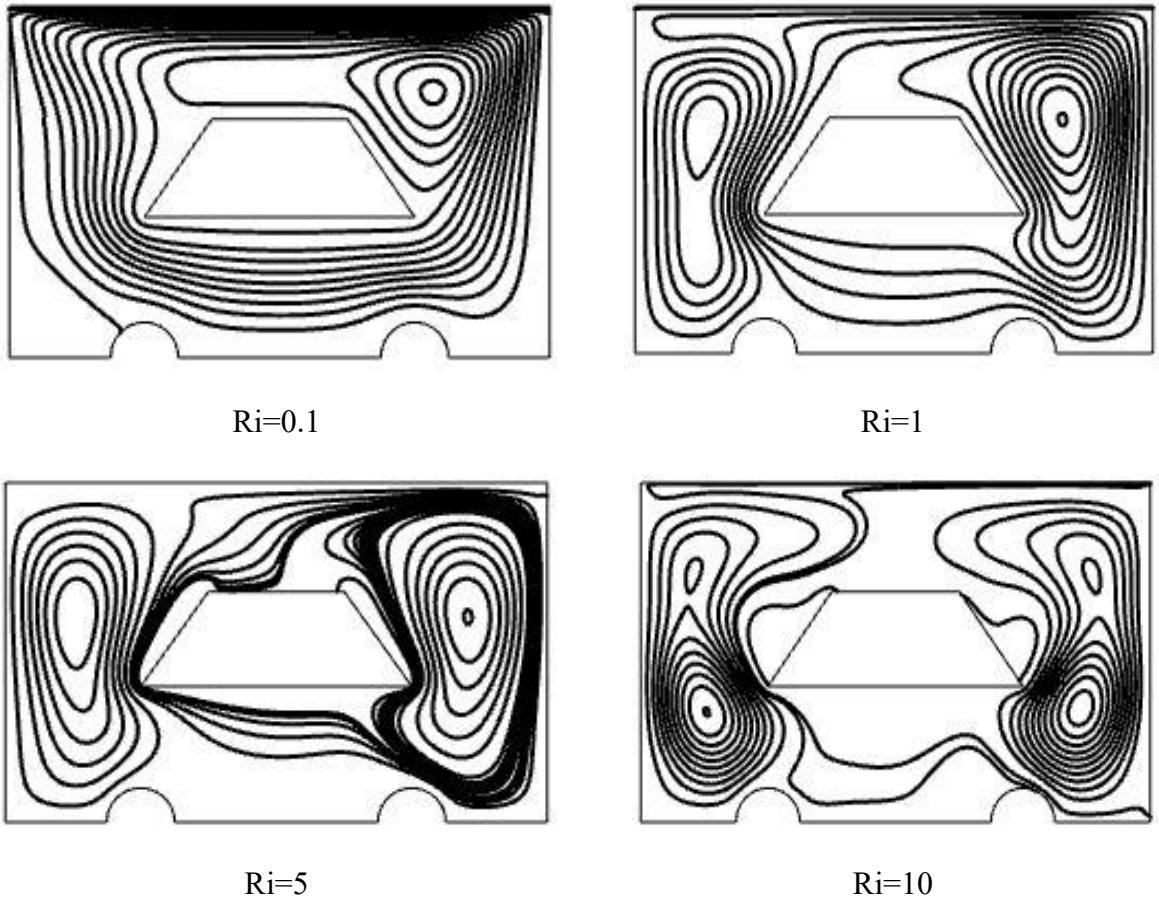

Figure 6.1: Streamlines for different values of Ri without MHD while Re=100, Pr=7, A=0.042

For the variations of *Ri* in absence of magnetic field with trapezoidal heated block, the overall features of the streamlines are predicted in figure 6.1 where *Re=100, Pr=7, Br=20* and *A=0.042*. In absence of the magnetic field and in the forced convection region, the fluid flow is characterized by a primary rotating uni-cellular vortex occupying the bulk of the cavity generated by the movement of the upper lid. Without MHD and in the forced convection region i.e. *Ri=0.1*, the core of the vortex spreads in the whole cavity. When forced convection and natural convection are equally dominant, namely at mixed convection i.e. *Ri=1*, the core of the vortex divided in to two parts and form bi-cellular vortex at the two vertical walls. The density of streamlines increases at the right vertical wall than the left vertical wall because of

the upper moving lid in the positive x-direction. As *Ri* increases further i.e. *Ri=5*, the bi-cellular vortex become more symmetric than that at *Ri=1*. When *Ri=10*, i.e. the effect of forced convection is very much less compared to the natural convection effect, the bi-cellular vortex become more symmetric and also some small vortex are included. Also at the natural convection i.e. *Ri=10*, the density of the streamlines increases near the two semi-circular wall heater.

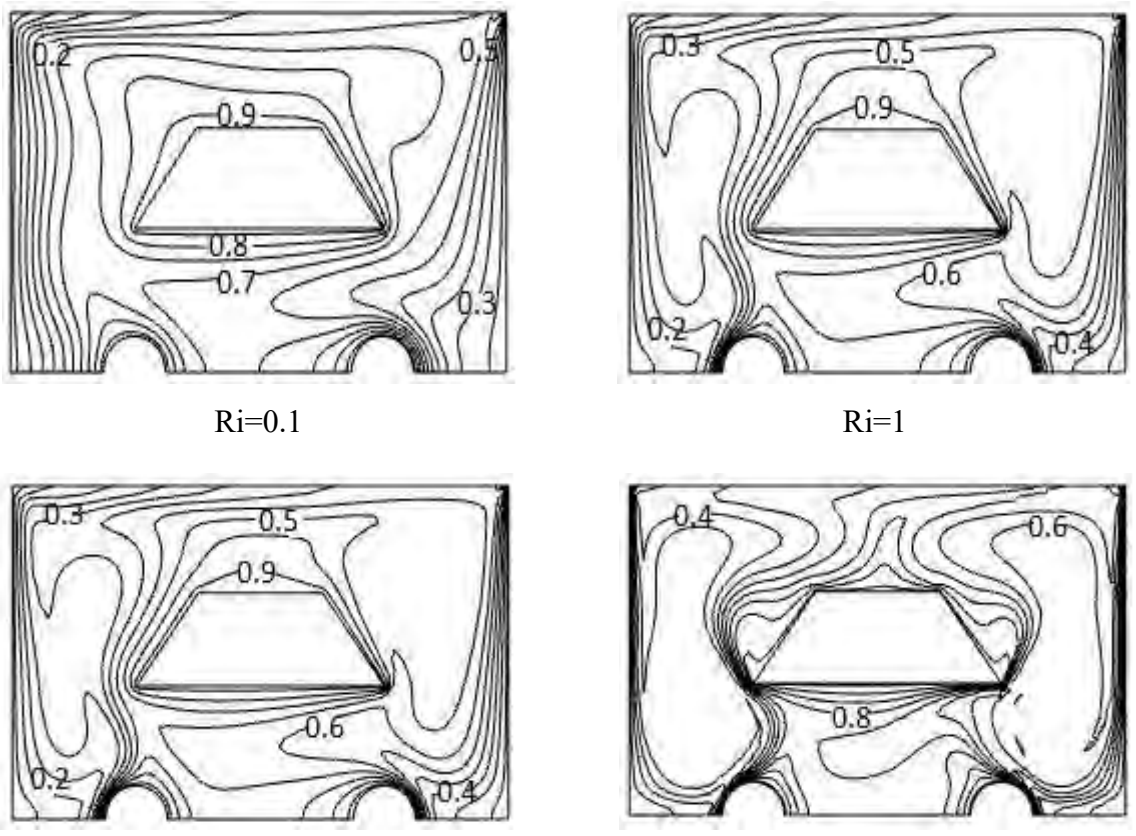

Ri=0.1 Ri=1

Ri=5 Ri=10

Figure 6.2: Isotherm for different values of Ri without MHD while Re=100, Pr=7, A=0.042

For the variations of *Ri* in absence of magnetic field with trapezoidal obstacle the overall feature of the isotherms are predicted in figure 6.2 where *Re=100,Pr=7, Br=20* and *A=0.042* are kept fixed. Without MHD and in the convection region i.e. *Ri=0.1*, the isotherms near the heated obstacle and around the semi-circular wall heater are rotated in parallel form. As *Ri* increases, the nonlinearity of isotherm increases and also it is observed that the temperature at the right side of the heated block is higher than the temperature of the left side of the heated block. With the increase of *Ri* two void are forms at the left and right side of the heated block and still the temperature at the right side of the block is higher than the temperature at the left

side. But in the natural convection dominated region (*Ri=10*) in absence of magnetic field, the non-linearity of the isotherm are so high that they are almost symmetric at the left and right side of the heated block and semi-circular wall heater. The density of isotherm increases around the heated block and the semi-circular wall heater. And it behaves in to parallel form. Also the temperature is still higher at the right side of the heated block than the left side of the heated block.

For variations of *Ri* in absence of magnetic field with rectangular heated block the overall features of the streamlines are presented in figure 6.3 where *Re=100, Pr=7, Br=20* and *A=0.028* are kept fixed. from the above figure 6.3 it is observed that as *Ri* increases from 0.1 to 10 the changes are similar to the changes with trapezoidal heated block. There are one difference between this two cases. That is, with trapezoidal heated block the overall shapes of streamlines are looks like mango seeds and with rectangular heated block the overall shapes of streamlines are looks like oval shapes. At forced convection region i.e. *Ri=0.1*, streamlines are looks similar in both cases.

Figure 6.4 illustrates the variation of isotherms for different values of *Ri* in absence of magnetic field with rectangular heated block where *Re=100, Pr=7, Br=20* and *Ri=0.028*. We observed that the patterns of the isotherm looks same as in figure 6.2 but the shapes in this figure is oval. Also the temperature at the right side of the rectangular block is higher than the temperature at the left side of the rectangular heated block.

The variations of *Ha* and *Ri* with trapezoidal heated block, the overall features of the streamlines are illustrated in figure 6.5 and figure 6.6 where *Re=100, Pr=7, Br=20* and *A=0.042.* At forced convection region *(Ri=0.1)* as *Ha* increases from 0 to 150 the density of streamlines increases near the upper horizontal wall and decreases near the lower part of the heated block. For highest value of *Ha* we observed that all the streamlines gathered at the top of the heated obstacle. At mixed convection region *(i.e. Ri=1*) in absence of magnetic field the core divided into two parts positioned at the left and right side of the heated block. This divided parts are looks like mango seed and symmetric. The density of streamlines nearer to moving lid decreases with the increases of *Ha* and so the results are no more symmetric with the increase of *Ha* at *Ri=1*. Also streamlines contained three more minor vortex with the increase of *Ha* at *Ri=1*. At natural convection (*i.e. Ri=10*) figure illustrates that with the increase of *Ha* the velocity field form two large bi-cellular vortex with four minor vortices. For highest value of *Ha* the streamlines looks more symmetric for *Ri=10*. This is because of

the application of transverse magnetic fields which slow down the movement of the buoyancy-induced flow in the cavity.

6.1.2 Effect of fluid flow and temperature with rectangular obstacle in absence of magnetic field

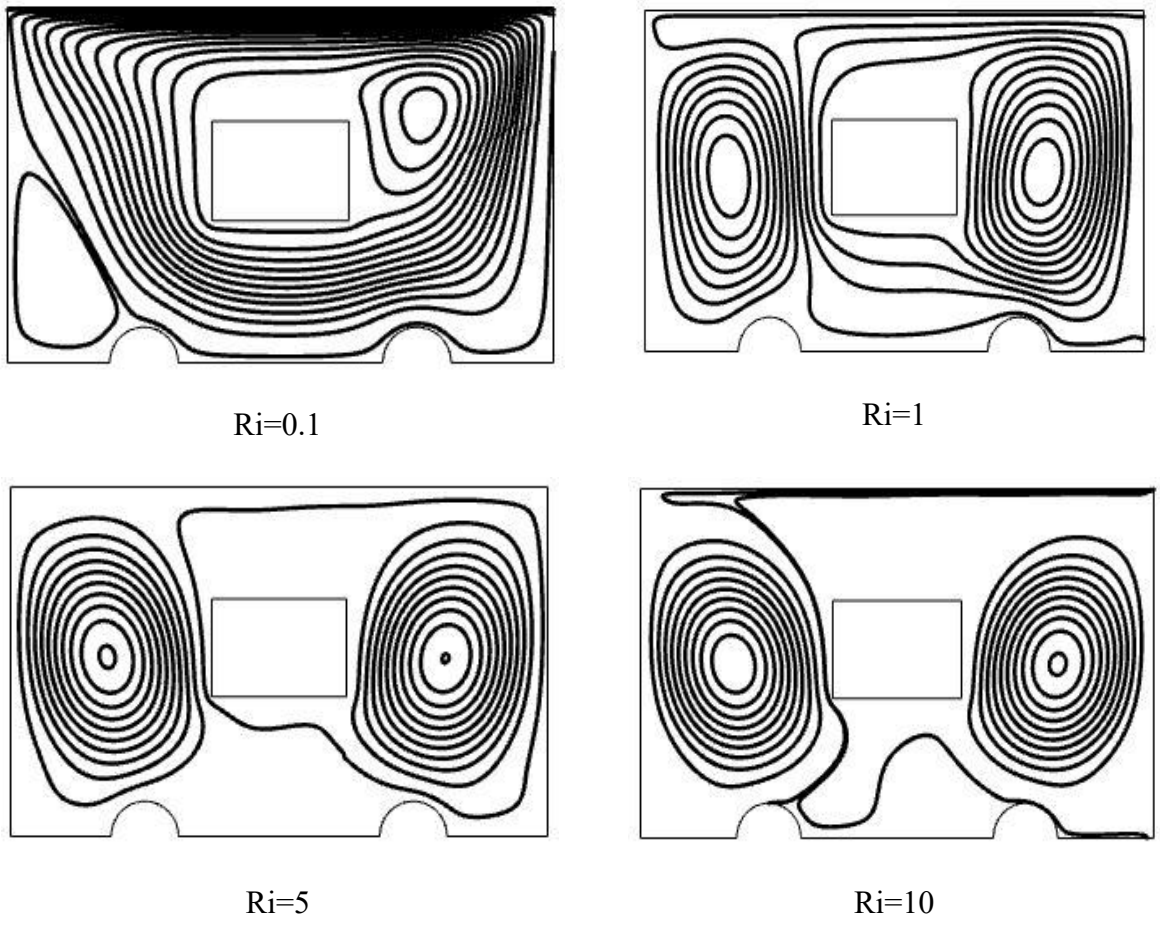

Figure 6.3: Streamlines for different values of Ri without MHD while Re=100, Pr=7, A=0.028

The corresponding effect on the temperature fields are shown in figure 6.7 and figure 6.8. The isotherms are almost parallel to both vertical walls for highest value of *Ha* at the forced convection region *i.e. Ri=0.1,* indicating that most of the heat transfer process is carried out by conduction. However some deviations in the conduction dominated isotherms lines are initiated near the left top surface of the cavity. With the increase of *Ha* at the mixed convection region *i.e. Ri=1*, isotherms line taken shape from linear to nonlinear zigzag shape. As *Ri* increases with increase of *Ha*, the nonlinearity in the isotherms become higher and plume formation is profound at the left and right side of the trapezoidal heated block and

other isotherm tend to be parallel to the vertical walls. Moreover, the formation of the thermal boundary layers near the two vertical cold walls are to be initiated for the lower value of *Ha*. This is owing to the dominating influence of the convective current in the cavity. Also for highest value of *Ha* and *Ri* the isotherm lines are in symmetric form.

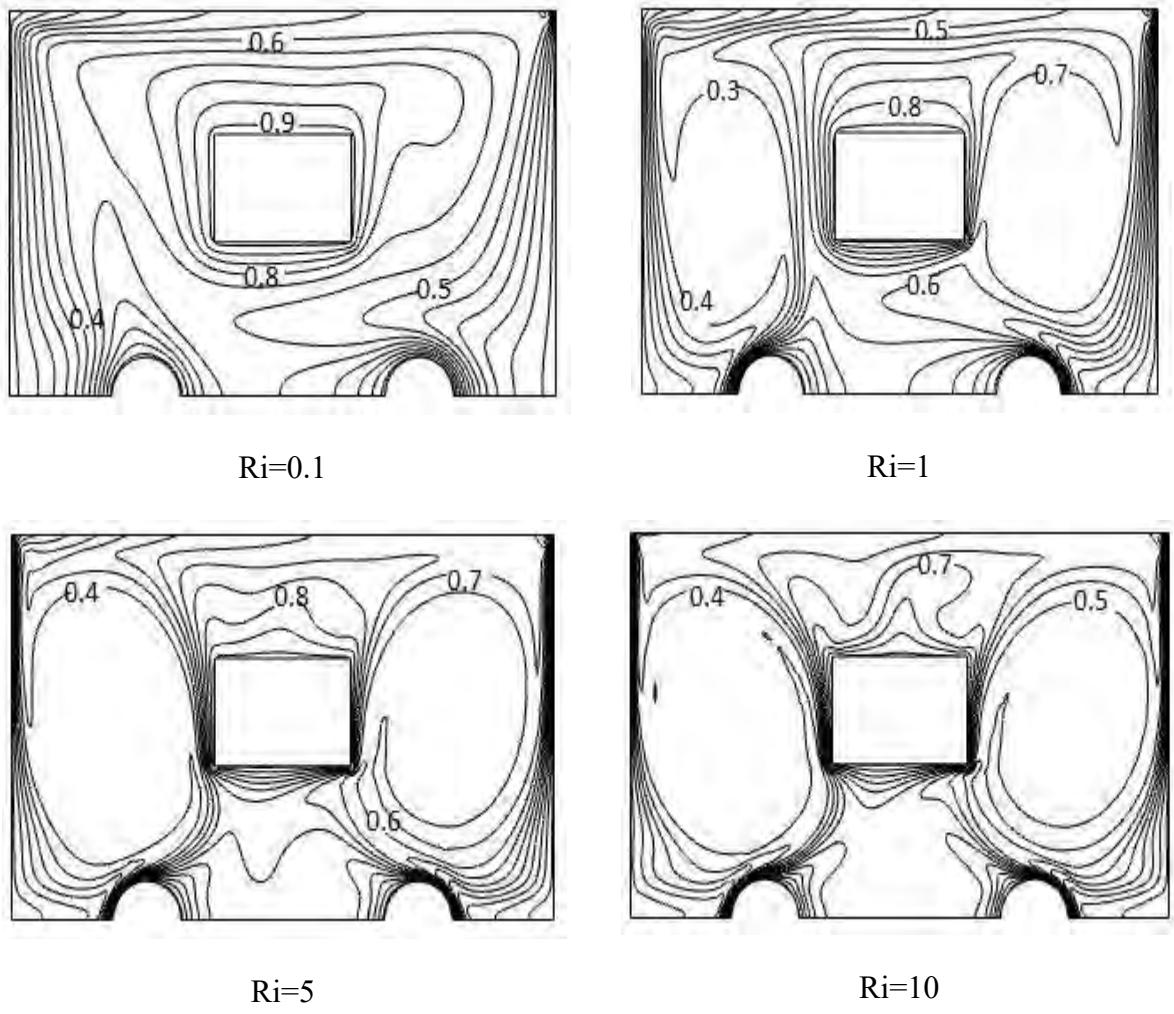

Ri=0.1 Ri=1

Ri=5 Ri=10

Figure 6.4: Isotherm for different values of Ri without MHD while Re=100, Pr=7, A=0.028

The variations of *Ri* and *Ha* with rectangular heated block in presence of magnetic field, the overall features are illustrated in figure 6.9 and figure 6.10 where *Re=100, Pr=7, Br=20* and *A=0.028*. we observed that the effect of *Ri* and *Ha* in the fluid flow is same as shown in figure 6.5 and figure 6.6. The only change in the effect of obstacle size on streamlines in presence of MHD is the isotherm lines are in oval shape for rectangular obstacle whereas it is looks like mango seeds for trapezoidal obstacle.

6.1.3 Effect of fluid flow and temperature with trapezoidal obstacle in presence of magnetic field

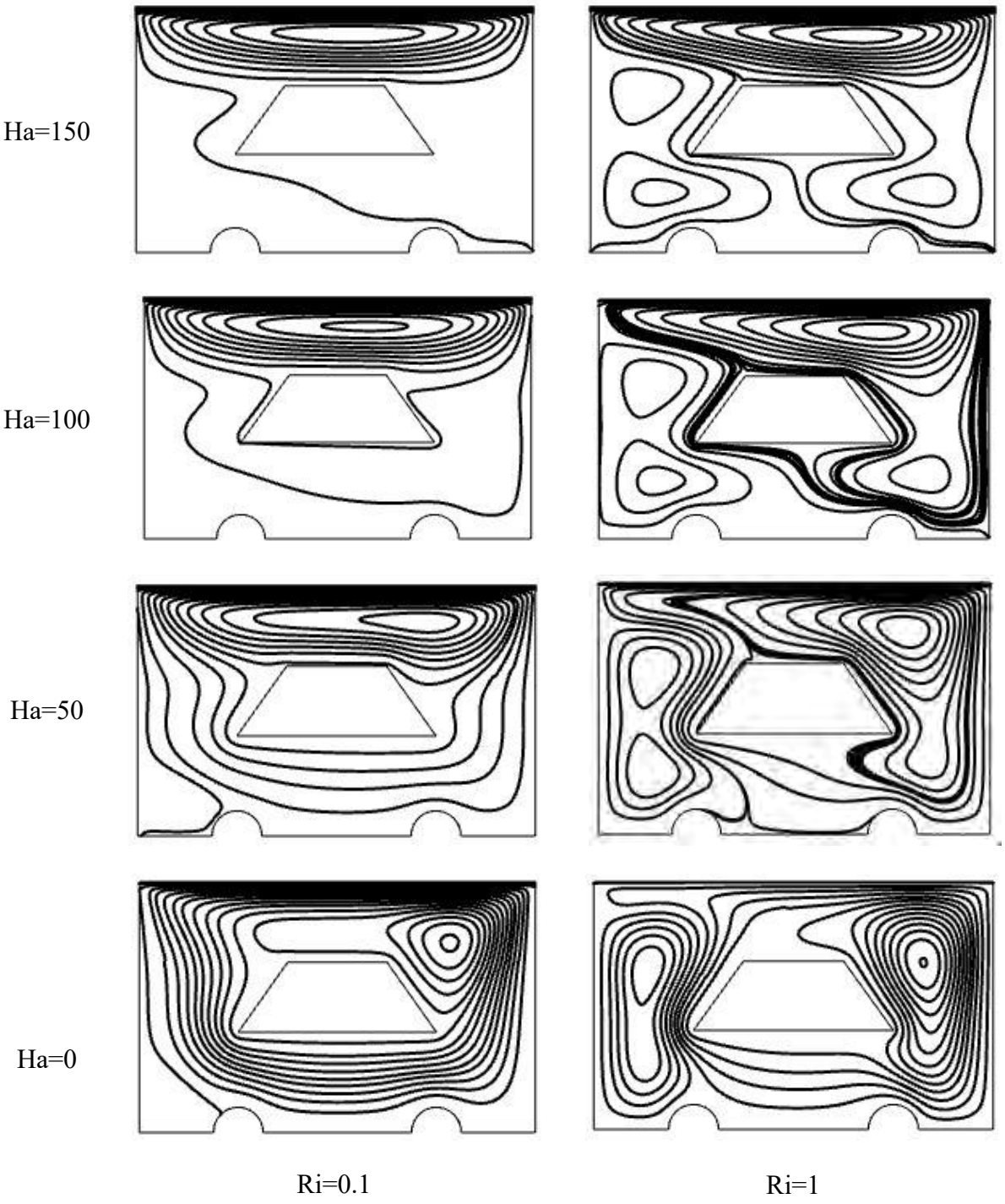

Figure 6.5: Streamlines for different values of Ha while Re=100, Pr=7, A=0.042 and Ri= 0.1 & 1

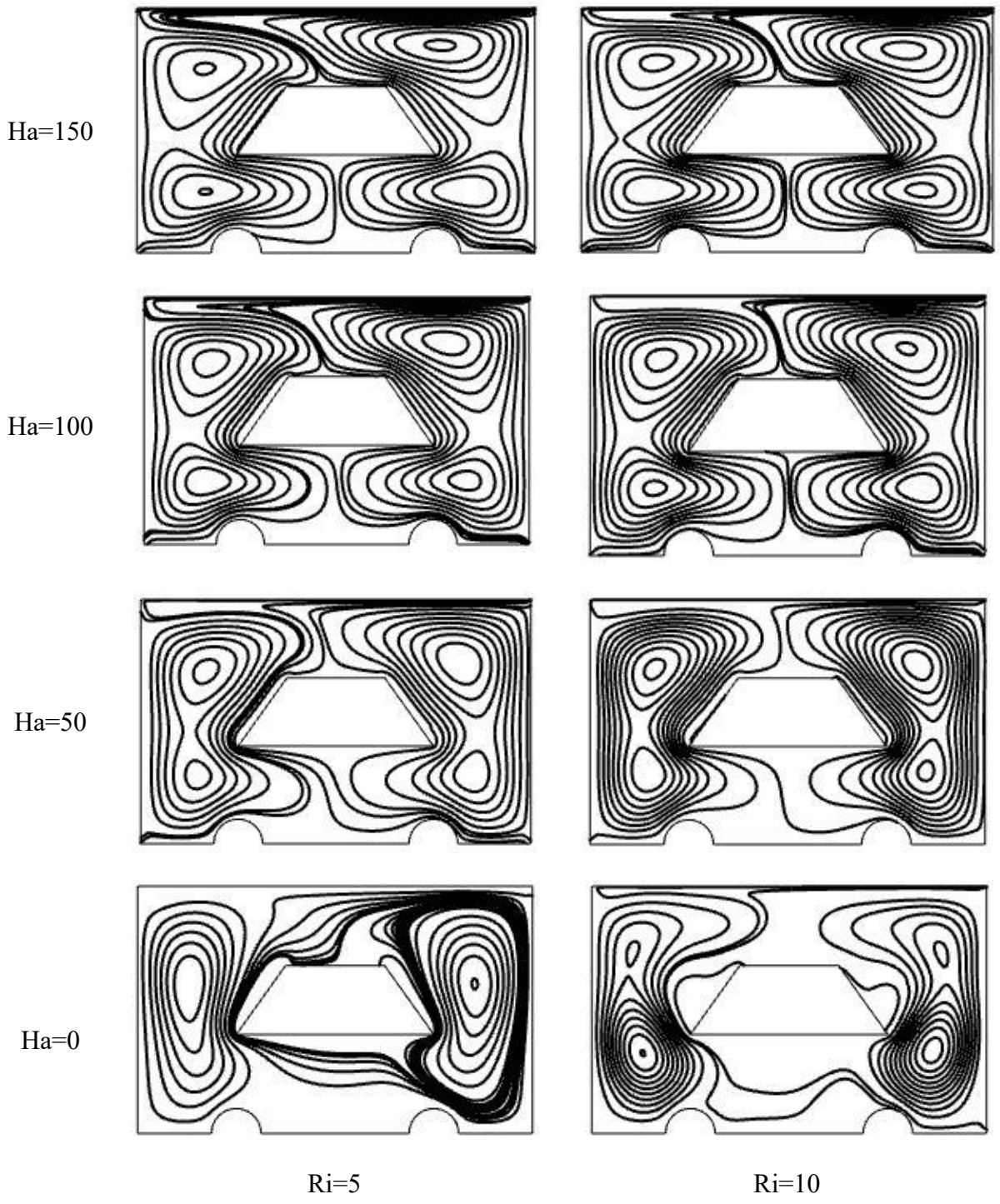

Figure 6.6: Streamlines for different values of Ha while Re=100, Pr=7, A=0.042 and Ri=5&10

The corresponding effect on the temperature fields are shown in figure 6.11 and figure 6.12. At forced convection region isotherms are almost parallel to the both vertical walls. But with the increase of *Ri* the isotherms become nonlinear. For further increase of *Ri* (*i.e. Ri=10*), at natural convection dominated region the nonlinearity become higher and plume formation is

profound at the left and right side of the rectangular heated block. Also we observed that the temperature at the right side of the heated block is higher than temperature at the left side of the heated block.

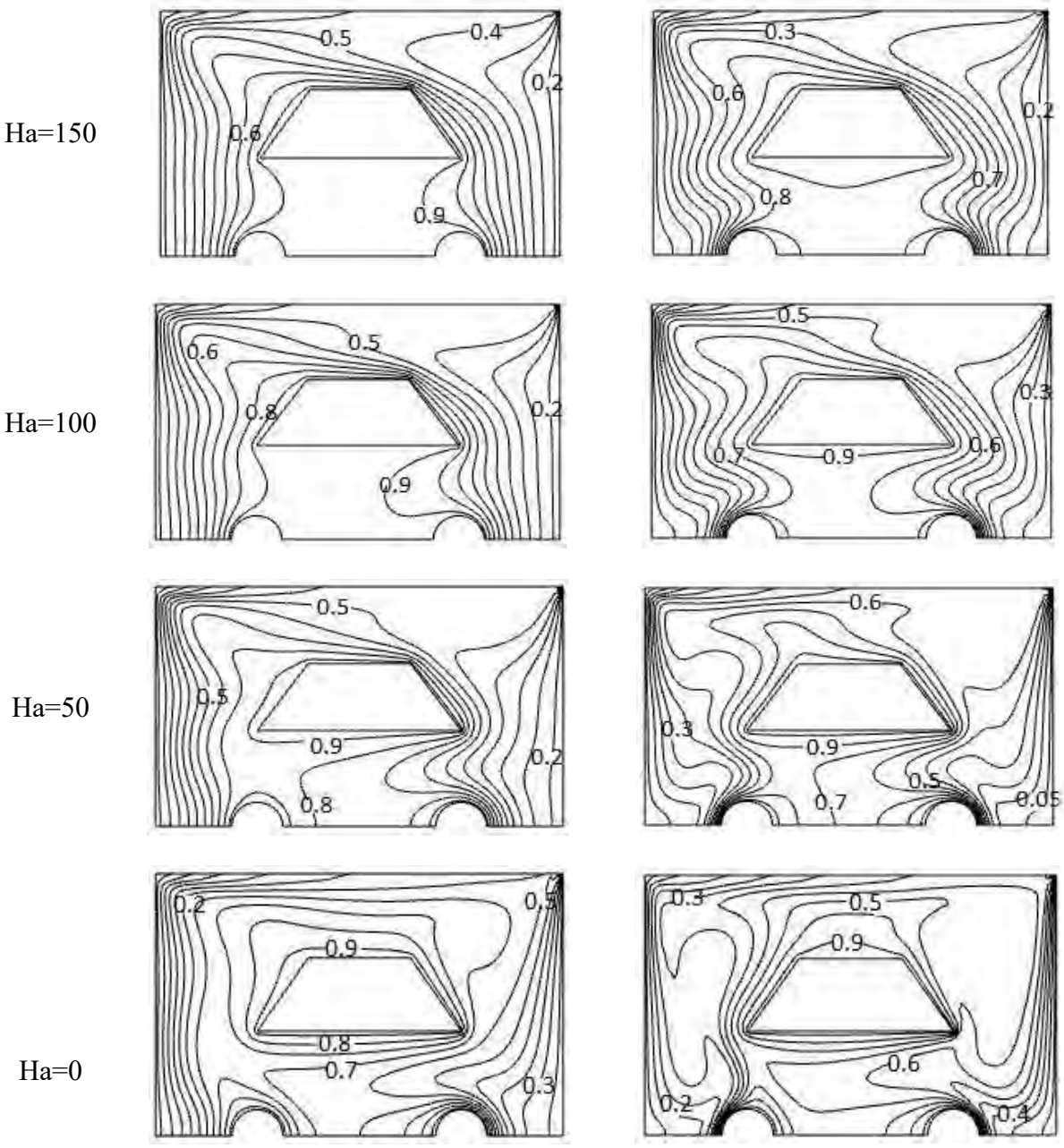

Figure 6.7: Isotherm for different values of Ha while Re=100, Pr=7, A=0.042 and Ri=0.1 &1

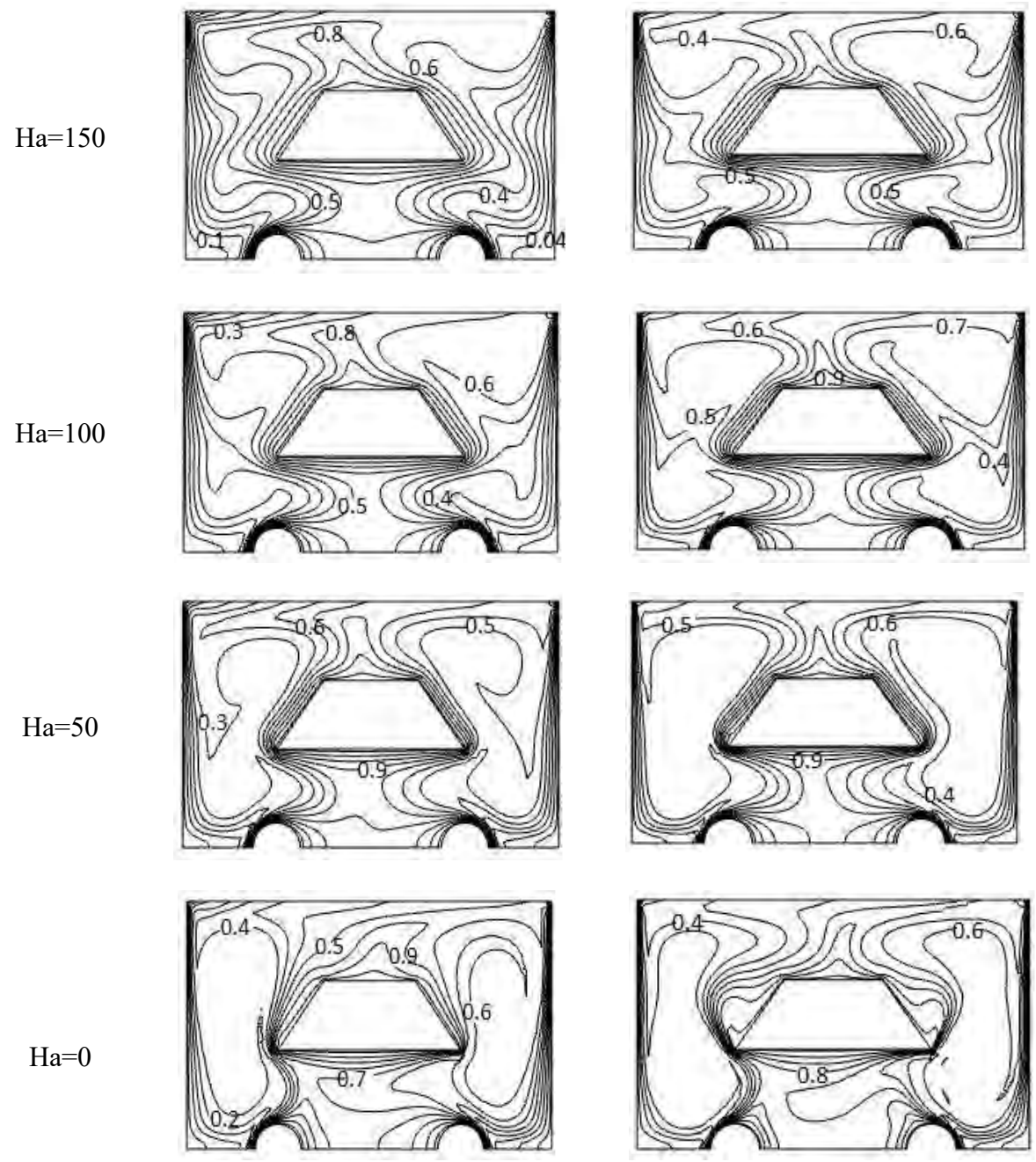

Figure 6.8: Isotherm for different values of Ha while Re=100, Pr=7, A=0.042 and Ri= 5&10

The corresponding effect on the temperature fields are shown in figure 6.11 and figure 6.12. At forced convection region isotherms are almost parallel to the both vertical walls. But with the increase of *Ri* the isotherms become nonlinear. For further increase of *Ri* (*i.e. Ri=10*), at natural convection dominated region the nonlinearity become higher and plume formation is profound at the left and right side of the rectangular heated block. Also we observed that the

temperature at the right side of the heated block is higher than temperature at the left side of the heated block.

6.1.4 Effect of fluid flow and temperature with rectangular obstacle in presence of magnetic field

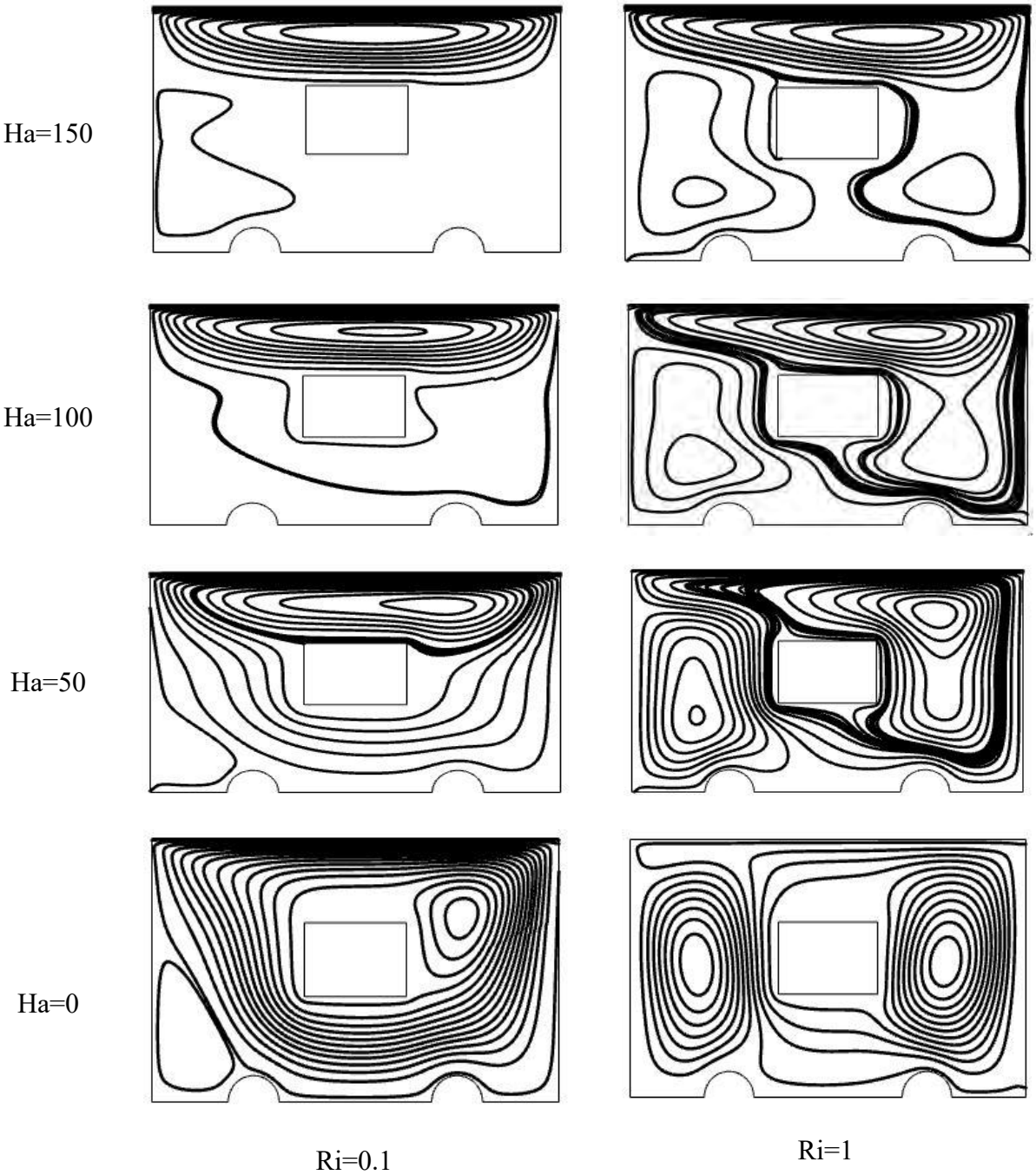

Figure 6.9: Streamlines for different values of Ha while Re=100, Pr=7, A=0.028 and Ri=0.1&1

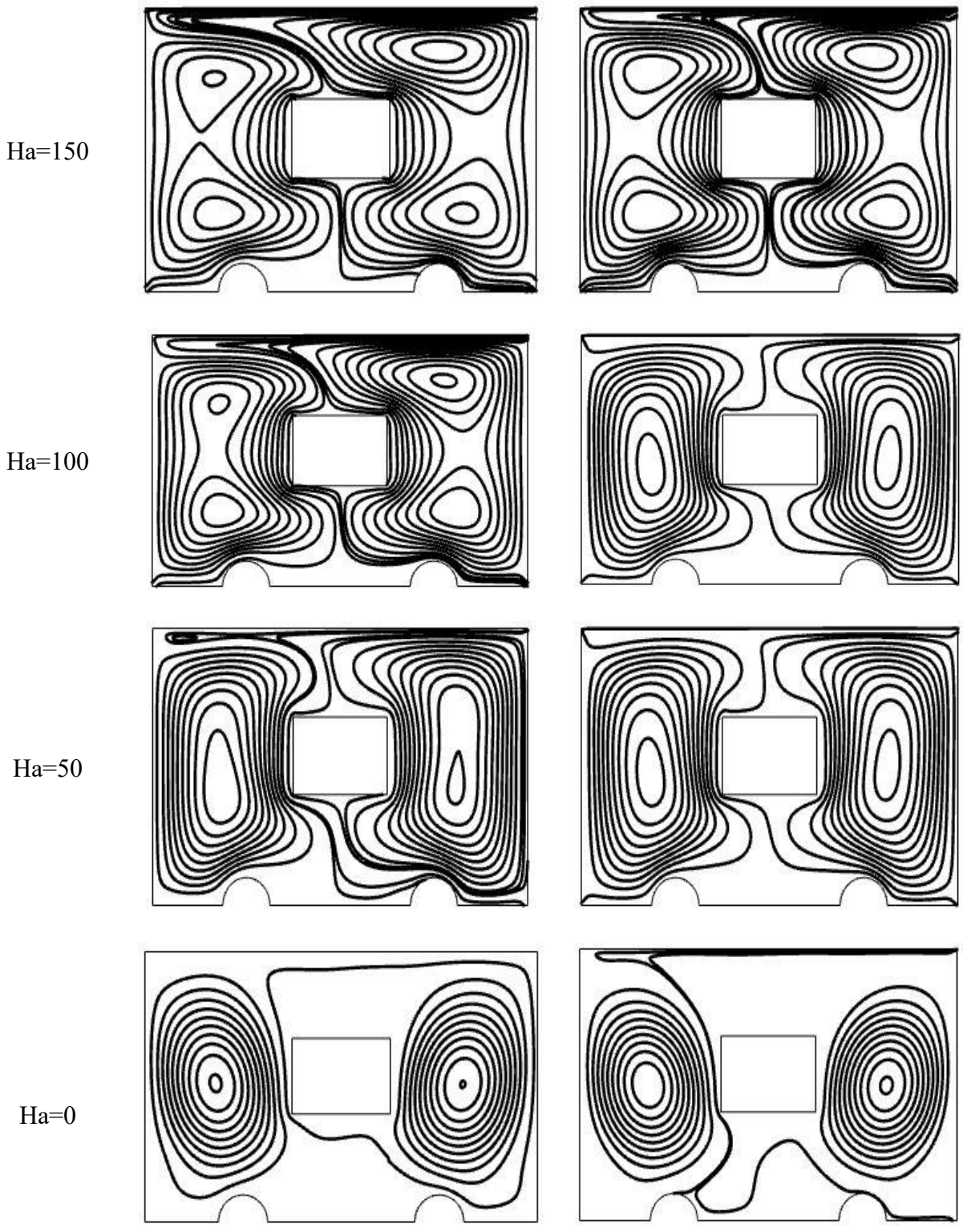

Figure 6.10: Streamlines for different values of Ha while Re=100, Pr=7, A=0.028 and Ri=5&10

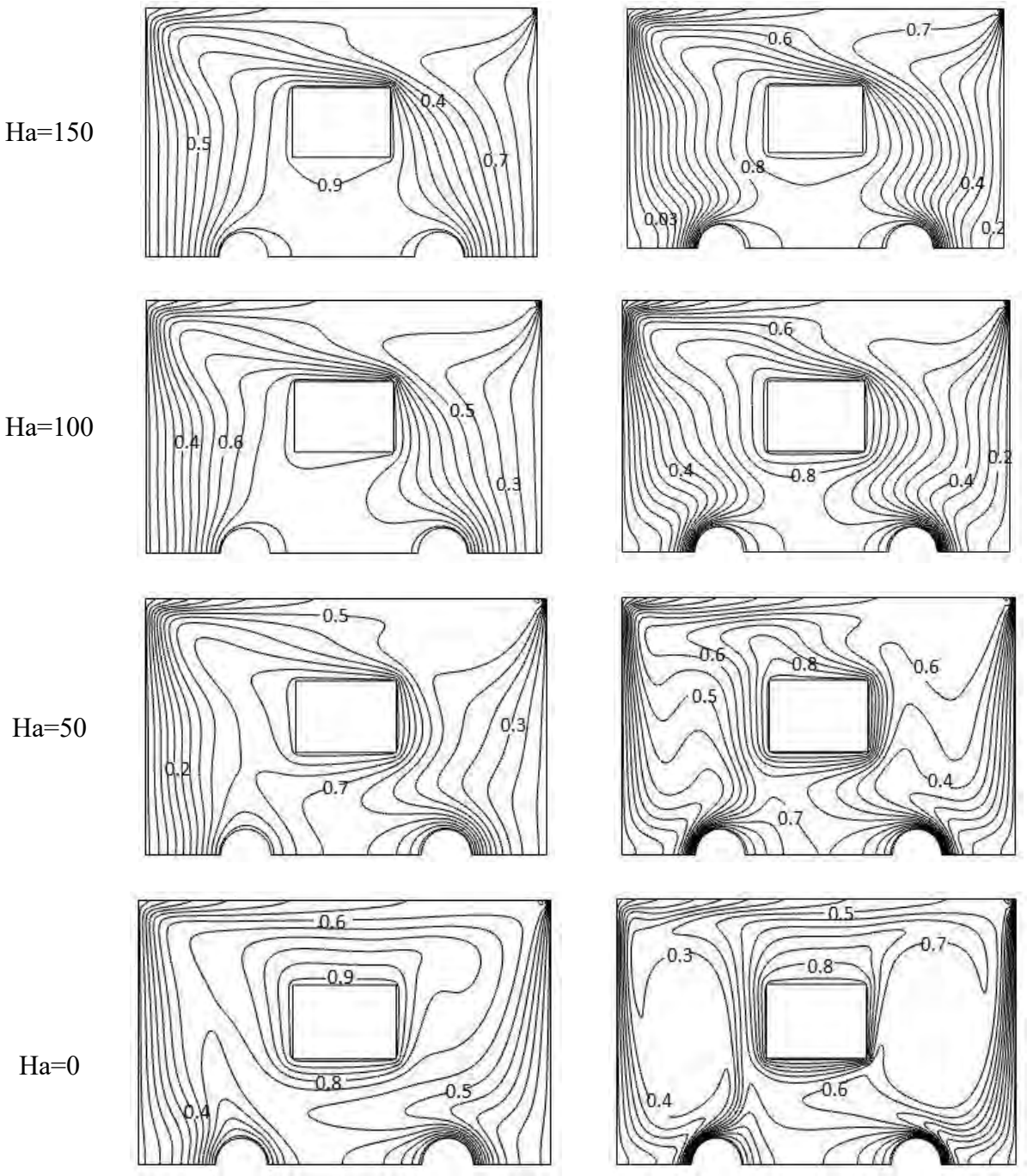

Figure 6.11: Isotherm for different values of Ha while Re=100, Pr=7, A=0.028 and Ri=0.1&1

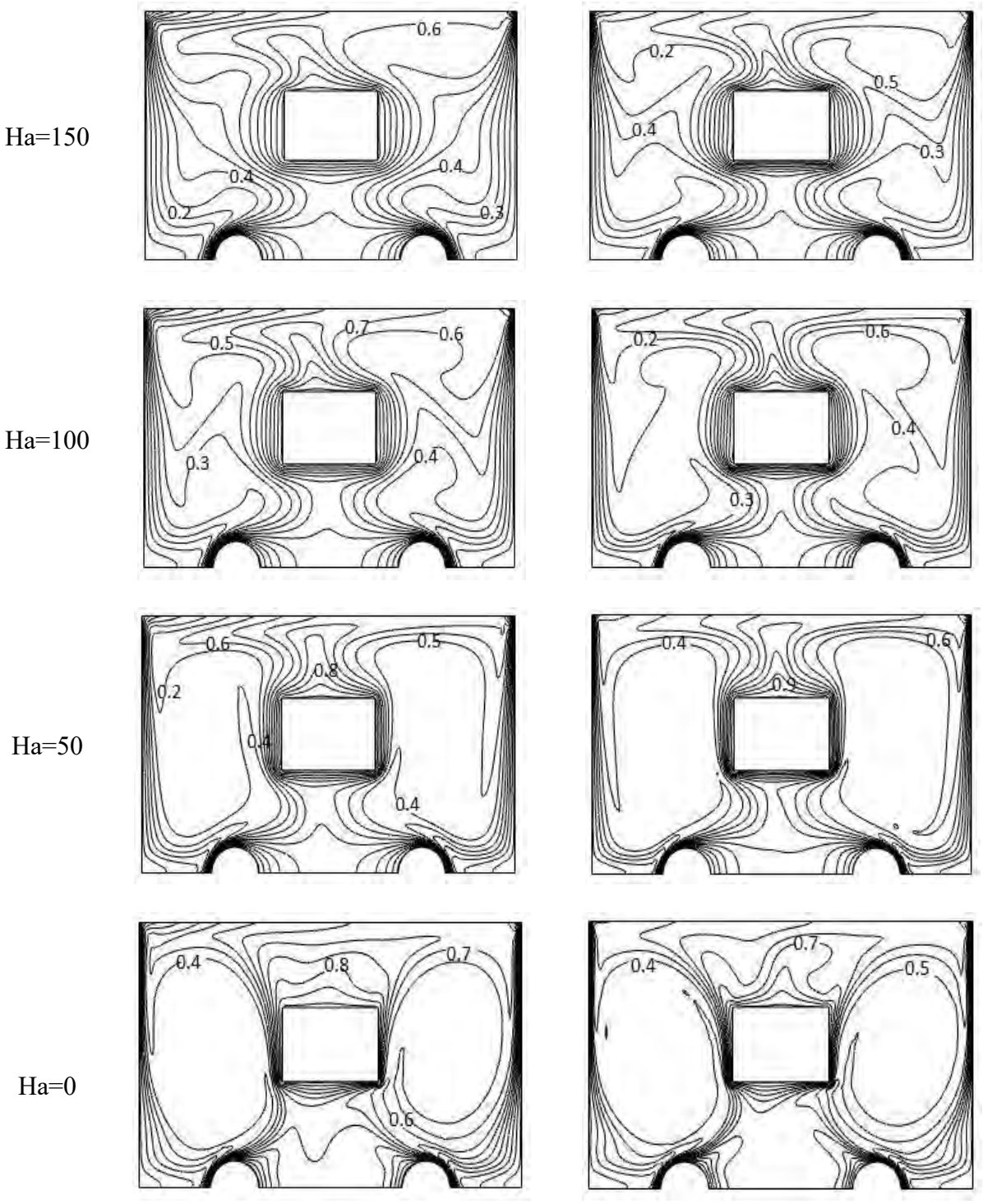

Figure 6.12: Isotherm for different values of Ha while Re=100, Pr=7, A=0.028 and Ri=5&10

6.1.5 Effect of fluid flow and temperature with trapezoidal obstacle without magnetic field for different values of buoyancy ratio and Richardson number:

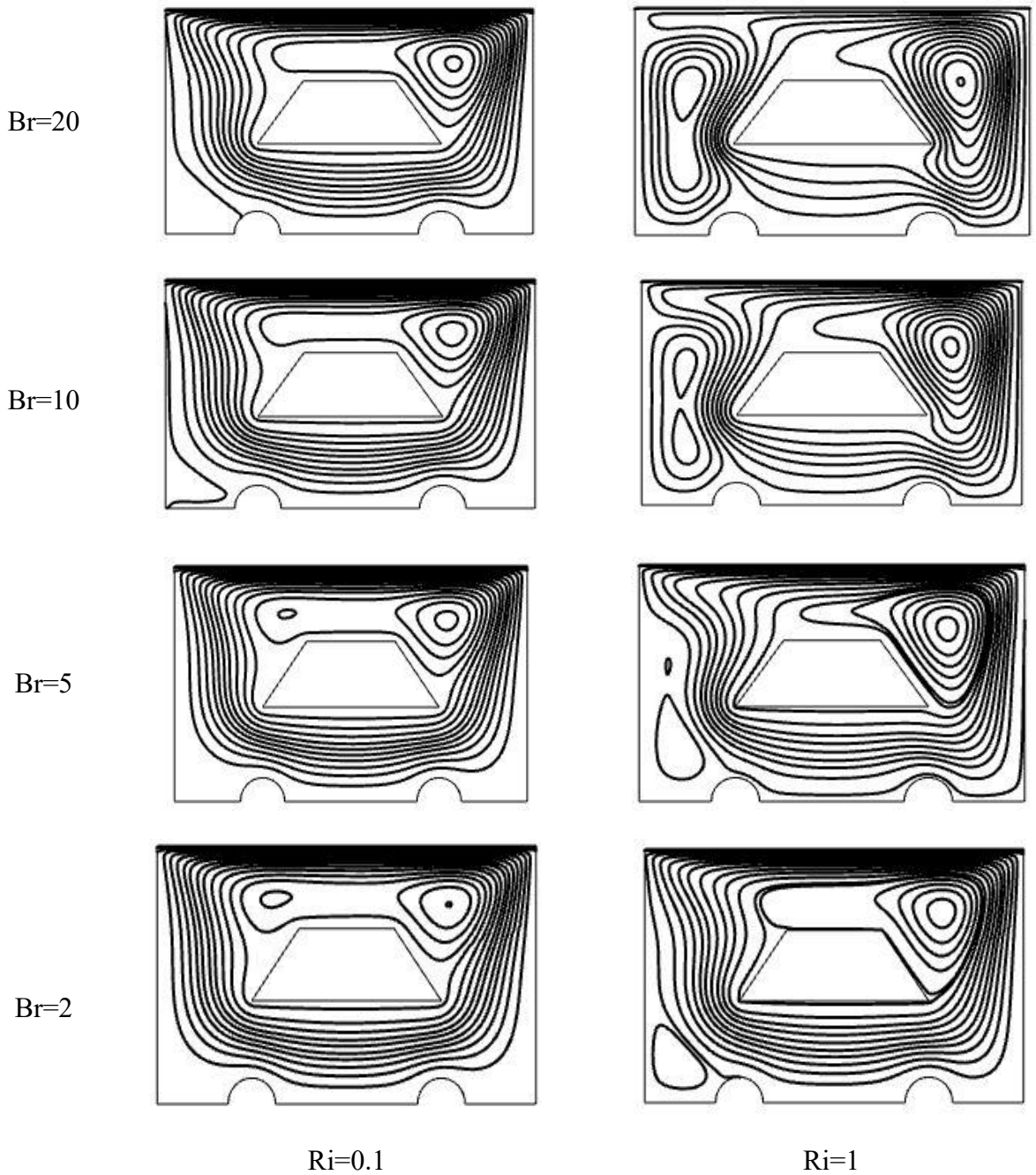

Figure 6.13: Streamlines for different values of Br without MHD while Re=100, Pr=7, A=0.042 and Ri=0.1&1

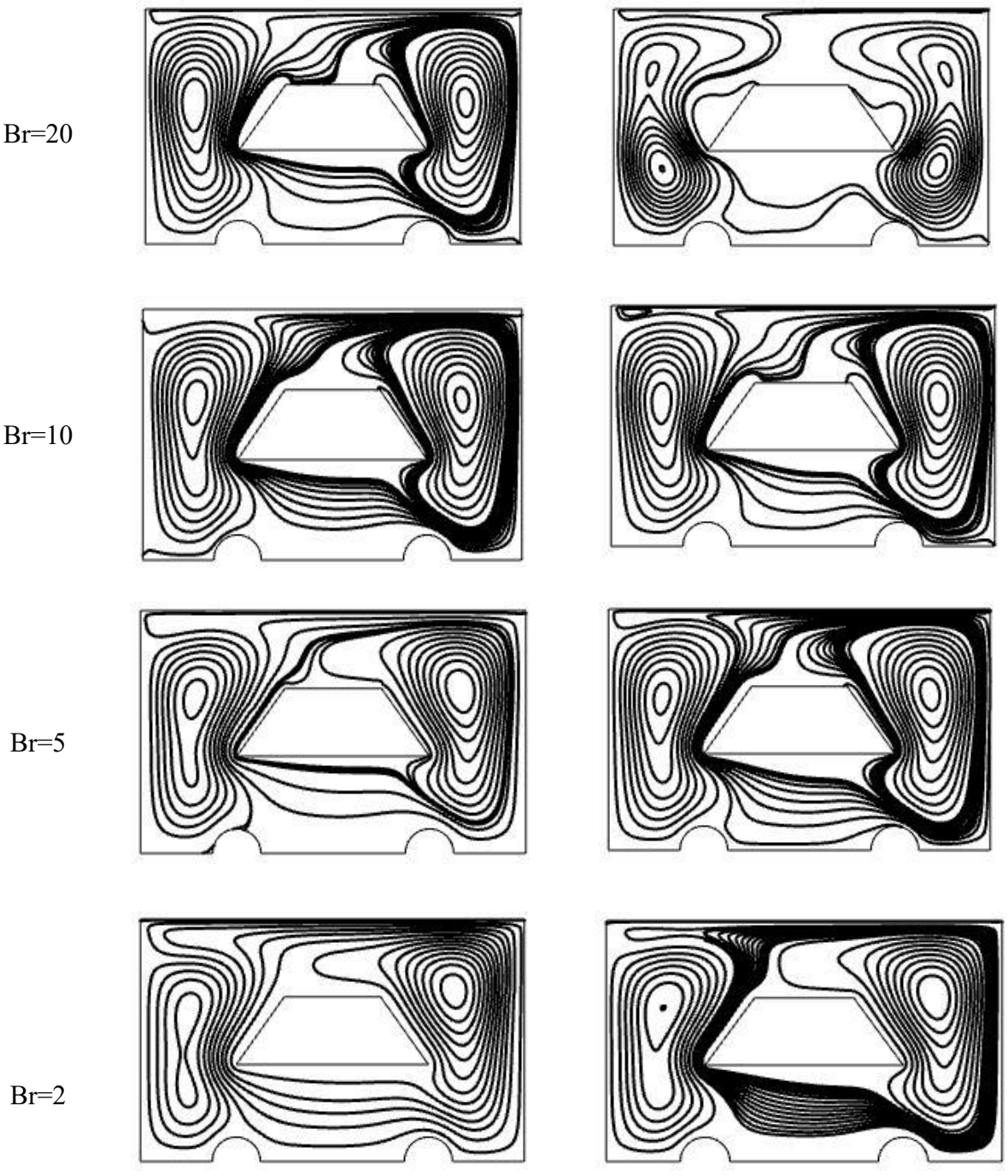

Figure 6.14: Streamlines for different values of Br without MHD while Re=100, Pr=7, A=0.042 and Ri=5 & 10

The effect of fluid flow for the variations of *Br* and *Ha* in absence of magnetic field with trapezoidal heated block, the overall features are illustrated in figure 6.13 and figure 6.14. In forced convection region (*i.e. Ri=0.1*) a uni-cellular vortex is characterized within

the whole cavity for all values of *Br*. The density of streamlines is high at the right top side of the heated obstacle because of the movement of upper lid. For highest value of *Br* a small single vortex is also formed at lower left side of the heated obstacle. At mixed convection region (*i.e. Ri=1*) the small vortex become large. With the increase of *Br* the streamlines are accumulated at the right side of the heated obstacle and the small vortex become larger and taking position at the left side of the heated obstacle vertically. For highest value of *Br* a bi-cellular vortex form at the two side of the heated obstacle.

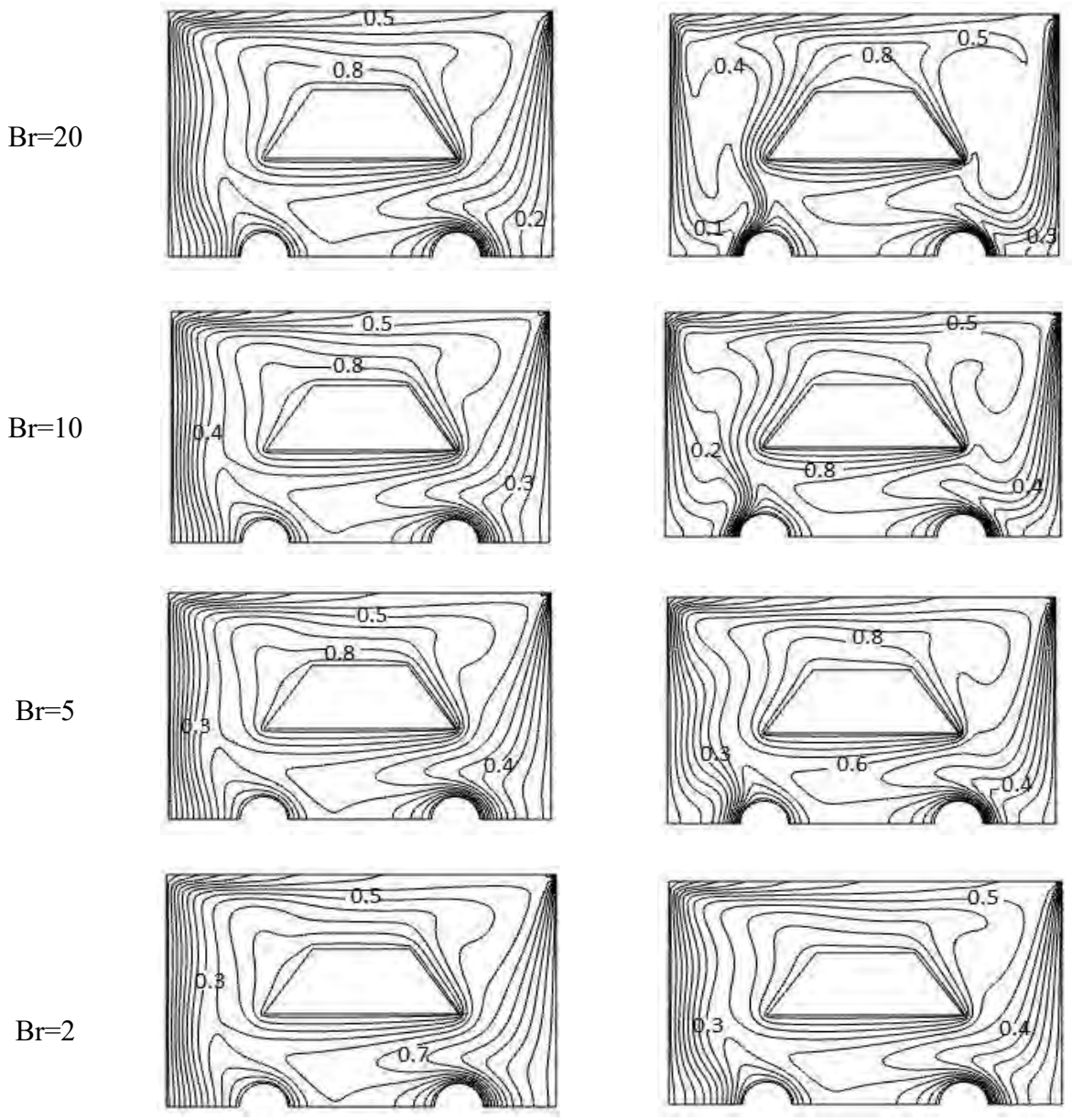

Figure 6.15: Isotherm for different values of Br without MHD while Re=100, Pr=7, A=0.042 and Ri=0.1 & 1

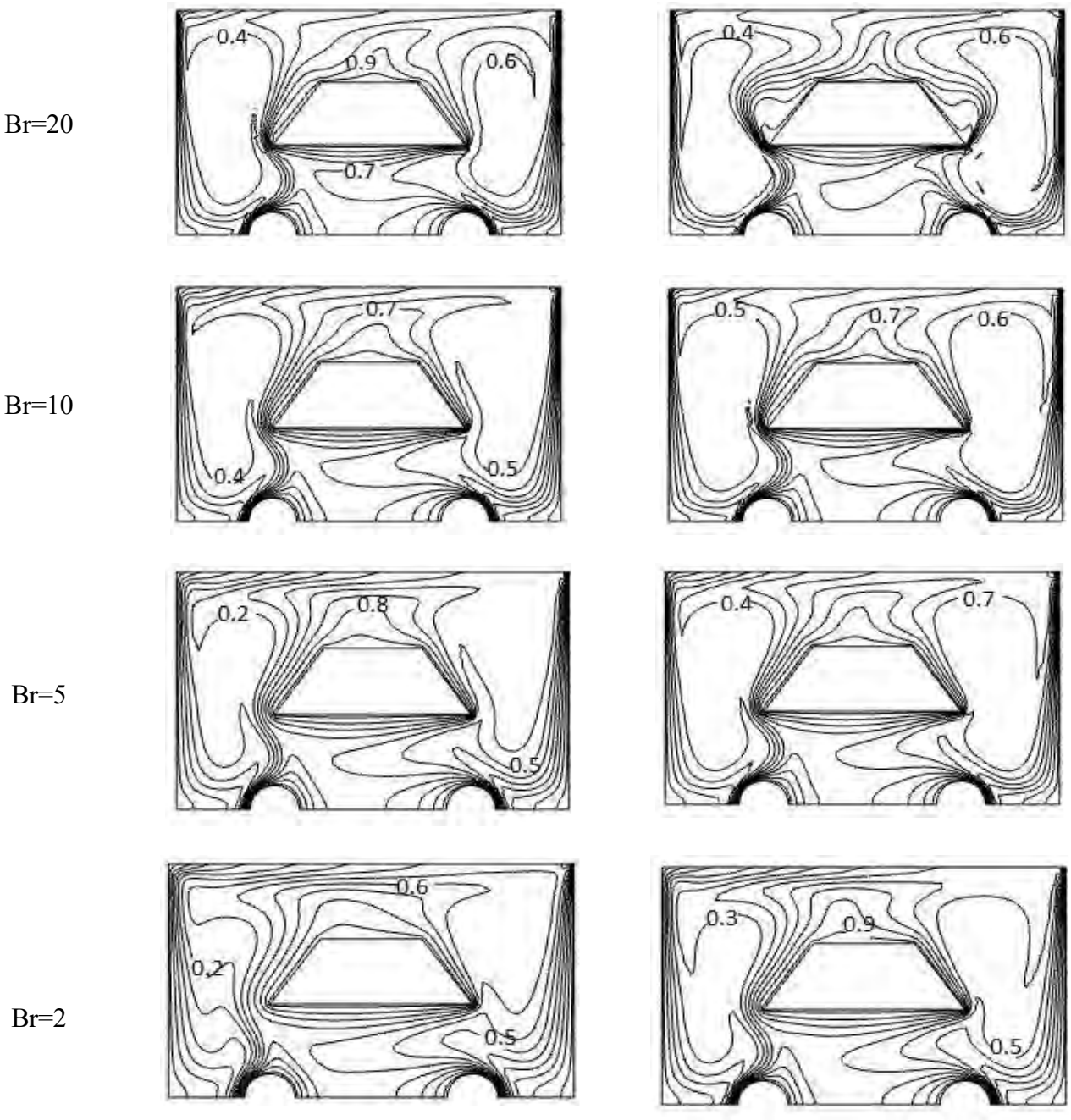

Figure 6.16: Isotherm for different values of Br without MHD while Re=100, Pr=7, A=0.042 and Ri=5 & 10

The density of streamlines are high at the right side of the heated obstacle in absence of MHD because of the moving lid. For further increase of *Ri* i.e. at natural convection region

6.1.6 Effect of fluid flow and temperature with rectangular obstacle without magnetic field for different values of buoyancy ratio and Richardson number:

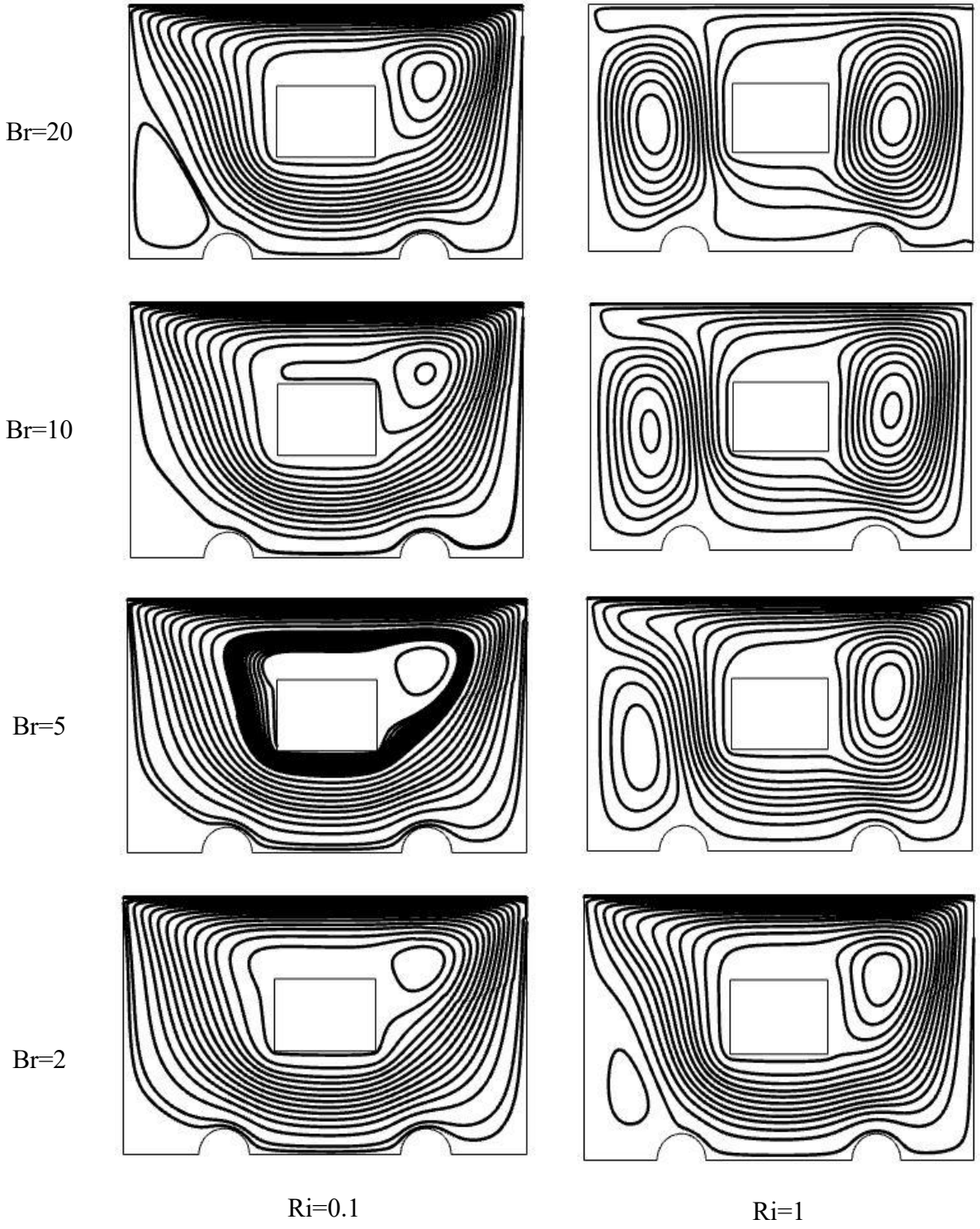

Figure 6.17: Streamlines for different values of Br without MHD while Re=100, Pr=7, A=0.028 and Ri=0.1 & 1

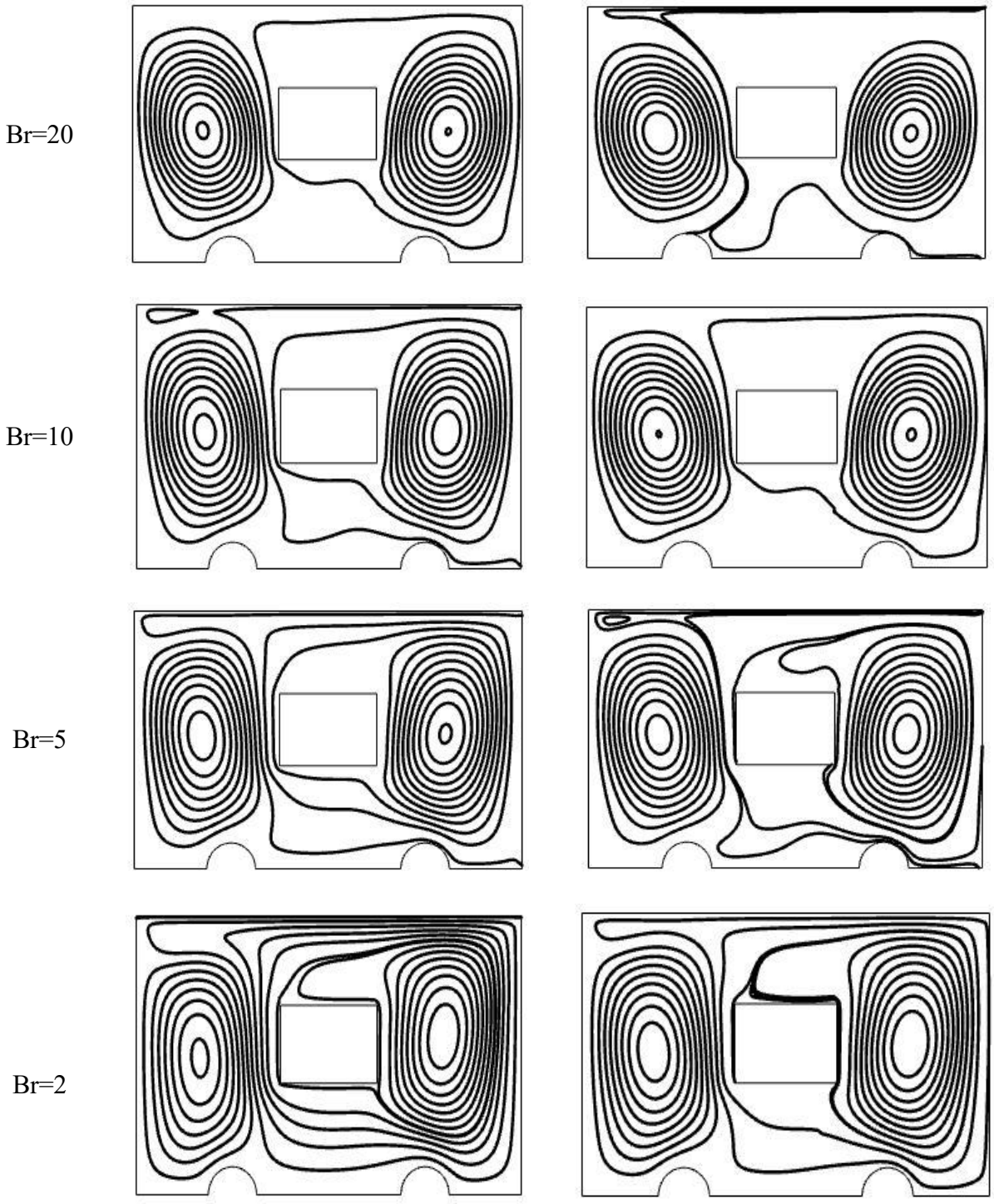

Figure 6.18: Streamlines for different values of Br without MHD while Re=100, Pr=7, A=0.028 and Ri=5 & 10

streamlines are divided into two parts at the both side of heated obstacle. In this case it is also looks symmetric for highest value of *Br* in absence of MHD.

The effect of temperature for the variations of *Br* and *Ri* in absence of MHD with trapezoidal heated obstacle, the overall features are illustrated in figure 6.15 and figure 6.16. At forced convection region (*i.e. Ri=0.1*) isotherms are rotated in parallel form around the heated obstacle and the two semi-circular wall heater. But the disturbance is observed at the right side of the heated obstacle and around the right semi-circular wall heater because of the moving lid for all values of *Br*. At mixed convection region (*i.e. Ri=1*) the disturbance in isotherm is increased. In this region it is observed that, the pattern of disturbance are not similar for the both sides of heated obstacle. At the left side isotherms are in zigzag pattern in parallel form but at the right

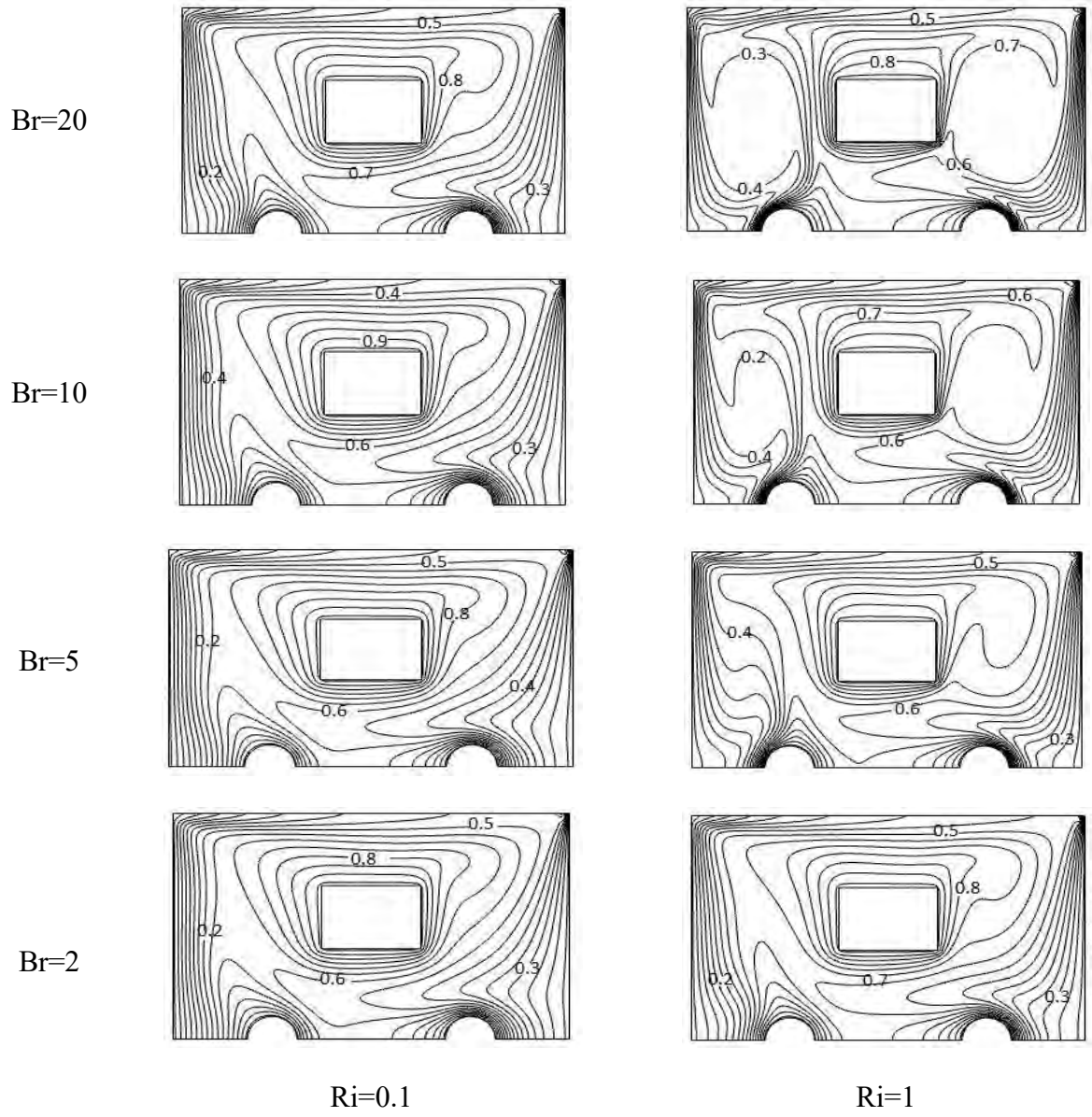

Figure 6.19: Isotherm for different values of Br without MHD while Re=100, Pr=7, A=0.028 and Ri=0.1 & 1

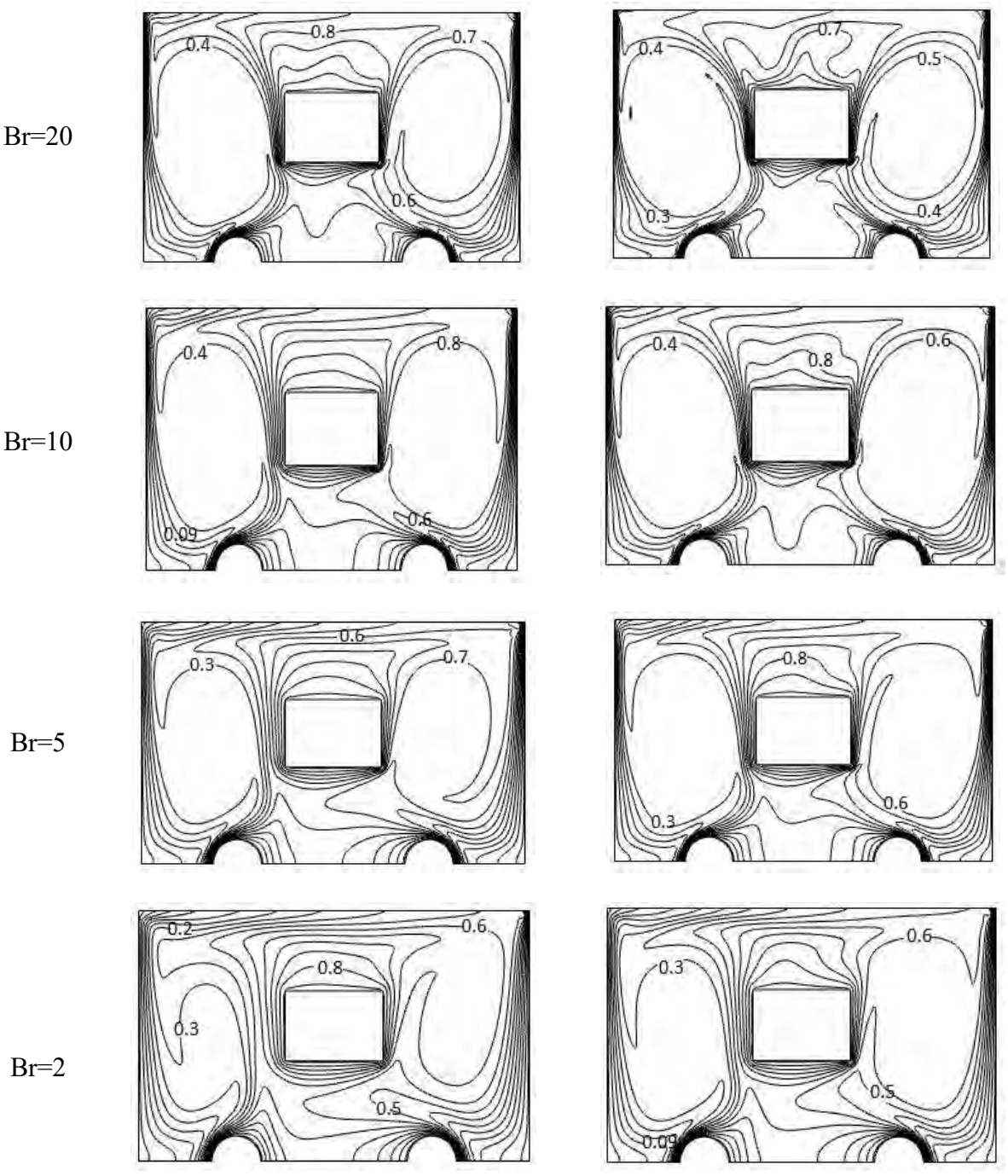

Figure 6.20: Isotherm for different values of Br without MHD while Re=100, Pr=7, A=0.028 and Ri=5 & 10

6.1.7 Effect of fluid flow and temperature with trapezoidal obstacle with magnetic field for different values of buoyancy ratio and Richardson number:

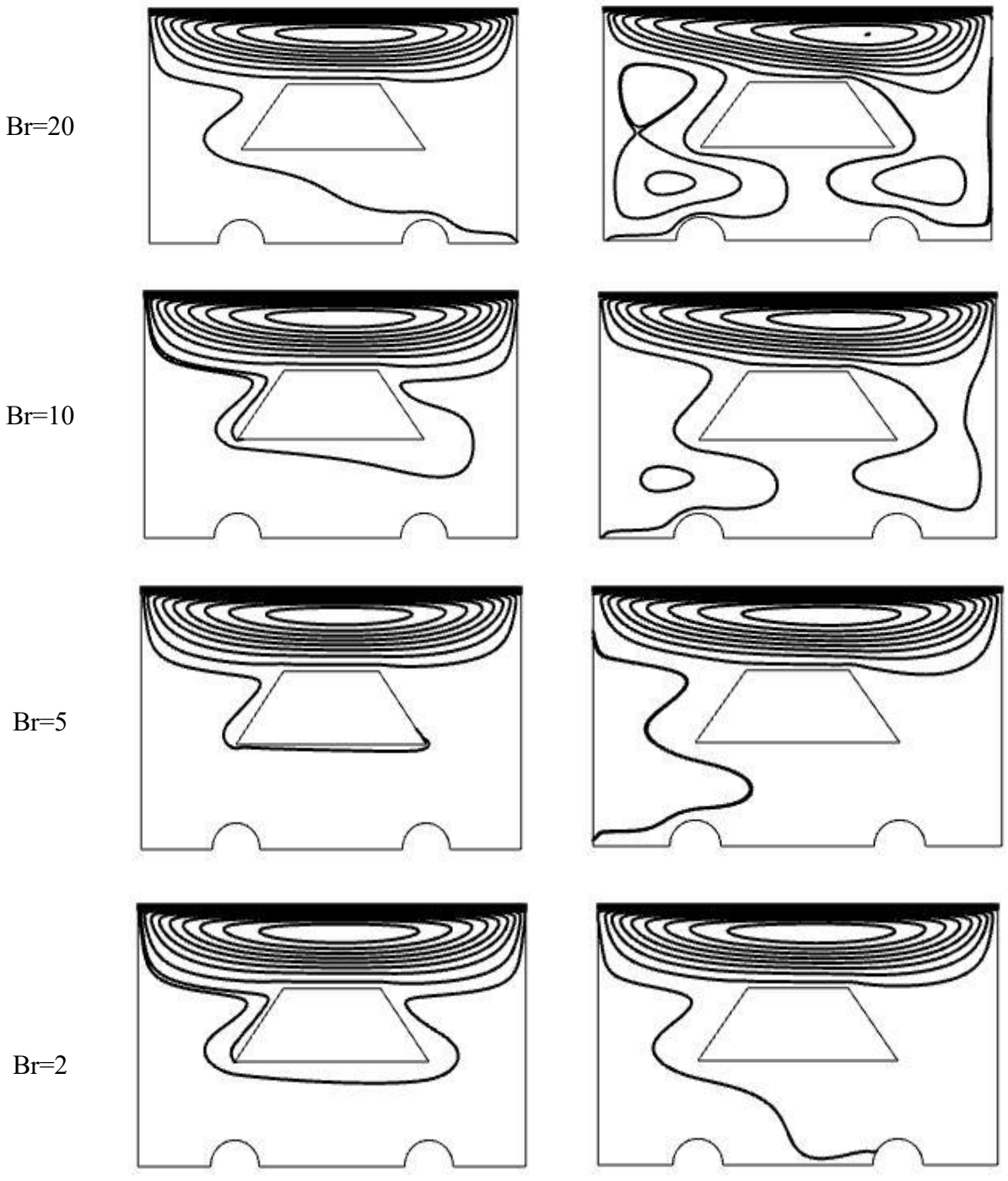

Figure 6.21: Streamlines for different values of Br with Ha=150 while Re=100, Pr=7, A=0.042 and Ri=0.1 & 1

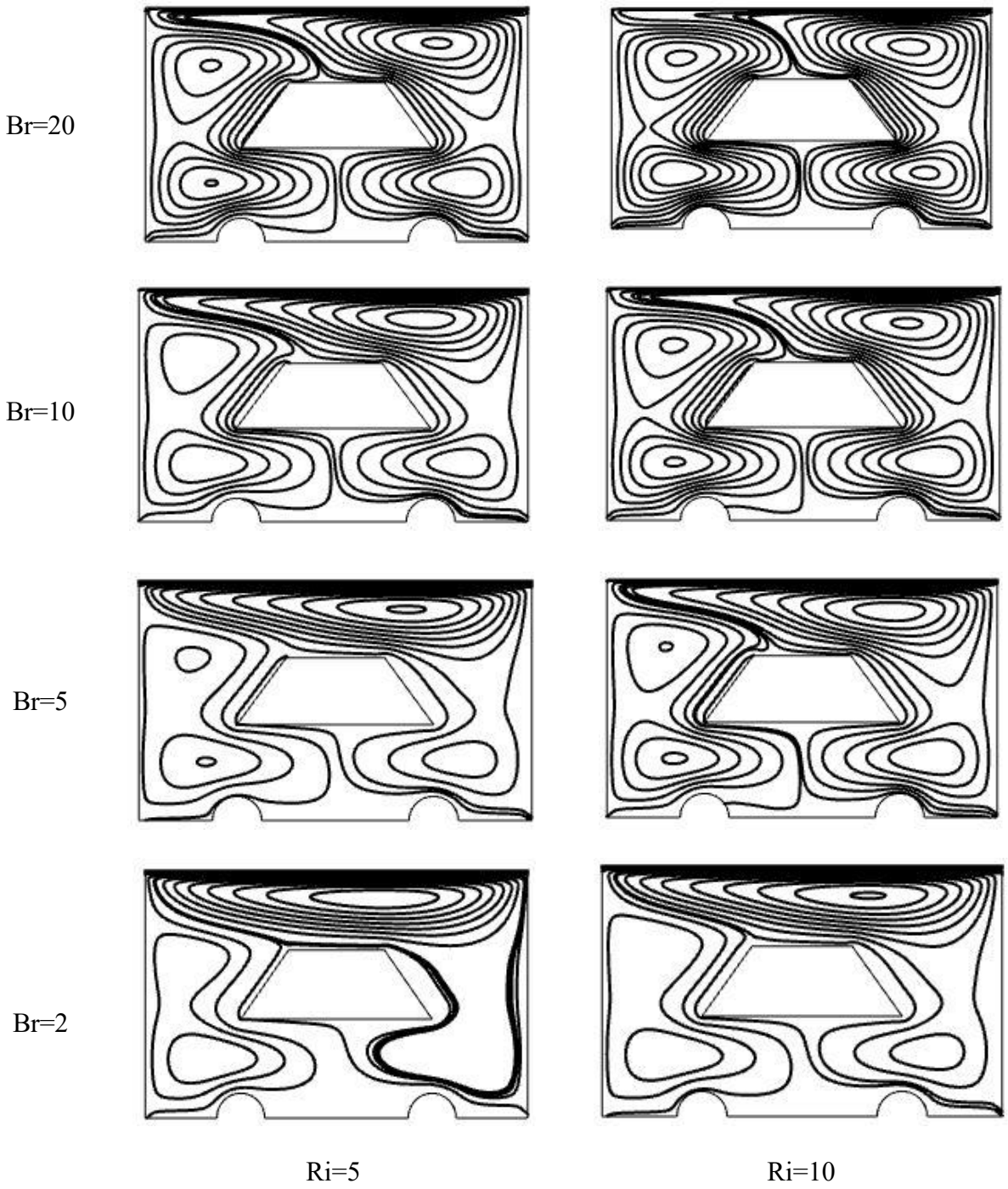

Figure 6.22: Streamlines for different values of Br with Ha=150 while Re=100, Pr=7, A=0.042 and Ri=5 & 10

side isotherms are in zigzag pattern which are not in parallel form. Also the temperature is higher at the right side of the heated obstacle than the left side of the heated obstacle. Isotherms are almost parallel at the two vertical cold walls. The difference at the two sides of heated obstacle is because of the moving lid in the positive x-direction and the increasing value of *Br*. At natural convection region (*i.e. Ri=10*) the disturbance increased and two void

created at the two sides of the heated obstacle. Also these voids looks like mango-seeds. Also temperature is higher at right side of the heated obstacle than the left side of the heated obstacle.

The effect of fluid flow for the variations of *Br* and *Ri* in absence of MHD with rectangular heated obstacle, the overall features are shown in figure 6.17 and figure 6.18. At forced convection region (*i.e. Ri=0.1*) a uni-cellular vortex characterized for all values of *Br*.

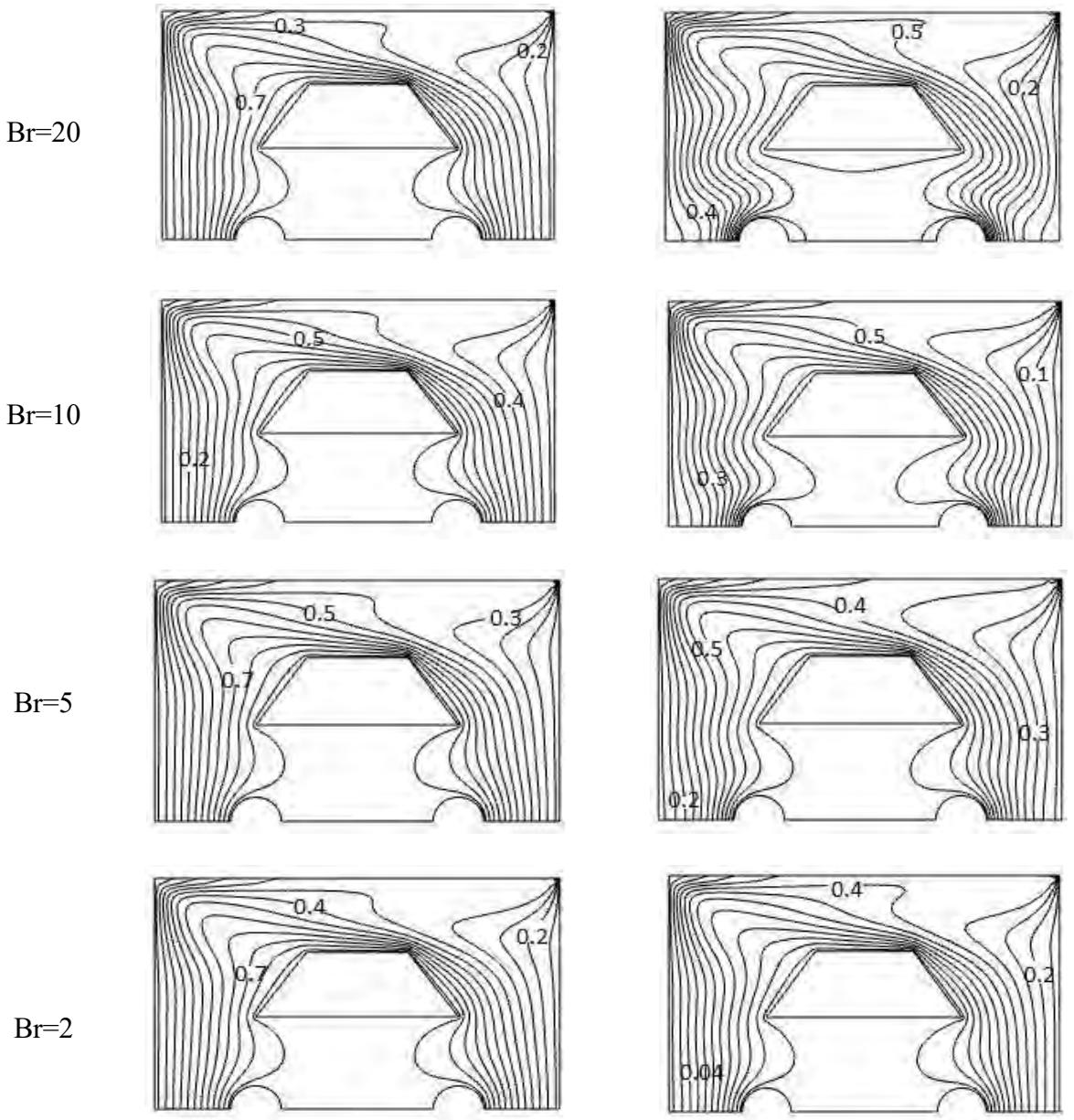

Figure 6.23: Isotherm for different values of Br with Ha=150 while Re=100, Pr=7, A=0.042 and Ri=0.1 & 1

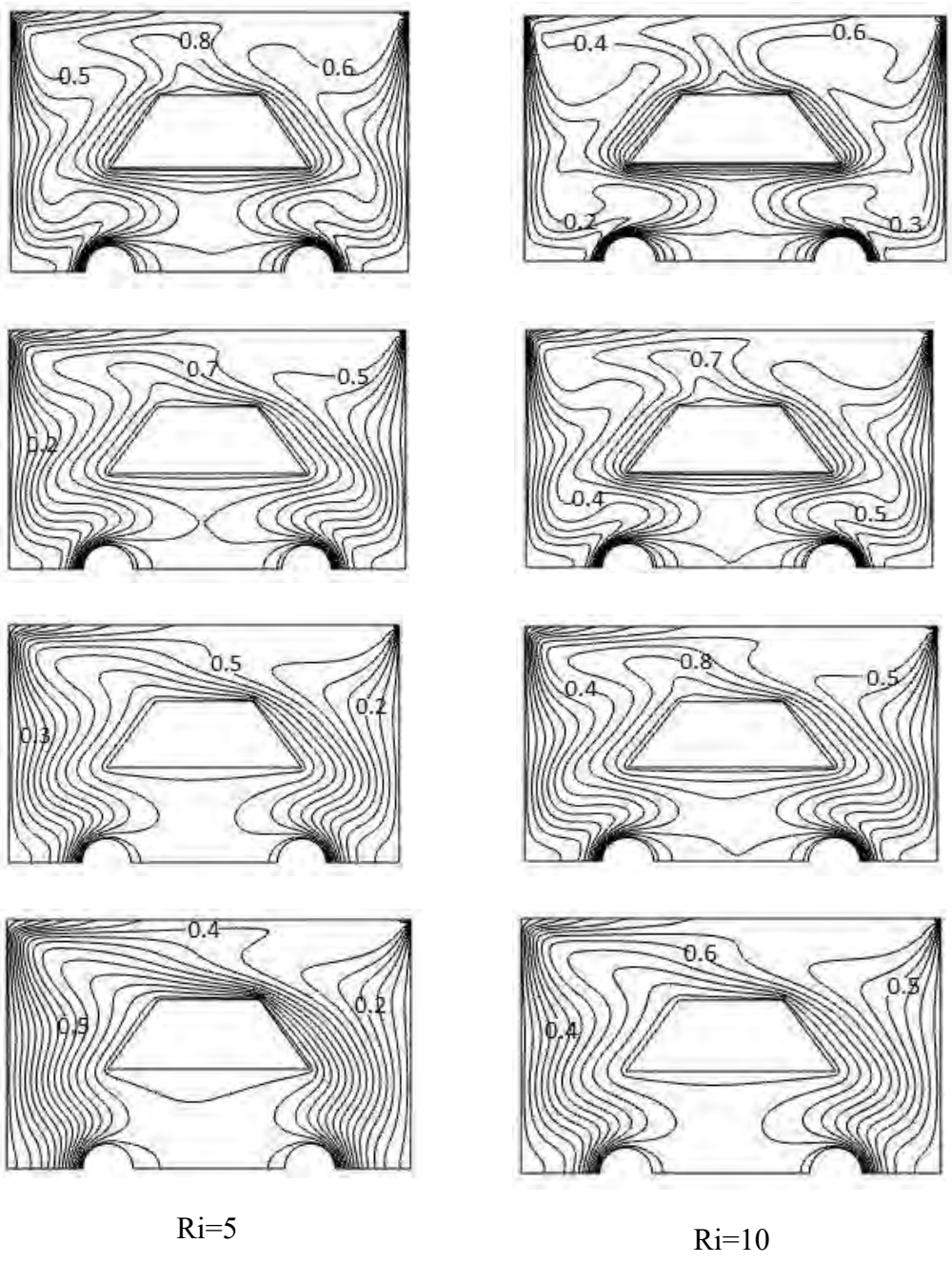

Figure 6.24: Isotherm for different values of Br with Ha=150 while Re=100, Pr=7, A=0.042 and Ri=5 & 10

At low value of *Br* the density of streamlines increases around the rectangular heated obstacle. With the increase of *Br* the density decreases around the heated rectangular obstacle. At highest value of *Br* a oval shape vortex is observed at the left corner of the cavity and the density increases at the right vertical wall. At mixed convection region (*i.e. Ri=1*) the oval shape vortex become large for the lowest value of *Br*. With the increase of *Br* this oval shape vortex become larger and bi-cellular vortex formed at the right and left side of the

heated obstacle. The density of streamlines are higher at the right side of the heated obstacle than the left side. At natural convection dominated region *(i.e. Ri=10*) with the increase of *Br* in absence of MHD streamlines

6.1.8 Effect of fluid flow and temperature with rectangular obstacle with magnetic field for different values of buoyancy ratio and Richardson number:

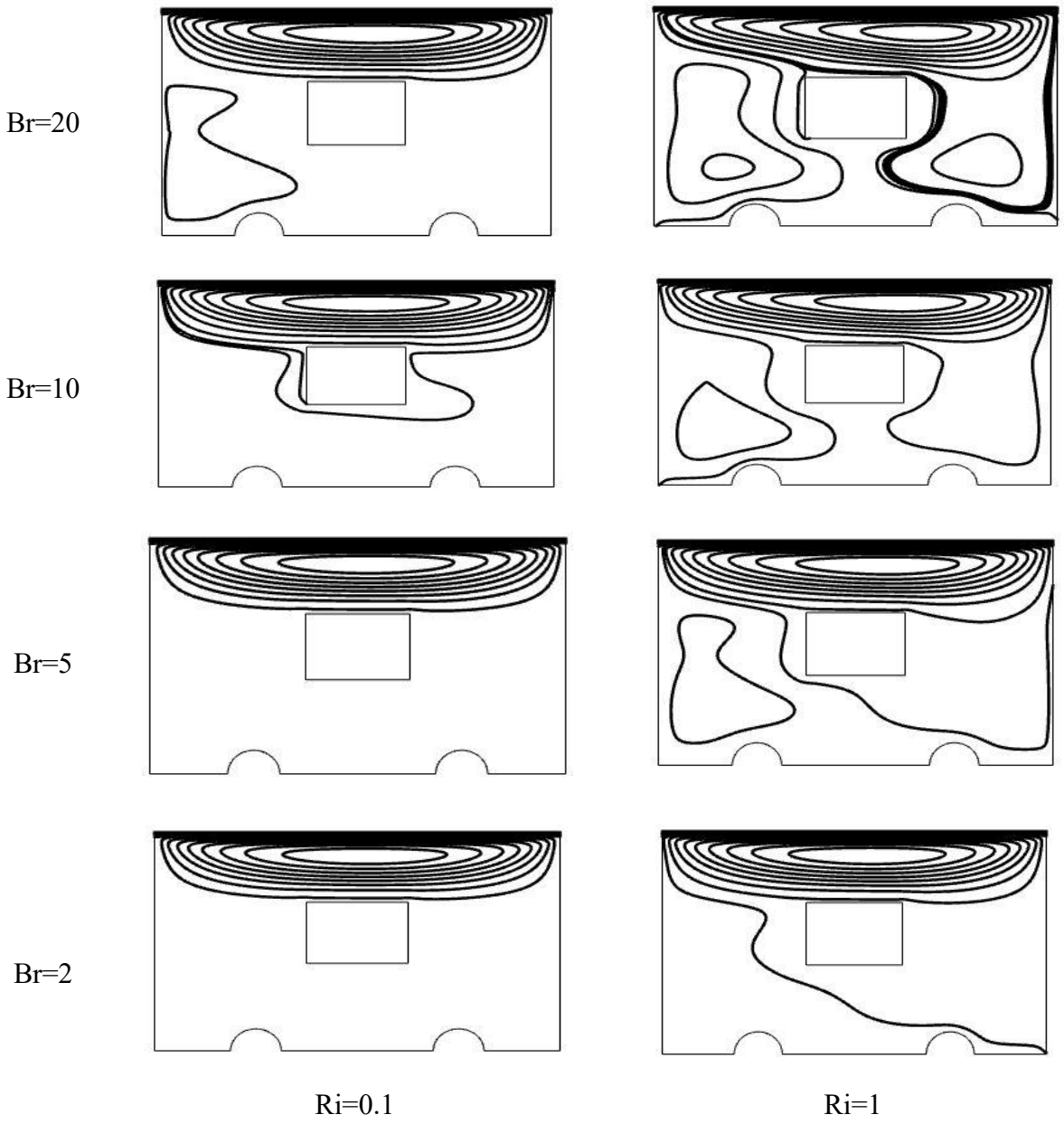

Figure 6.25: Streamline for different values of Br with Ha=150 while Re=100, Pr=7, A=0.028 and Ri=0.1 & 1

divided into two parts and situated at the left and right side of the heated rectangular obstacle and they are symmetric.

The corresponding effect on temperature for the variations of *Br* and *Ri* with rectangular heated block in absence of MHD, the overall features are illustrated in figure 6.19 and figure 6.20. At forced convection region isotherms are rotated parallel around the heated rectangular block and the two semi-circular wall heater. Some isotherms are bended at the right semi-circular wall heater but they bended in parallel form for all values of *Br.* With the increase of *Ri i.e.* at mixed convection region *Ri=1*, the nonlinearity increases at both sides around the heated obstacle. For highest value of Br the isotherm lines are accumulated at the two vertical wall and makes oval shape voids on both sides of the heated rectangular obstacle. Also the temperature at right side is higher than the temperature at the left side. Further increase of *Ri* with the increase of Br isotherm lines form more clear oval shape voids and they looks symmetric. Only the disturbance is found at the top of the heated rectangular obstacle. Also the temperature is high at the right side than the left side.

The effect of fluid flow for different values of *Br* and *Ri* with the trapezoidal obstacle and fixed *Ha=150*, the overall features are illustrated in figure 6.21 and figure 6.22. At the forced convection region i.e. *Ri=0.1*, all the streamlines are accumulated at the top of the heated trapezoidal block for each value of *Br*. At mixed convection region i.e. *Ri=1*, with the increase of *Br* a single vortex is formed. At highest value of *Ha*, the fluid flow experiences a Lorentz force due to the influence of the magnetic field. Further increase of *Ri i.e.* at natural convection region *Ri=10*, streamlines creates a bi-cellular vortex at the left and right side of the block. The heated block divided the vortex into two parts and they looks symmetric.

The corresponding effect of temperature are shown in figure 6.23 and figure 6.24. Isotherm lines are almost parallel in forced and mixed convection region. With the increase of *Ri* isotherm lines become nonlinear. At natural convection region the nonlinearity become higher and plume formation is profound at the left and right side of the heated block.

The effect of fluid flow for variations *Br* and *Ri* with rectangular heated block and fixed *Ha=150*, the overall features are illustrated in figure 6.25 and figure 6.26. We observed that the results in this case is similar as shown in figure 6.21 and figure 6.22.

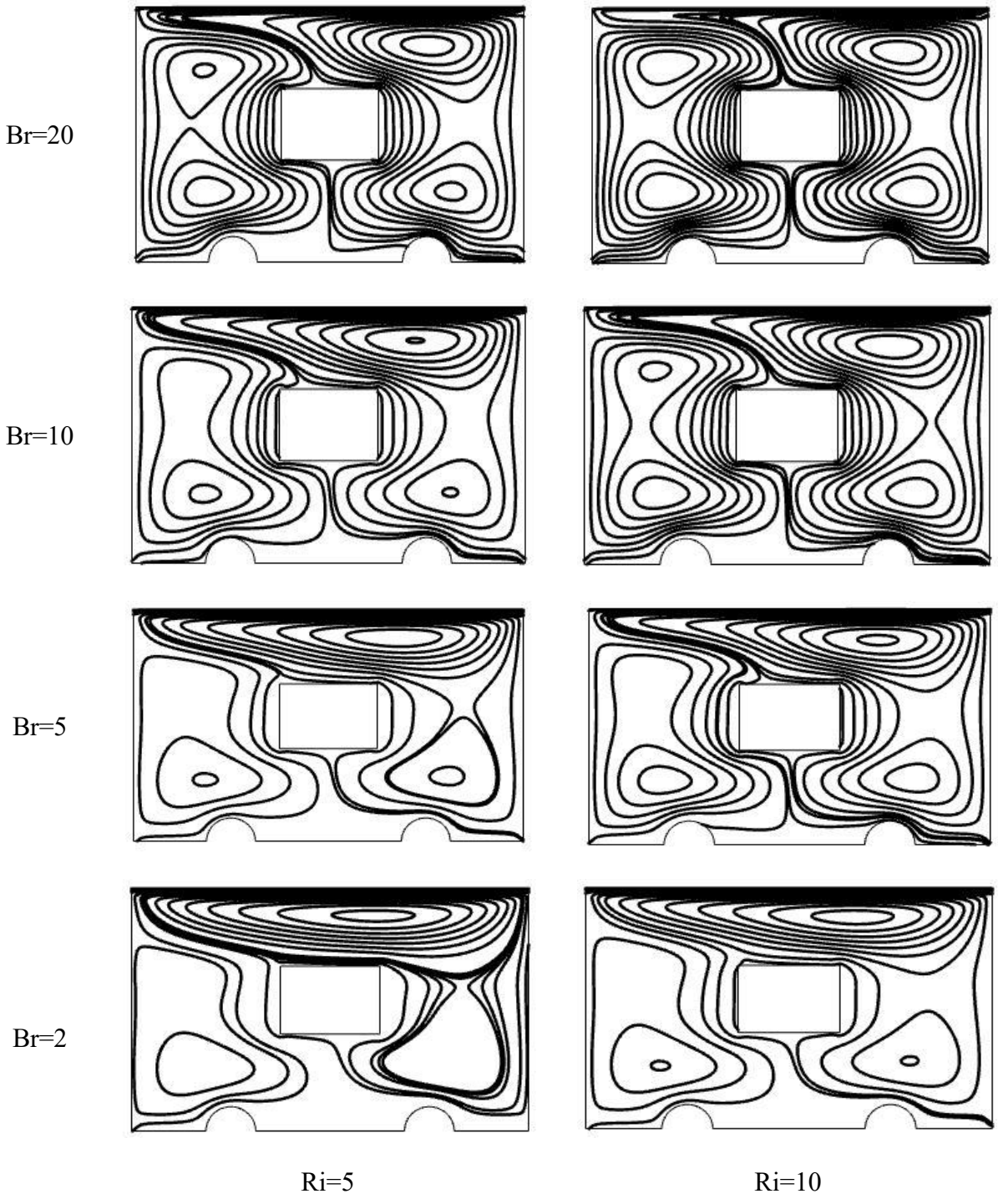

Figure 6.26: Streamline for different values of Br with Ha=150 while Re=100, Pr=7, A=0.028 and Ri=5 & 10

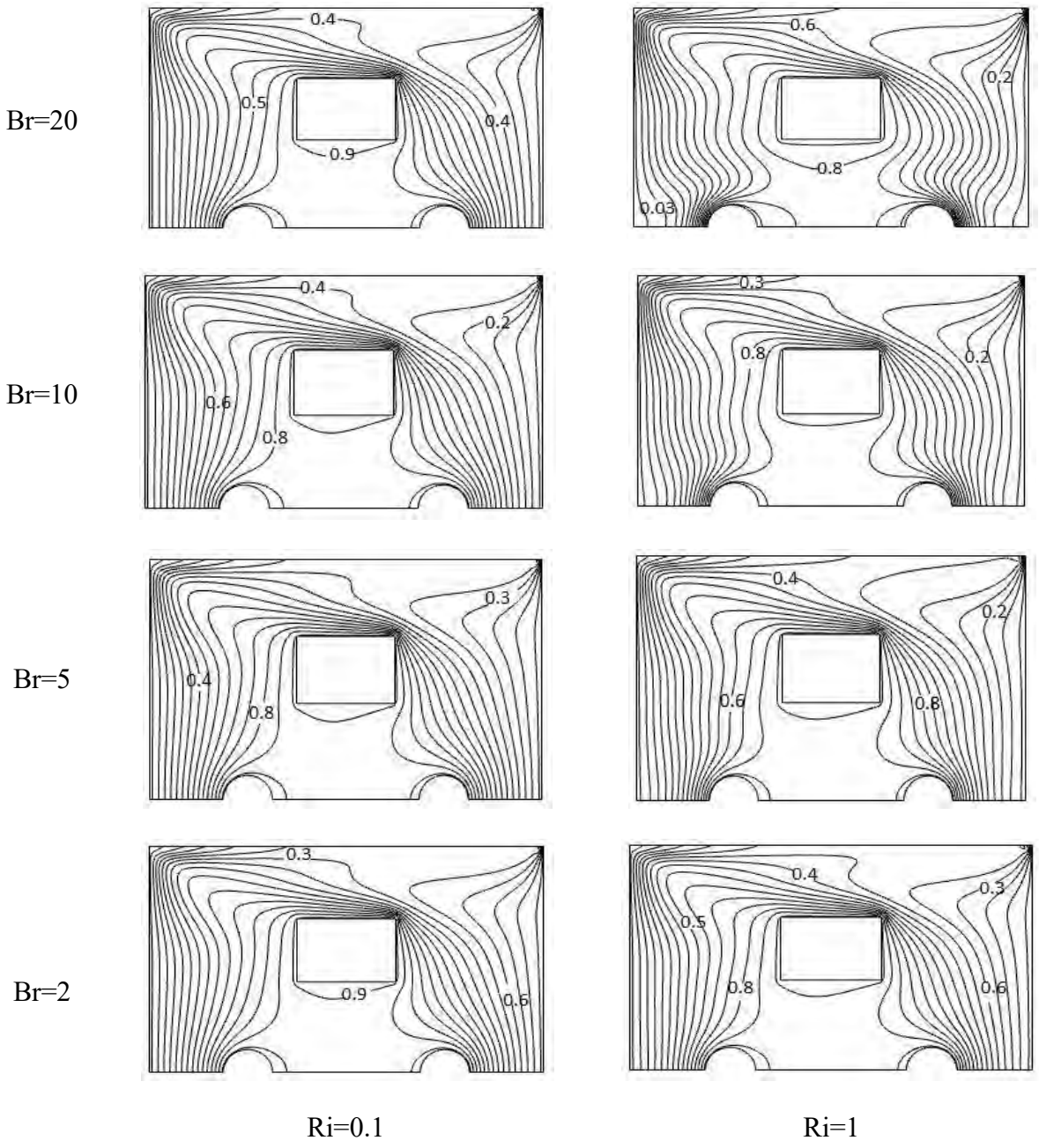

Figure 6.27: Isotherm for different values of Br with Ha=150 while Re=100, Pr=7, A=0.028 and Ri=0.1 & 1

The corresponding effect of temperature the variations of *Br* and *Ri* and fixed *Ha=150* with rectangular heated block, the overall features are shown in figure 6.27 and figure 6.28. This results is similar as the results shown in figure 6.23 and figure 6.24.

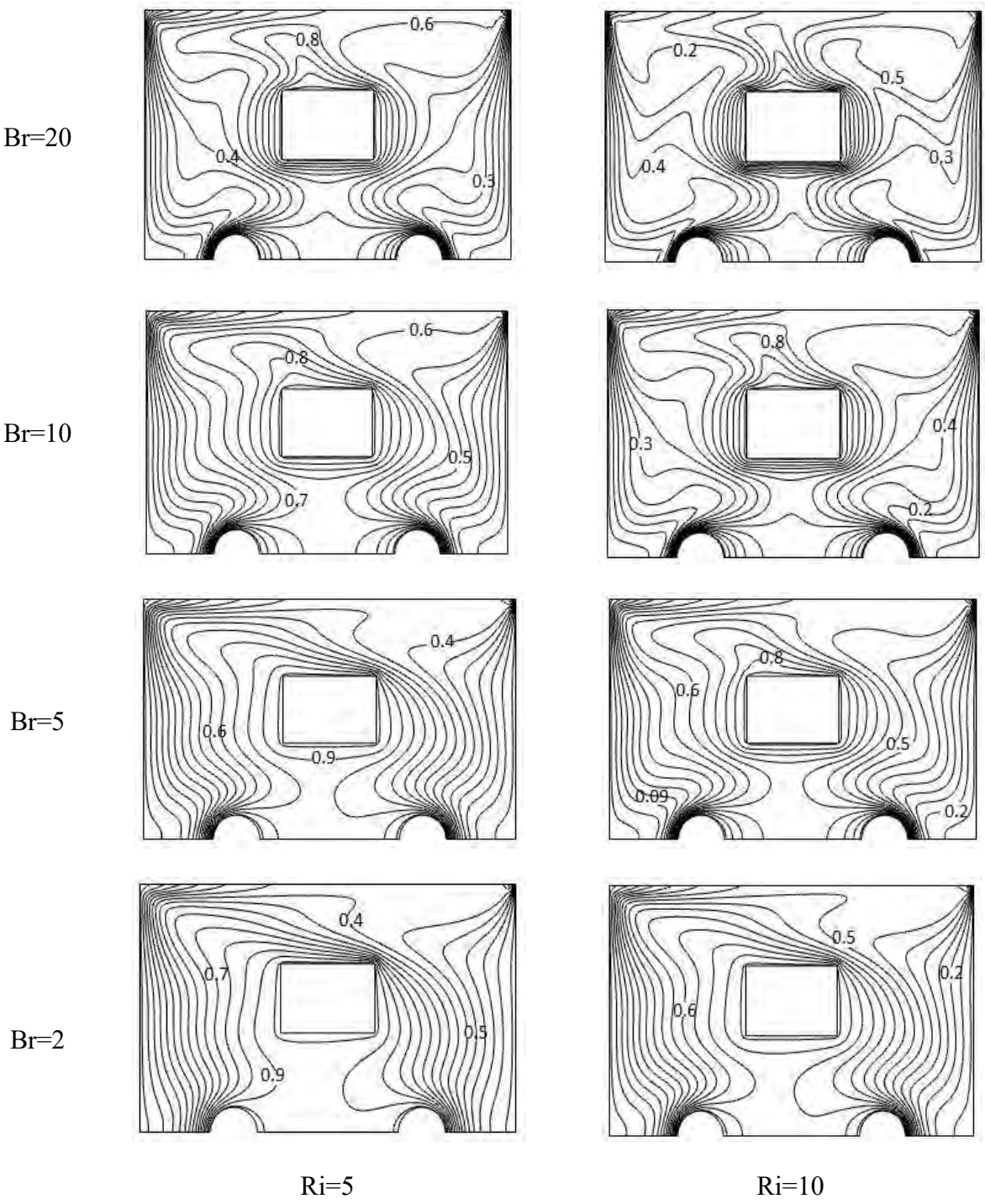

Figure 6.28: Isotherm for different values of Br with Ha=150 while Re=100, Pr=7, A=0.028 and Ri=5 & 10

6.2 Heat Transfer Rates: Average Nusselt number Vs the effect of various parameters

In order to evaluate how different shapes of heated obstacle effect heat transfer rate or how variations of parameter effect the heat transfer rate the following figures are illustrated. Figure 6.29 and figure 6.30 shows how different shapes of heated obstacle effect the heat transfer rate for different values of *Ri* without MHD along the left and right semi-circular wall heater. Heat transfer rate is higher with rectangular heated obstacle than the trapezoidal heated obstacle along the left and right semi-circular wall heater. But the difference between heat transfer is high at the right semi-circular wall heater than the left semi-circular wall heater. This means that, heat transfer rate is high at the right semi-circular wall heater for two different shapes of heated obstacle. i.e. when the area of heated obstacle decreases heat transfer rate increases along the both semi-circular wall heater.

To evaluate the effect of different shapes of obstacle in presence of magnetic field how heat transfer rate behave along the two semi-circular wall heater we illustrate figure 6.31 and figure 6.32. We observed that, heat transfer rate is high for rectangular obstacle than the trapezoidal obstacle along the two semi-circular wall heater. But the difference between heat transfer rate is decreases in both case in presence of MHD. Also the value of heat transfer rate is almost same along the left and right semi-circular wall heater in presence of MHD.

Figure 6.33 and figure 6.34 shows the effect of hear transfer rate for different values of *Ha* with trapezoidal heated obstacle along the left and right semi-circular wall heater. Along the left semi-circular wall with trapezoidal heated obstacle in absence of magnetic field heat transfer rate is highest for all values of *Ri* except natural convection dominated region. In the forced convection to mixed convection dominated region it increases gradually but in the mixed to natural convection dominated region in increases abruptly. Presence and increasing values of magnetic field decreases the heat transfer rate. In presence of magnetic field, heat transfer decreases slightly in the region $\mathbf{0.1} \leq \boldsymbol{Ri} \leq \mathbf{1}$ but it decreases abruptly in the region $\mathbf{1} \leq \boldsymbol{Ri} \leq \mathbf{10}$. In absence of MHD and low values of *Ha* , the highest value of heat transfer rate is same for natural convection dominated region along the left semi-circular wall heater with trapezoidal obstacle. But this value is not same along the right semi-circular wall heater. For highest value of *Ha* heat transfer rate is same for all values of *Ri* along the two semi-circular wall heater.

6.2.1 Effect of Average Nusselt number for different values of Ri along the semi-circular wall heater for different obstacle without MHD

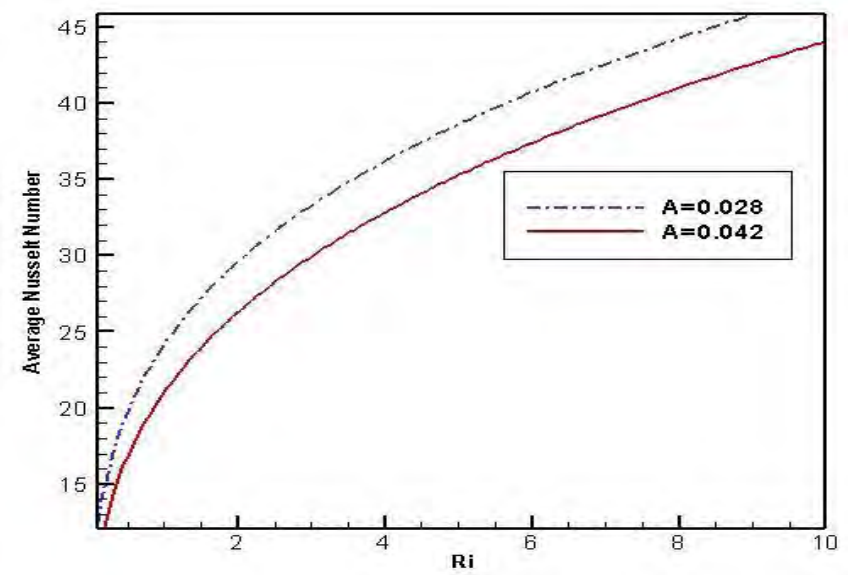

Figure 6.29: Average Nusselt number Vs Ri for different obstacle without MHD along the left semi-circular wall heater

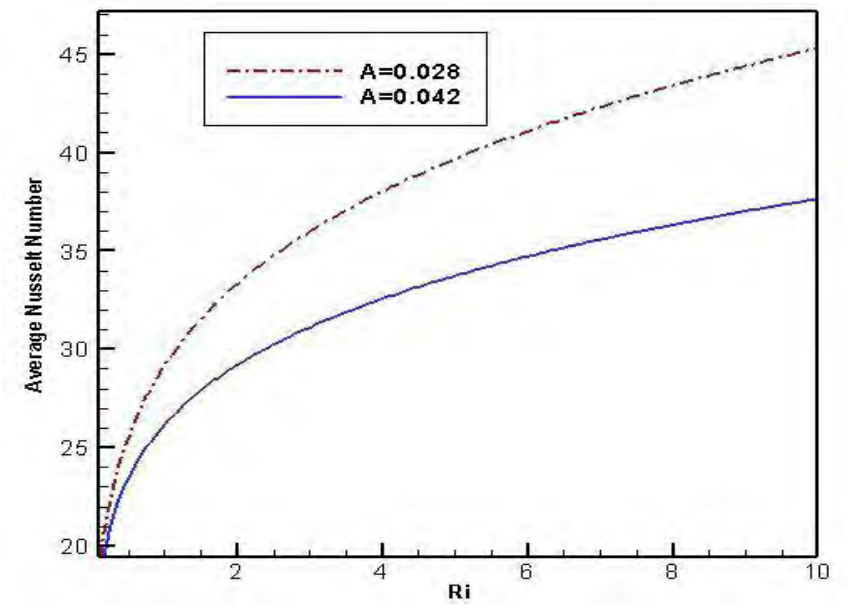

Figure 6.30: Average Nusselt number Vs Ri for different obstacle without MHD along the right semi-circular wall heater

6.2.2 Effect of Average Nusselt number for different values of Ri along the semi-circular wall heater for different obstacle with MHD

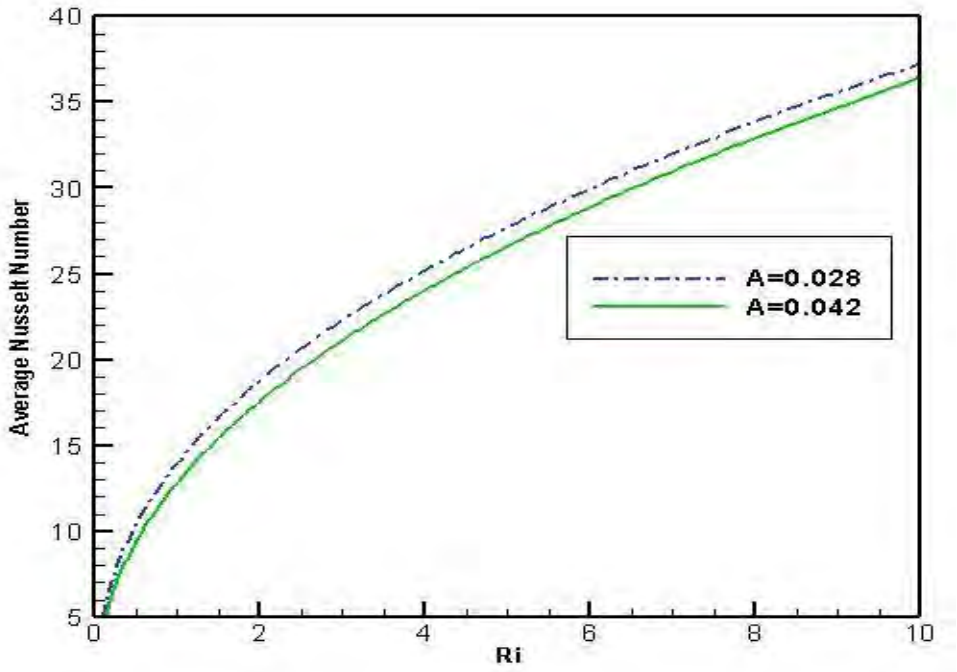

Figure 6.31: Average Nusselt number Vs Ri for different obstacle with MHD along the left semi-circular wall heater

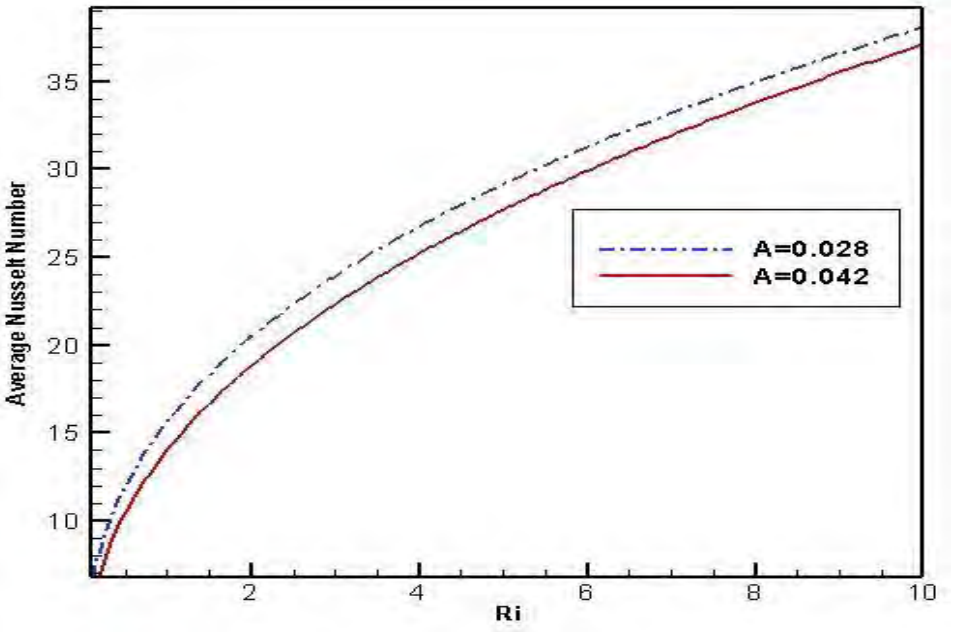

Figure 6.32: Average Nusselt number Vs Ri for different obstacle with MHD along the right semi-circular wall heater

6.2.3 Effect of Average Nusselt number Vs Ri along the semi-circular wall heater for different values of Ha with trapezoidal obstacle

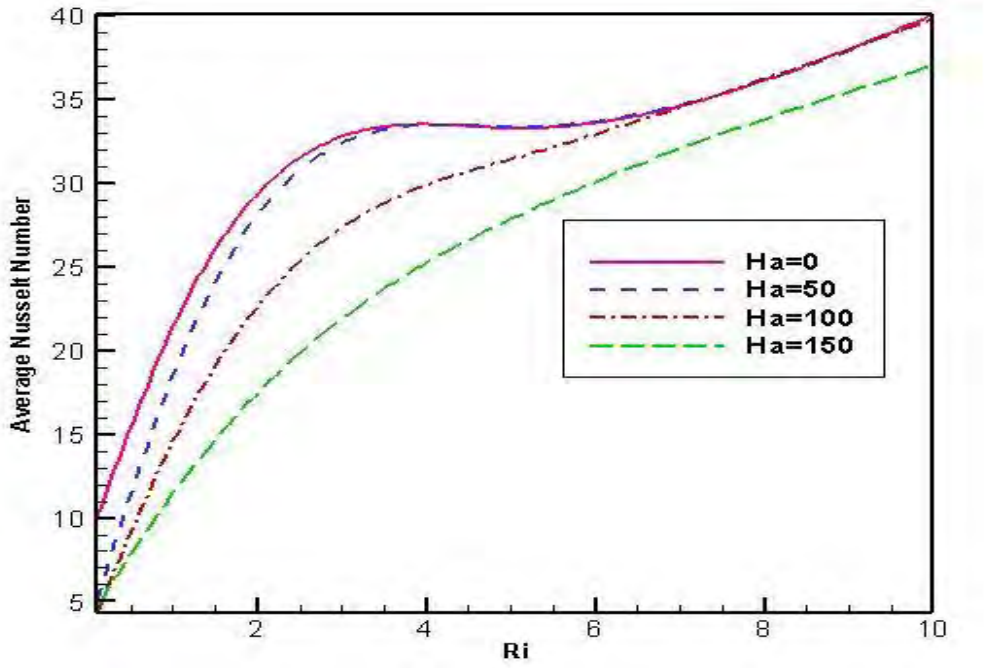

Figure 6.33: Average Nusselt number Vs Ri for different values of Ha with trapezoidal obstacle along the left semi-circular wall heater

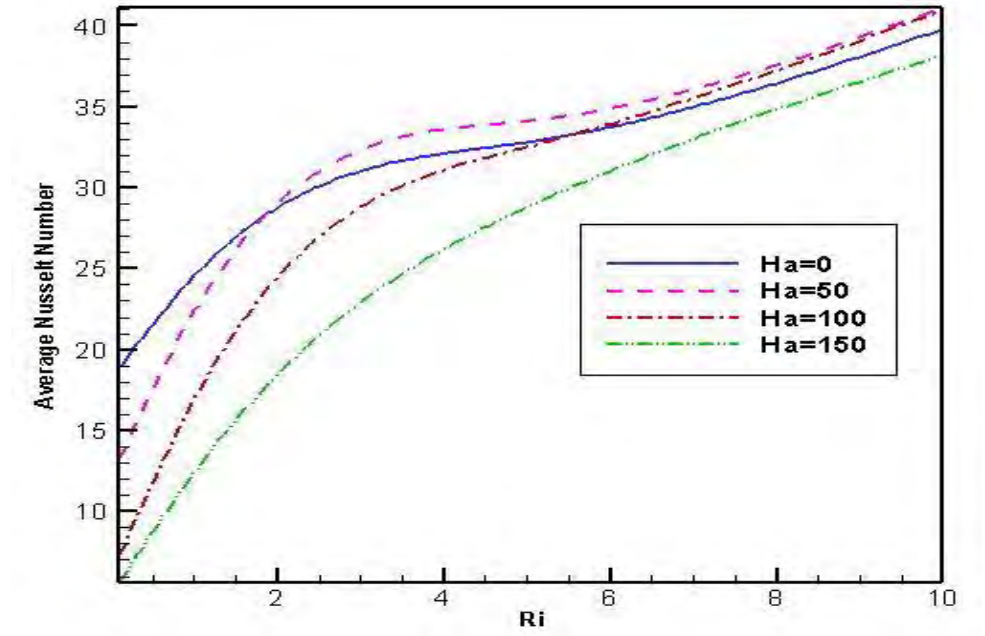

Figure 6.34: Average Nusselt number Vs Ri for different values of Ha with trapezoidal obstacle along the right semi-circular wall heater

6.2.4 Effect of Average Nusselt number Vs Ri along the semi-circular wall heater for different values of Ha with rectangular obstacle

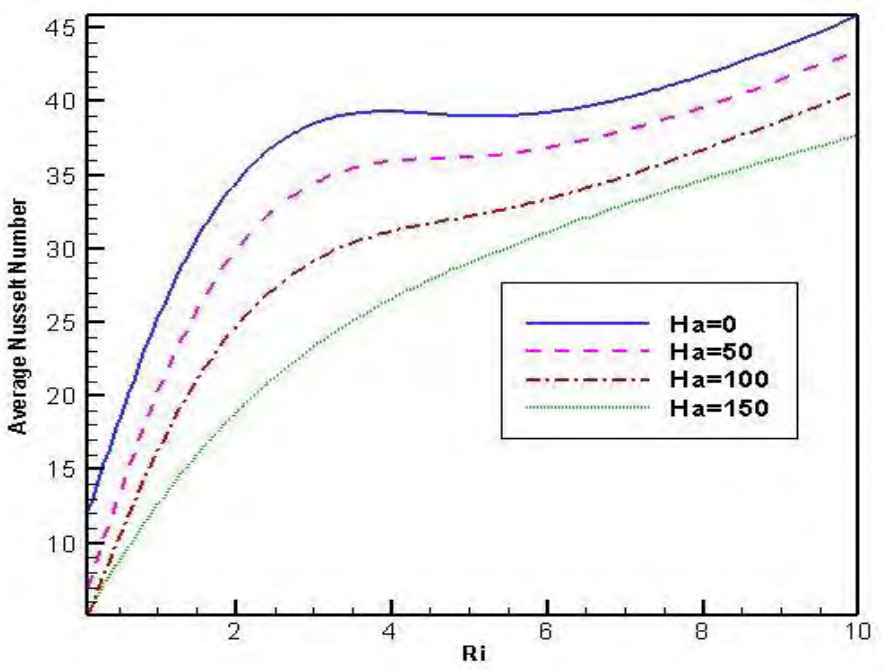

Figure 6.35: Average Nusselt number Vs Ri for different values of Ha with rectangular obstacle along the left semi-circular wall heater

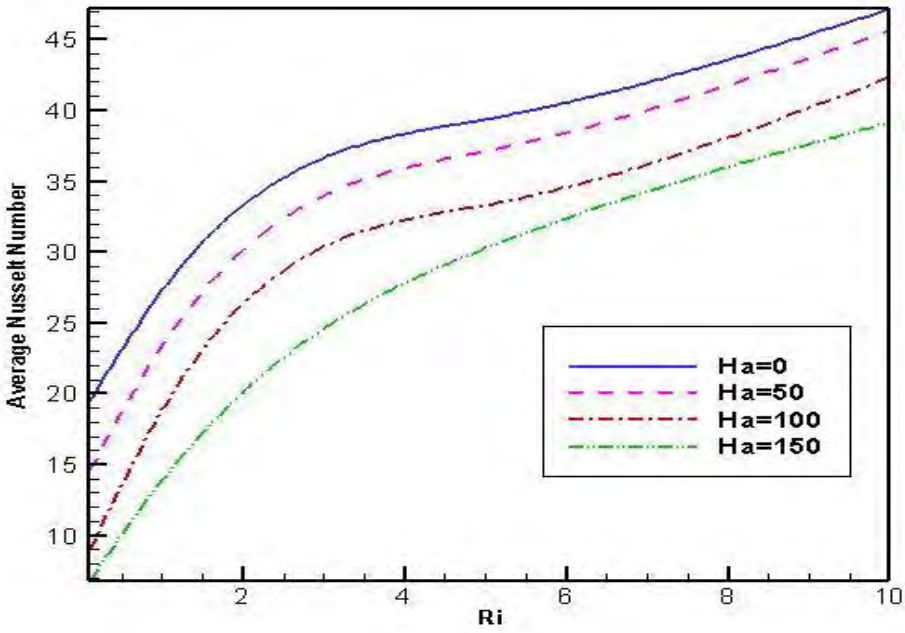

Figure 6.36: Average Nusselt number Vs Ri for different values of Ha with rectangular obstacle along the right semi-circular wall heater

6.2.5 Effect of Average Nusselt number Vs Ri along the semi-circular wall heater for different values of Br for trapezoidal obstacle with MHD

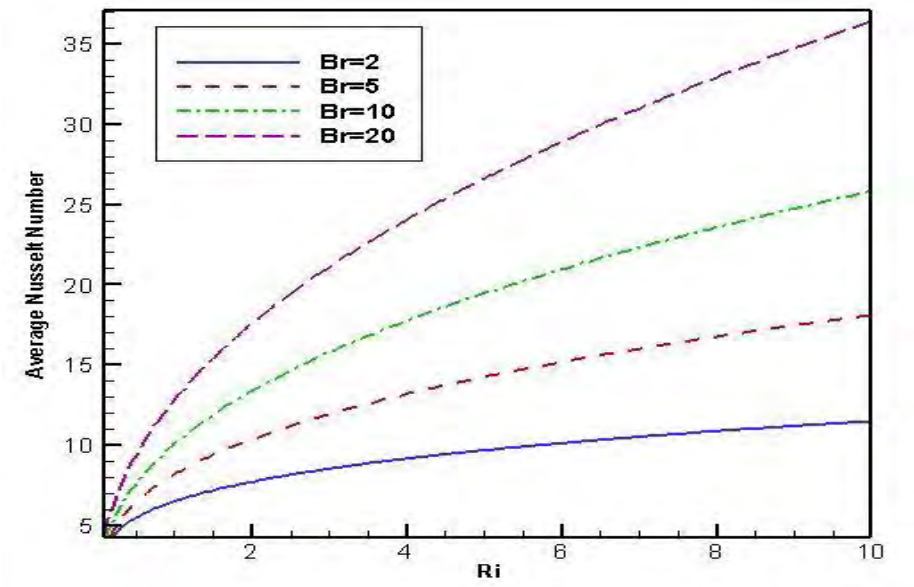

Figure 6.37: Average Nusselt number Vs Ri for different values of Br with MHD trapezoidal obstacle along the left semi-circular wall heater

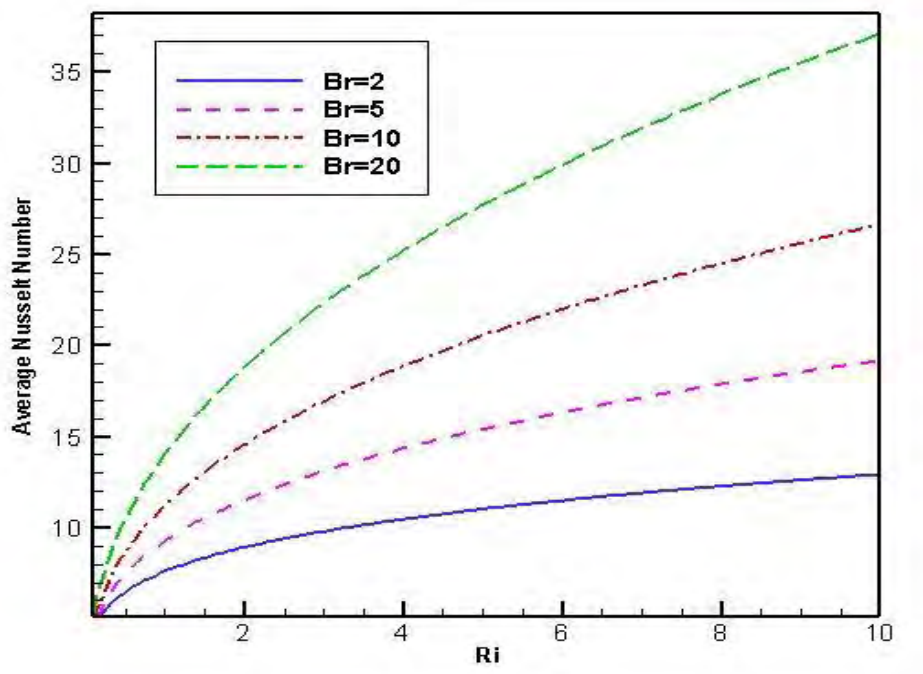

Figure 6.38: Average Nusselt number Vs Ri for different values of Br with MHD trapezoidal obstacle along the right semi-circular wall heater

Figure 6.35 and figure 6.36 shows the effect of heat transfer rate for different values of *Ha* with rectangular heated obstacle along the left and right semi-circular wall heater respectively. In absence of magnetic field, $\boldsymbol{Nu_{av}}$ is highest for all values of *Ri*. In the forced to mixed convection dominated region it increases gradually but in the mixed to natural convection region it increases abruptly. Presence and increasing value of magnetic field decreases the heat transfer rate. In presence of magnetic field $\boldsymbol{Nu_{av}}$ decreases slightly in the region $\boldsymbol{0.1 \leq Ri \leq 1}$ but it decreases abruptly in the region $\boldsymbol{1 \leq Ri \leq 10}$. For highest value of *Ha* the curve is smooth along the left and right semi-circular wall heater. With the increase of *Ha*, this four curve behaves parallel for both cases. Also heat transfer rate is high along the right semi-circular wall heater than the left semi-circular wall heater.

Figure 6.37 and figure 6.38 illustrates the effect of *Br* in presence of MHD with trapezoidal obstacle along the left and right semi-circular wall heater. This figures shows that for different values of *Br* heat transfer rate increases with the increases of *Ri*. Also heat transfer rate increases with the increases of *Br*. For highest value of *Br* heat transfer rate is high along the both left and right semi-circular wall heater. $\boldsymbol{Nu_{av}}$ increases slightly in the region $\boldsymbol{0.1 \leq Ri \leq 1}$ but increases abruptly in the region $\boldsymbol{1 \leq Ri \leq 10}$. For lowest value of *Br*, the variation of $\boldsymbol{Nu_{av}}$ is nominal in forced to mixed and mixed to natural convection region with trapezoidal obstacle along the two semi-circular wall heater.

Figure 6.39 and figure 6.40 shows the effect of *Br* in presence of MHD with rectangular heated obstacle along the left and right semi-circular wall heater. This figures shows the same results shown in figure 6.37 and figure6.38.

6.2.6 Effect of Average Nusselt number Vs Ri along the semi-circular wall heater for different values of Br for rectangular obstacle with MHD

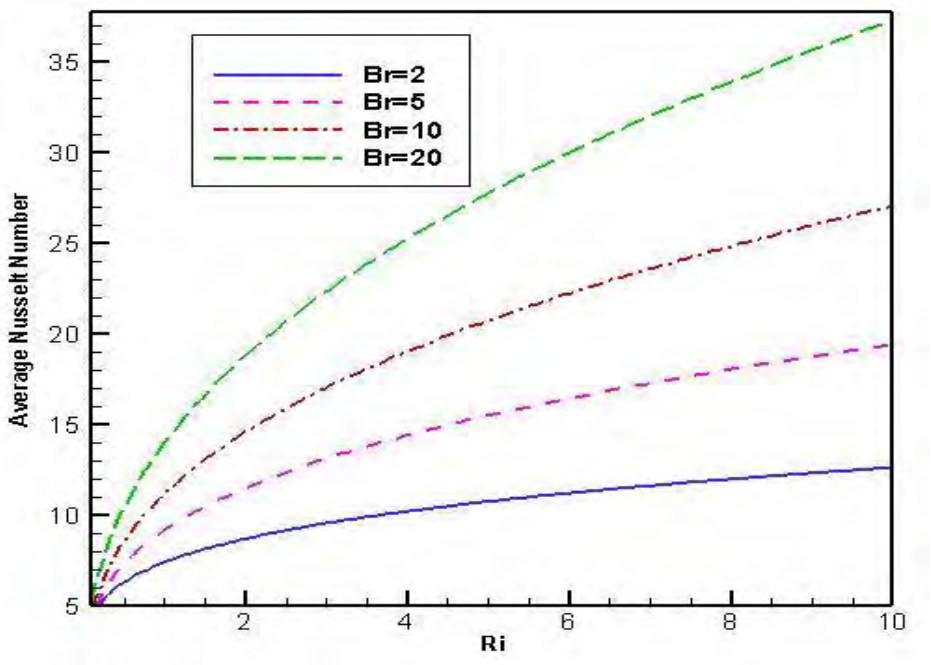

Figure 6.39: Average Nusselt number Vs Ri for different values of Br with MHD rectangular obstacle along the left semi-circular wall heater

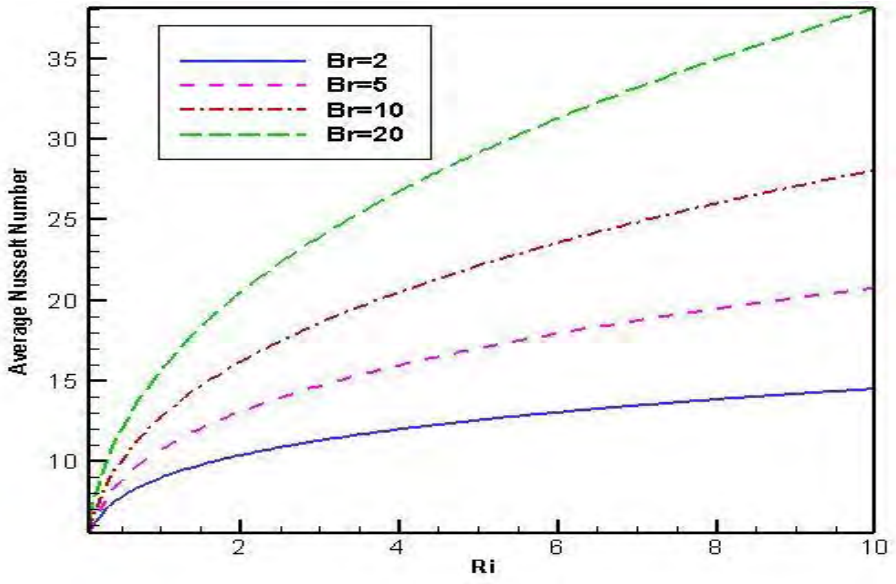

Figure 6.40: Average Nusselt number Vs Ri for different values of Br with MHD rectangular obstacle along the right semi-circular wall heater

CONCLUSIONS

A Finite element method is used to study the present investigation on MHD mixed convection flow around a heated obstacle (*i.e.* trapezoidal or rectangular) placed in a lid driven rectangular cavity. From this investigation, it is found that all the parameters *e.g.* magnetic field, Richardson number, Buoyancy ratio and size of the heated obstacle plays significant role on average heat transfer. The major outcomes have been drawn as follows:

- The heat transfer rate increases for increasing Richardson number.
- Heat transfer rate is decreases with increases of the size of the heated obstacle in absence and presence of MHD. But the ratio of differences in size is high in absence of MHD than the presence of MHD along the left and right semi-circular wall heater. In absence of MHD the ratio of differences are not similar along the left and right semi-circular wall heater. But in presence of MHD the ratio of differences are same along the left and right semi-circular wall heater.
- The magnetic field plays an important role on the flow pattern and temperature. The fluid flow and temperature become weak for increasing the value of Hartmann number.
- Heat transfer rate is higher in absence of magnetic field. Presence of magnetic field decreases $\boldsymbol{Nu_{av}}$ drastically. Increasing value of $\boldsymbol{Ha}$ decreases $\boldsymbol{Nu_{av}}$ gradually in the region $\mathbf{0.1} \leq \boldsymbol{Ri} \leq \mathbf{1}$ but decreases $\boldsymbol{Nu_{av}}$ abruptly in the region $\mathbf{1} \leq \boldsymbol{Ri} \leq \mathbf{10}$.
- Heat transfer rate resisted with the increase of magnetic field.
- Buoyancy ratio plays an important role in absence and presence of magnetic field on heat transfer.
- With the increase of $\boldsymbol{Br}$ heat transfer rate increases. With the increases of $\boldsymbol{Br}$, $\boldsymbol{Nu_{av}}$ increases slightly in the region $\mathbf{0.1} \leq \boldsymbol{Ri} \leq \mathbf{1}$ and it increases abruptly in the region $\mathbf{1} \leq \boldsymbol{Ri} \leq \mathbf{10}$. For lower value of $\boldsymbol{Br}$ heat transfer rate nominal in forced to mixed and mixed to natural convection region.
- Buoyancy ratio plays an important role on temperature distribution for both cases trapezoidal and rectangular heated obstacle with and without MHD.

- Fluid flow is strongly dominated by buoyancy forces. Flow strength step-up with the increasing value of Richardson number.
- Heat transfer rate is high along the right semi-circular wall heater than the left semi-circular wall heater for all the cases.
- For rectangular heated obstacle heat transfer rate is higher than the trapezoidal heated obstacle for all cases.
- In mixed convection dominated region streamlines and isotherms are not symmetric in both presence and absence of magnetic field. But in natural convection region streamlines and isotherms are symmetrical in both presence and absence of magnetic field.
- There is no significant effect on fluid flow for increasing values of Lewis number.
- There is no significant effect of Lewis number on temperature distribution.

REFERENCES

Al-Amiri, A., Khanafer, K., Bull, J., Pop, I., Effect of sinusoidal wavy bottom surface on mixed convection heat transfer in a lid-driven cavity, Int. J. Heat Mass Transfer, 50, 1771–1780, 2007.

Al-Salem, K., Öztop, H. F., Pop, I. & Varol, Y. , Effects of moving lid direction on MHD mixed convection in a linearly heated cavity, Int. J. Heat Mass Transfer, 55, 1103–1112, 2012.

Aydin, O., Ünal, A., & Ayhan, T., A numerical study on buoyancy-driven flow in an inclined square enclosure heated and cooled on adjacent walls, Numerical Heat Transfer, 36, 585–599, 1999.

Basak, T., Roy, S., Sharma, P. K. & Pop, I., Analysis of mixed convection flows within a square cavity with linearly heated side wall, Int. J. Heat Mass Transfer, 52, 2224–2242, 2009.

Basak, T., Roy, S., Singh, S. K. & Pop, I, Finite element simulation of natural convection within porous trapezoidal enclosures for various inclination angles: effect of various wall heating, Int. J. Heat Mass transfer, 52, 4135–4150, 2009.

Bhuiyan, A.H., Uddin, M. N. and Alim, M. A., Combined effect of Hartmann and Rayleigh numbers on free convective flow in a square cavity with different positions of heated elliptic obstacle, Annals of Pure and Applied Mathematics, 6, 41-56, 2014.

Billah, M. M., Rahman, M. M., Sharif, U.M, Rahim, N. A., Saidur, R. & Hasanuzzaman, M., Numerical analysis of fluid flow due to mixed convection in a lid-driven cavity having a heated circular hollow cylinder, Int. Commun. Heat Mass Transfer, 38, 1093–1103, 2011.

Buchanan, G. R., Finite Element Analysis, Schaum's Outline Series, McGraw-Hill, 1995.

Chandra, A. & Chhabra, R. P., Flow over and forced convection heat transfer in Newtonian fluids from a semi-circular cylinder, Int. J. Heat Mass Transfer, 54, 225–241, 2011.

Ching, Y.C., Öztop, H. F., Rahman, M. M., Islam, M. R. & Ahsan, A., Finite element simulation of mixed convection heat and mass transfer in a right triangular enclosure, Int. Commun. Heat Mass Transfer, 39, 689–696, 2012.

Dong, S.F. & Li, Y. T., Conjugate of natural convection and conduction in a complicated enclosure, Int. J. Heat Mass Transfer, 47, 2233–2239, 2004.

Hasanuzzaman, M., Öztop, H. F., Rahman, M. M., Rahim, M. M., Saidur, R. & Varol, Y., Magnetohydrodynamic natural convection in trapezoidal cavities, Int. Commun. Heat Mass Transfer 39, 1384–1394,2012.

Hasanuzzaman, M., Rahman, M. M., Öztop, H. F., Rahim, N. A. & Saidur, R., Effects of Lewis number on heat and mass transfer in a triangular cavity, Int. Commun. Heat Mass Transfer, 39, 1213–1219, 2012.

Hossain, M.S. & Alim, M. A., MHD free convection within trapezoidal cavity with non-uniformly heated bottom wall, Int. J. Heat Mass Transfer 69, 327–336, 2014.

House, J.M., Beckermann, C. & Smith, T. F., Effect of a centered conducting body on natural convection heat transfer in an enclosure, Numerical Heat Transfer, 18, 213–225,1990.

Islam, A.W., Sharif, M. A. R. & Carlson, E. S., Mixed convection in a lid driven square cavity with an isothermally heated square blockage inside, Int. J. Heat Mass Transfer, 55, 5244-5255, 2012.

Khalil Khanafer, comparison of flow and heat transfer characteristics in a lid-driven cavity between flexible and modified geometry of a heated bottom wall, Int. J. Heat Mass Transfer, 78, 1032–1041, 2014.

Khanafer, K. & Aithal, S. M., Laminar mixed convection flow and heat transfer characteristics in a lid driven cavity with a circular cylinder, Int. J. Heat Mass Transfer, 66, 200–209, 2013.

Koca, A., Oztop, H. F. & Varol, Y., The effects of Prandtl number on natural convection in triangular enclosures with localized heating from below, Int. Commun. Heat Mass Transfer, 34, 511–519, 2007.

Lewis, R. W., Nithiarasu, P. & Seetharamu, K. N., Fundamentals of Finite Element Method for Heat and Fluid Flow, John Wiley & Sons, Ltd, 2004.

Moallemi, M. K. and Jang, K. S., Prandtl number effect on laminar mixed convection heat transfer in a lid-driven cavity, Int. J. Heat Mass transfer, 35, 1881-1892, 1992.

Nasrin, R., Alim, M. A. & Chamkha, A. J., Combined convection flow in triangular wavy chamber filled with water–CuO nanofluid: Effect of viscosity models, Int. Commun. Heat Mass Transfer, 39, 1226–1236, 2012.

Nithyadevi, N. & Yang, R., Double diffusive natural convection in a partially heated enclosure with Soret and Dufour effects, Int. J. Heat Fluid Flow, 30, 902–910, 2009.

Oztop, H.F., Al-Salem, K. & Pop, I., MHD mixed convection in a lid-driven cavity with corner heater, Int. J. Heat Mass Transfer, 54, 3494–3504, 2011.

Öztop, H.F., Rahman, M. M., Ahsan, A., Hasanuzzaman, M. & Saidur, R., MHD natural convection in an enclosure from two semi-circular heaters on the bottom wall, Int. J. Heat Mass Transfer, 55, 1844–1854, 2012.

Öztop, H.F., Zhao, Z. and Yu, B., Fluid flow due to combined convection in lid-driven enclosure having a circular body, Int. J. Heat and Fluid Flow, 30, 886-901, 2009.

Parvin, S. & Hossain, N. F., Finite element simulation of MHD combined convection through a triangular wavy channel, Int. Commun. Heat Mass Transfer, 39, 811–817, 2012.

Patankar, S. V., Numerical Heat Transfer and Fluid Flow, Hemisphere McGraw-Hill, Washington DC, 1980.

Rahman, M. M., Alim, M. A. & Sarker, M. M. A., Numerical study on the conjugate effect of joule heating and magnato-hydrodynamics mixed convection in an obstructed lid-driven square cavity, Int. Commun. Heat Mass Transfer, 37, 524–534, 2010.

Rahman, M. M., Öztop, H. F., Ahsan, A. & Orfi, J., Natural convection effects on heat and mass transfer in a curvilinear triangular cavity, Int. J. Heat Mass Transfer, 55, 6250–6259, 2012.

Rahman, M. M., Parvin, S., Saidur, R., Rahim, N. A., Magnetohydrodynamic mixed convection in a horizontal channel with an open cavity, Int. Commun. Heat Mass Transfer, 38, 184-193, 2011.

Rahman, M. M., Saidur, R. & Rahim, N. A., Conjugated effect of joule heating and magneto-hydrodynamic on double-diffusive mixed convection in a horizontal channel with an open cavity, Int. J. Heat Mass Transfer, 54, 3201–3213, 2011.

Rahman, M.M., Öztop, H. F., Rahim, N. A., Saidur, R. & Al-Salem, K., MHD Mixed convection with joule heating effect in a lid-driven cavity with a heated semi-circular source using finite element technique, Numerical Heat Transfer, 60, 543–560, 2011.

Rahman, M.M., Öztop, H. F., Rahim, N. A., Saidur, R., Al-Salem, K., Amin, N., Mamun, M. A. H. & Ahsan, A., Computational analysis of mixed convection in a channel with a cavity heated from different sides, Int. Commun. Heat Mass Transfer, 39, 78–84, 2012.

Ray, S. & Chatterjee, D., MHD mixed convection in a lid-driven cavity including heat conducting circular solid object and corner heaters with Joule heating, Int. Commun. Heat Mass Transfer, 57, 200–207, 2014.

Serrano-Arellano, J., Gijón-Rivera, M., Riesco-Ávila, J. M., Xamán, J. & Álvarez, G., Numerical investigation of transient heat and mass transfer by natural convection in a ventilated cavity: Outlet air gap located close to heat source, Int. J. Heat Mass Transfer, 76, 268–278, 2014.

Sivasankaran, S., Malleswaran, A., Lee, J. & Sundar, P., Hydro-magnetic combined convection in a lid-driven cavity with sinusoidal boundary conditions on both sidewalls, Int. J. Heat Mass Transfer, 54, 512–525, 2011.

Sivasankaran, S., Sivakumar, V. & Prakash, P., Numerical study on mixed convection in a lid-driven cavity with non-uniform heating on both sidewalls, Int. J. Heat Mass Transfer, 53, 4304–4315, 2010.

Teamah, M. A., Numerical simulation of double diffusive natural convection in rectangular enclosure in the presences of magnetic field and heat source, Int. J. Thermal Sciences, 47, 237–248, 2008.

Varol, Y., Koca, A. & Öztop, H.F., Natural convection in a triangle enclosure with flush mounted heater on the wall, Int. Commun. Heat Mass Transfer, 33, 951–958, 2006.
